Center for Research and Advanced Studies
of the National Polytechnic Institute

Physics Department

Graphene generalized coherent states

A thesis by

Daniel Ortiz Campa

In partial fulfillment of the requirements
for the degree of

Doctor of Philosophy
in Physics

Advised by

Dr. David José Fernández Cabrera

Mexico City.
May 30, 2022

Centro de Investigación y de Estudios Avanzados del Instituto Politécnico Nacional

Departamento de Física

ESTADOS COHERENTES GENERALIZADOS DEL GRAFENO

Tesis presentada
como requisito parcial para la obtención del grado de
Doctor en Ciencias en la Especialidad de Física

por

Daniel Ortiz Campa

asesorado por

Dr. David José Fernández Cabrera

Ciudad de México

Junio 2022

En memoria de mi padre.

Agradecimientos

- A mi padre Juan Ortiz Mendoza, gracias por formar parte de mi vida, tu recuerdo siempre me acompañará.
- A mi madre Estela Guadalupe Campa Jiménez, gracias por tu esfuerzo y cariño, sin ti nada de esto sería posible.
- A mi familia, amigos y colegas, gracias por cada uno de los valiosos momentos a su lado.
- A mi asesor, el Dr. David José Fernández Cabrera, le agradezco su mentoría a lo largo de estos años, este trabajo no sería posible sin su conocimiento, consejos y apoyo.
- A Juan Domingo, le agradezco la colaboración y retroalimentación continua, fundamentales en el desarrollo de este trabajo.
- A los Doctores Héctor Hugo García Compean, Alonso Contreras Astorga, Erik Díaz Bautista y Mario Pérez González, les agradezco por fungir como sinodales de esta tesis y por los valiosos comentarios sobre la misma.
- Al Departamento de física del CINVESTAV, por darme la oportunidad de realizar mis estudios de posgrado, a todos y cada uno de sus integrantes, gracias por brindarme una estancia placentera.
- Al CONACYT (México) por el apoyo brindado a través de la beca de doctorado 703048 y el proyecto FORDECYT-PRONACES/61533/2020 que permitieron la realización de este trabajo.

Resumen

En este trabajo comenzaremos describiendo la mecánica cuántica supersimétrica (SUSY QM) de primero y segundo orden, la cual nos proporciona un método mediante el cual se obtienen nuevos sistemas cuánticos con soluciones exactas partiendo de un sistema conocido.

Después, identificaremos el Hamiltoniano efectivo para la monocapa y la bicapa de grafeno bajo la acción de campos magnéticos ortogonales a dichos materiales y resolveremos el problema de eigenvalores para tales operadores, mostrando algunos ejemplos en los cuales se obtienen soluciones exactas al problema de eigenvalores del Hamiltoniano efectivo para la bicapa.

Posteriormente, construiremos una familia de operadores de escalera para los eigenestados de los Hamiltonianos efectivos de la monocapa y bicapa. Más tarde, calcularemos los estados coherentes generalizados de la monocapa y la bicapa de grafeno mediante tres definiciones distintas, analizaremos cada uno de los estados resultantes y determinaremos las condiciones que nos llevan a la mutua equivalencia entre ellos.

Finalmente, estudiaremos la evolución temporal de estos estados haciendo uso de la fidelidad, función que nos permite encontrar los cuasiperiodos para los cuales el estado coherente evolucionado coincidirá con el inicial.

Abstract

In this work we begin by describing the first and second-order supersymmetric quantum mechanics (SUSY QM), that provides us a method through which new exactly-solvable quantum systems are obtained departing from a known one.

Then, we will identify the effective Hamiltonian for monolayer and bilayer graphene under the action of magnetic fields orthogonal to the surface of these materials and we will solve the eigenvalue problem, showing some examples for which exact analytical solutions to the eigenvalue problem for the effective Hamiltonian of bilayer graphene are obtained.

Subsequently, we will build a family of ladder operators for the eigenstates of the effective Hamiltonians of monolayer and bilayer graphene. Later, we will calculate the generalized coherent states for the monolayer and bilayer graphene using three different definitions, we will analyze each of them and determine the conditions leading to their mutual equivalence.

Finally, we will study the time evolution of these states using the quantum fidelity, a function allowing us to find the quasiperiods for which the coherent state at time t will coincide with the initial one.

Contents

List of Figures

CHAPTER 1

Introduction

The thinnest ever known material is called graphene, term coined by Hanns-Peter Boehm and promoted by Saito in order to describe a material that consists of a hexagonal arrangement of carbon atoms [1, 2]. Graphene was isolated for the first time by André Geim, Konstantin Novoselov and their collaborators, but a theoretical description of the band structure of the material was available since 1957 [3, 4]. Due to its interesting properties, the electronic structure of graphene at low energies has been widely studied through the tight-binding model. In fact, at low energies the material can be effectively described by the massless Dirac equation [5, 6]. Besides, when graphene is placed in an external magnetic field the conduction and valence bands turn out to be discrete (Landau levels) [7–9]. On the other hand, the material made up of two graphene layers stacked one on top of the other is known as bilayer graphene. At low energies, bilayer graphene is not described by the massless Dirac equation, since its dispersion relation is quadratic, and its energy levels are also discrete under an external magnetic field [5].

In general, to find the energy levels and associated wave functions for monolayer and bilayer graphene in external magnetic fields is not a simple task. Nevertheless, for some magnetic fields expressed in the Landau gauge the problem can be solved by implementing the techniques of supersymmetric quantum mechanics (SUSY QM) [10–13]. Let us stress that SUSY QM is a technique that intertwines pairs of Hamiltonians by means of a differential operator, allowing us to find the solutions of one Hamiltonian from the other [14]. The fundamental ideas of SUSY QM, Darboux transformation and factorization method are closely related. The last one is widely used in physics to solve eigenvalue problems in quantum mechanics, since it allows us to factorize a differential operator in terms of less order ones. In 1951, Infeld and Hull gave an exhaustive classification of systems solvable by this method, thus the subject was believed to be exhausted [15, 16]. However, in 1984 Bogdan Mielnik found a new factorization that led him to derive isospectral potentials to the harmonic oscillator that were not contained in the Infeld and Hull classification, thus reviving interest

in the search for potentials solvable through this method [17]. After this, Nieto, Andrianov, Borisov, Iofe, and Sukumar found the connection between factorization method and the supersymmetry concept introduced by Witten [18–21].

Going back to graphene, let us note that the first and second-order SUSY QM allows us to determine the energy levels for monolayer and bilayer graphene respectively. Since the corresponding wave functions are stationary, the flux of probability current associated with the electrical resistivity and conductivity for the material in these states is time-independent [6]. With this in mind, a different approach has been used in several papers, where it is tried to find information of the system through the coherent states [22–26]. Let us remember that the coherent states (CS), term coined in 1963 by Glauber [27, 28], were originally found by Schrödinger as states associated with the harmonic oscillator that saturate the Heisenberg uncertainty relation [29]. These states also fulfill a series of properties that can be seen as mutually equivalent definitions. However, for arbitrary systems this is not the case. Therefore, when working with the graphene coherent states, the definition used to generate them becomes fundamental.

In this work we have taken as motivation the non-uniqueness of the graphene CS proposed by several authors, and we want to carry out an analysis of the different CS definitions as well as to look for the conditions allowing to recover the uniqueness seen for the harmonic oscillator. In order to do that we have structured this analysis as follows: in chapter 2, we will describe the most relevant elements employed in the first and second-order SUSY QM, using a direct approach for the latter instead of an iterative one. We will make special emphasis on the conditions necessary to obtain non-singular potentials through this method. Subsequently, in chapter 3 the general aspects leading to the effective Hamiltonians of monolayer and bilayer graphene will be described, and their connection with SUSY QM when magnetic fields are involved. Throughout chapter 4, several exact solutions for electrons in bilayer graphene will be shown, and three kinds of SUSY partner potentials will be considered: shape-invariant, rational modifications and confluent partner potentials. For each case the magnetic field generating them will be determined. Then, in chapter 5 we start by defining the ladder operators for the previously found eigenstates, allowing us to analyze the different definitions of graphene generalized CS; as part of this process, the algebra fulfilled by the ladder operators will be determined. In chapter 6 we will show an example of these coherent states, showing also that the mutual equivalence between CS definitions is possible in some cases. We will also make a description of the time evolution of these states by means of a quantum fidelity analysis. Finally, in chapter 7 we will give our conclusions and some perspectives for this work.

CHAPTER 2

Supersymmetric quantum mechanics

In quantum mechanics, solving systems with Schrödinger-like Hamiltonians is not trivial. One of the most used techniques to accomplish this task is the so-called factorization method, which for many years was believed to be exhausted after the Infeld and Hull classification was introduced [15, 16]. But in 1984 Mielnik found a new family of operators allowing to factorize the harmonic oscillator Hamiltonian and led him to new exactly solvable potentials. Shortly after Fernández did the same treatment for the hydrogen atom [17, 30]. Previously, in 1981, Witten had proposed a mechanism through which pairs of isospectral Hamiltonians could be obtained [18], nowadays called supersymmetric partners. It was Nieto, Andrianov, Borisov, Iofe, and Sukumar who formally established the connection between the factorization method and Witten's supersymmetry [19–21].

Next, we will overview briefly the general ideas behind the first and second-order supersymmetric quantum mechanics (SUSY QM), widely described in the literature (see e.g. [14, 31] and references therein). The main purpose will be to generate new solvable Hamiltonians from a given known one, with the new potential being isospectral (or almost isospectral) to the initial one.

SECTION 2.1

First-order SUSY QM

Let H_1^- and H_1^+ be two hermitian Schrödinger-like Hamiltonians

$$H_1^{\pm} = -\frac{d^2}{dx^2} + V_1^{\pm}(x), \tag{2.1.1}$$

which are intertwined by means of a first-order differential operator $\mathcal{L}_1^-$ in the way

$$H_1^+ \mathcal{L}_1^- = \mathcal{L}_1^- H_1^-, \tag{2.1.2}$$

with

$$\mathcal{L}_1^- = \frac{d}{dx} + W(x), \tag{2.1.3}$$

where $\mathcal{L}_1^-$ is known as intertwining operator and the so-called superpotential $W(x)$ is a real function to be determined. Assuming that H_1^- is a solvable Hamiltonian, whose normalized eigenfunctions and eigenvalues $\psi_n^-(x)$, $\mathcal{E}_n^-$ are such that $\mathcal{E}_n^- < \mathcal{E}_{n+1}^- \; \forall \; n \in \{\mathbb{N} \cup 0\}$, then from equation (2.1.2) it turns out that

$$\phi_n^+(x) = \mathcal{L}_1^- \psi_n^-(x), \tag{2.1.4}$$

is a non-normalized formal eigenfunction of H_1^+, whose norm is given by

$$\langle \phi_n^+ | \phi_n^+ \rangle = \langle \psi_n^- | \, \mathcal{L}_1^+ \mathcal{L}_1^- \, | \psi_n^- \rangle \, , \tag{2.1.5}$$

with

$$\mathcal{L}_1^+ = -\frac{d}{dx} + W(x), \tag{2.1.6}$$

i.e., $\mathcal{L}_1^+ \equiv \left(\mathcal{L}_1^-\right)^\dagger$ is an intertwining operator which is the hermitian conjugate of $\mathcal{L}_1^-$. Equation (2.1.5) will be relevant later for our analysis. By substituting the explicit form of the operator $\mathcal{L}_1^-$ into the intertwining relation (2.1.2), we get that

$$H_1^+ \mathcal{L}_1^- = -\frac{d^3}{dx^3} - W\frac{d^2}{dx^2} + \left(V_1^+ - 2W^{'}\right)\frac{d}{dx} + \left(WV_1^+ - W^{''}\right), \tag{2.1.7a}$$

$$\mathcal{L}_1^- H_1^- = -\frac{d^3}{dx^3} - W\frac{d^2}{dx^2} + V_1^-\frac{d}{dx} + \left(WV_1^- + V_1^{'-}\right). \tag{2.1.7b}$$

Since the right-hand side expressions (2.1.7a) and (2.1.7b) must be equal, by comparing the powers of d/dx, it follows that

$$V_1^+ = V_1^- + 2W^{'}, \tag{2.1.8a}$$

$$WV_1^+ - W^{''} = WV_1^- + V_1^{'-}. \tag{2.1.8b}$$

Substituting the V_1^+ of equation (2.1.8a) into (2.1.8b) and integrating the results, it turns out that W satisfies the following Riccati equation

$$W^2 - W^{'} = V_1^- - \epsilon, \tag{2.1.9}$$

where ϵ is an arbitrary real constant known as factorization energy. Then, the potentials $V_1^\pm$ can be written as follows

$$V_1^- = W^2 - W^{'} + \epsilon, \tag{2.1.10a}$$

$$V_1^+ = W^2 + W^{'} + \epsilon. \tag{2.1.10b}$$

In order to determine the superpotential, it is proposed the following change of variable

$$W = -\frac{u^{'}}{u}, \tag{2.1.11}$$

then, equation (2.1.10a) becomes

$$-u'' + V_1^- u = \epsilon u. \tag{2.1.12}$$

This means that u is a formal eigenfunction of the Hamiltonian H_1^- associated with the eigenvalue ϵ, which is called seed solution in the literature. Note that, for a fixed ϵ, by solving equation (2.1.12) the superpotential will be determined. On the other hand, equations (2.1.10) allow to factorize both Hamiltonians as follows:

$$H_1^- = \mathcal{L}_1^+ \mathcal{L}_1^- + \epsilon, \tag{2.1.13a}$$

$$H_1^+ = \mathcal{L}_1^- \mathcal{L}_1^+ + \epsilon. \tag{2.1.13b}$$

Using equation (2.1.13a), the relation for the norm of ϕ_n^+ given in equation (2.1.5) becomes

$$\langle \phi_n^+ | \phi_n^+ \rangle = \mathcal{E}_n^- - \epsilon \geq 0. \tag{2.1.14}$$

Since ϵ is an arbitrary real constant, if we take it such that $\mathcal{E}_{n-1}^- < \epsilon < \mathcal{E}_n^-$ it implies that ϕ_n^+ would be a normalizable physical solution of H_1^+ but at the same time ϕ_{n-1}^+ would not. On the other hand, due to the oscillation theorem for the Schrödinger equation (2.1.12) it turns out that W and V_1^+ would diverge at some $x-$points when $\mathcal{E}_0^- < \epsilon$. In order to avoid this divergent behavior we restrict ourselves to $\epsilon \leq \mathcal{E}_0^-$, which fulfills (2.1.14) for all n [21, 32, 33].
Nevertheless, there are still two different cases, which depend on the value of ϵ:

- If $\epsilon = \mathcal{E}_0^-$ and the seed solution is taken as $u \equiv \psi_0^-(x)$, thus equation (2.1.14) indicates that $\phi_0^+ = 0$, which is not considered as eigenstate of H_1^+. Then, the spectrum of H_1^+ is $\mathrm{Sp}(H_1^+) = \{\mathcal{E}_n^+\} = \{\mathcal{E}_n^- | n = 1, 2, ...\}$, with associated normalized eigenfunctions given by

$$\psi_n^+(x) = \frac{\mathcal{L}_1^- \psi_n^-(x)}{\sqrt{\mathcal{E}_n^- - \mathcal{E}_0^-}} \quad \text{for} \quad n = 1, 2, ... \tag{2.1.15}$$

- If $\epsilon < \mathcal{E}_0^-$, the seed solution u is not a physical eigenfunction of H_1^-. However, from equation (2.1.10b) there exists $\psi_\epsilon^+(x)$ which is in the kernel of $\mathcal{L}_1^+$ and could be a physical eigenfunction of H_1^+ with eigenvalue ϵ, depending on whether or not it is normalizable. Thus, $\mathrm{Sp}(H_1^+) = \{\mathcal{E}_n^+\} = \{\mathcal{E}_n^- | n = 0, 1, ...\}$ when $\psi_\epsilon^+(x)$ is not normalizable, with corresponding eigenfunctions

$$\psi_n^+(x) = \frac{\mathcal{L}_1^- \psi_n^-(x)}{\sqrt{\mathcal{E}_n^- - \epsilon}}, \quad n = 0, 1, ... \tag{2.1.16}$$

  otherwise $\mathrm{Sp}(H_1^+) = \{\mathcal{E}_n^+\} = \{\epsilon, \mathcal{E}_n^- | n = 0, 1, ...\}$ with corresponding eigenfunctions

$$\psi_\epsilon^+(x), \quad \psi_n^+(x) = \frac{\mathcal{L}_1^- \psi_n^-(x)}{\sqrt{\mathcal{E}_n^- - \epsilon}}, \quad n = 0, 1, ... \tag{2.1.17}$$

with $\psi_\epsilon^+(x)$ being the normalized eigenfunction such that $\mathcal{L}_1^+\psi_\epsilon^+(x) = 0 \Rightarrow \psi_\epsilon^+(x) \propto \frac{1}{u(x)}$.

The two operators $H_1^\pm$ and their associated $V_1^\pm$ are called partner Hamiltonians and partner potentials respectively, or simply SUSY partners in the literature; from now on we will refer to them interchangeably.

It is important to stress some points: 1) a similar analysis can be performed if we consider that the solvable Hamiltonian is H_1^+ instead of H_1^-, by taking just the Hermitian conjugate of equation (2.1.2); 2) the superpotential depends implicitly on ϵ and its form does not modify H_1^- but it does with H_1^+, which means that we have endless SUSY partners for H_1^-, labeled by the factorization energy ϵ; 3) the constraint that the superpotential must be real is taken by simplicity. In fact, there are several ways to complexify the method [34].

In order to exemplify the technique, let us consider the shifted harmonic oscillator potential V_1^- as follows

$$V_1^- = \frac{\omega^2}{4}\left(x + \frac{2k}{\omega}\right)^2 - \frac{\omega}{2}, \tag{2.1.18}$$

its corresponding eigenfunctions and eigenvalues are

$$\psi_n^-(x) = \sqrt{\frac{1}{2^n n!}\left(\frac{\omega}{2\pi}\right)^{\frac{1}{2}}} e^{-\frac{1}{2}\zeta^2}\mathrm{H}_n(\zeta), \quad \mathcal{E}_n = n\omega \quad \text{for} \quad n = 0, ... \tag{2.1.19}$$

with $\zeta = \sqrt{\omega/2}(x + 2k/\omega)$ and H_n being the Hermite polynomials. For an arbitrary factorization energy ϵ, which for simplicity we will suppose to be real, the general solution associated to this potential is

$$u = e^{-\frac{\zeta^2}{2}}\left[{}_1\mathrm{F}_1\left(a, \frac{1}{2}; \zeta^2\right) + 2\nu\zeta\frac{\Gamma\left(a + \frac{1}{2}\right)}{\Gamma(a)}\,{}_1\mathrm{F}_1\left(a + \frac{1}{2}, \frac{3}{2}; \zeta^2\right)\right], \tag{2.1.20}$$

where $a = -\epsilon/2\omega$, ν is an arbitrary real constant and ${}_1\mathrm{F}_1$ is the hypergeometric (Kummer) function

$${}_1\mathrm{F}_1\left(a_1, b_1; y\right) = \frac{\Gamma(b_1)}{\Gamma(a_1)}\sum_{n=0}^{\infty}\frac{\Gamma(a_1 + n)}{\Gamma(b_1 + n)}\frac{y^n}{n!}. \tag{2.1.21}$$

Notice that, for $\epsilon < 0$ and $|\nu| \leq 1$ the solution u is nodeless. Figure 2.1 shows a plot of the potential V_1^- of equation (2.1.18) and two of its SUSY partners, which were generated as described above.

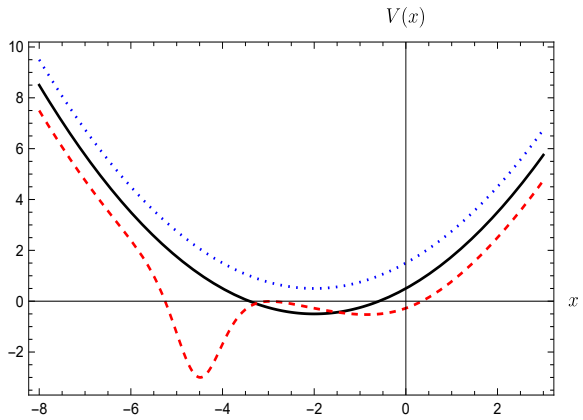

Figure 2.1: First-order SUSY partner potentials V_1^+ of the shifted harmonic oscillator (black curve) generated by using the seed solution (2.1.20) for $\epsilon = \mathcal{E}_0^- = 0$ (blue dotted curve) and $\epsilon = -\omega$ (red dashed). The parameters were taken as $\omega = 1$, $k = 1$ and $\nu = 0.98$.

SECTION 2.2

Second-order SUSY QM

The second-order SUSY QM is a technique connecting two SUSY partner Hamiltonians by a second-order differential intertwining operator (see [14, 35–37] and references therein). It can be addressed by using iteratively the first-order SUSY discussed in the previous section, but instead we will use next a direct approach.

Let H_2^- and H_2^+ be two hermitian Schrödinger-like Hamiltonians

$$H_2^\pm = -\frac{d^2}{dx^2} + V_2^\pm(x), \tag{2.2.1}$$

which are intertwined as follows

$$H_2^+ \mathcal{L}_2^- = \mathcal{L}_2^- H_2^-, \tag{2.2.2}$$

where the intertwining operator is given by

$$\mathcal{L}_2^- = \frac{d^2}{dx^2} + \eta(x)\frac{d}{dx} + \gamma(x). \tag{2.2.3}$$

Assuming that H_2^- is a solvable Hamiltonian whose normalized eigenfunctions and eigenvalues $\psi_n^-(x)$ and $\mathcal{E}_n^-$ are given, such that $\mathcal{E}_n^- < \mathcal{E}_{n+1}^-$ for $n = 0, 1, ...$, then from equation (2.2.2) it follows that

$$\phi_n^+(x) = \mathcal{L}_2^- \psi_n^-(x), \tag{2.2.4}$$

is a formal eigenfunction of H_2^+ whose norm is given by

$$\langle \phi_n^+ | \phi_n^+ \rangle = \langle \psi_n^- | \, \mathcal{L}_2^+ \mathcal{L}_2^- \, | \psi_n^- \rangle \geq 0, \tag{2.2.5}$$

where we have defined the hermitian conjugate of the intertwining operator $\mathcal{L}_2^-$ in the way:

$$\mathcal{L}_2^+ = \left(\mathcal{L}_2^-\right)^\dagger = \frac{d^2}{dx^2} - \eta(x)\frac{d}{dx} + \gamma(x) - \eta^{'}(x). \tag{2.2.6}$$

Now, by substituting the explicit expression of $\mathcal{L}_2^-$ into the intertwining relation (2.2.2), we will get

$$H_2^+ \mathcal{L}_2^- = -\frac{d^4}{dx^4} - \eta\frac{d^3}{dx^3} + \left(V_2^+ - 2\eta^{'} - \gamma\right)\frac{d^2}{dx^2} + \left(\eta V_2^+ - \eta^{''} - 2\gamma^{'}\right)\frac{d}{dx} + \left(\gamma V_2^+ - \gamma^{''}\right), \tag{2.2.7a}$$

$$\mathcal{L}_2^- H_2^- = -\frac{d^4}{dx^4} - \eta\frac{d^3}{dx^3} + \left(V_2^- - \gamma\right)\frac{d^2}{dx^2} + \left(\eta V_2^- + 2V_2^{'-}\right)\frac{d}{dx} + \left(V_2^{''-} + \eta V_2^{'-} + \gamma V_2^-\right). \tag{2.2.7b}$$

By comparing the same powers on d/dx of the previous right-hand sides it turns out that

$$V_2^+ = V_2^- + 2\eta^{'}, \tag{2.2.8a}$$

$$\eta V_2^+ - \eta^{''} - 2\gamma^{'} = \eta V_2^- + 2V_2^{'-}, \tag{2.2.8b}$$

$$\gamma V_2^+ - \gamma^{''} = V_2^{''-} + \eta V_2^{'-} + \gamma V_2^-. \tag{2.2.8c}$$

If we plug equation (2.2.8a) in (2.2.8b) and then integrate the result, it is obtained

$$\gamma = \frac{\eta^2}{2} - \frac{\eta^{'}}{2} - V_2^- + d, \tag{2.2.9}$$

with d being a real integration constant. In addition, we can substitute the V_2^+ of equation (2.2.8a) into (2.2.8c) to get

$$\gamma^{''} = 2\gamma\eta^{'} - V_2^{''-} - \eta V_2^{'-}. \tag{2.2.10}$$

Plugging equation (2.2.9) and its second derivative into (2.2.10), we will have

$$2\eta^{'} V_2^- + \eta V_2^{'-} = \frac{\eta^{'''}}{2} - 2(\eta^{'})^2 - \eta\eta^{''} + \eta^2\eta^{'} + 2\eta^{'} d. \tag{2.2.11}$$

We can integrate the previous equation, which after some algebra leads to

$$\frac{\eta\eta^{''}}{2} - \left(\frac{\eta^{'}}{2}\right)^2 - \eta^2\eta^{'} + \frac{\eta^4}{4} - \eta^2 V_2^- + \eta^2 d + c = 0, \tag{2.2.12}$$

with c being a new integration constant. The function γ is given in terms of η as follows:

$$\gamma = -\frac{\eta^{''}}{2\eta} + \left(\frac{\eta^{'}}{2\eta}\right)^2 + \frac{\eta^{'}}{2} + \frac{\eta^2}{4} - \frac{c}{\eta^2}. \tag{2.2.13}$$

We have obtained a non-linear second-order differential equation for η (see equation (2.2.12)) which looks complicated to be addressed. Nevertheless, let us try the following *anzats*

$$\eta^{'} = \eta^2 + 2\beta\eta - 2\xi, \tag{2.2.14}$$

where β and ξ are functions of x to be determined. Then, the second derivative of η reads

$$\eta^{''} = 2\eta\eta^{'} + 2\beta\eta^{'} + 2\beta^{'}\eta - 2\xi^{'}. \tag{2.2.15}$$

Plugging this expression in equation (2.2.12) and the *ansatz* once again, what we get after simplifying the result is

$$\left(\beta^{'} + \beta^2 - V_2^{-} + \xi + d\right)\eta^2 - \xi^{'}\eta + \left(c - \xi^2\right) = 0. \tag{2.2.16}$$

Since this formula has to be valid for any arbitrary η, the coefficients accompanying each of its powers must be zero. From these equations it is concluded that ξ is a constant with two possible values, $\xi_1 = \sqrt{c}$, $\xi_2 = -\sqrt{c}$. We get as well that

$$\beta_{1,2}^{'} + \beta_{1,2}^2 = V_2^{-} - \epsilon_{1,2}, \tag{2.2.17}$$

where $\epsilon_1 = d + \sqrt{c}$ and $\epsilon_2 = d - \sqrt{c}$. Similarly to the first-order SUSY, we propose the change $\beta_{1,2} = u_{1,2}^{'}/u_{1,2}$, which transforms the Riccati equation (2.2.17) into

$$-u_{1,2}^{''} + V_2^{-}u_{1,2} = \epsilon_{1,2}u_{1,2}. \tag{2.2.18}$$

This means that we need to have two seed solutions $u_{1,2}$ which are formal eigenfunctions of H_2^{-} with eigenvalues $\epsilon_{1,2}$, known as factorization energies.

On the other hand, after some algebra, the product $\mathcal{L}_2^{+}\mathcal{L}_2^{-}$ turns out to be

$$\mathcal{L}_2^{+}\mathcal{L}_2^{-} = \left(H_2^{-} - \epsilon_1\right)\left(H_2^{-} - \epsilon_2\right), \tag{2.2.19}$$

and the reversed product $\mathcal{L}_2^{-}\mathcal{L}_2^{+}$ becomes

$$\mathcal{L}_2^{-}\mathcal{L}_2^{+} = \left(H_2^{+} - \epsilon_1\right)\left(H_2^{+} - \epsilon_2\right). \tag{2.2.20}$$

Taking into account equations (2.2.5) and (2.2.19), it is obtained now the following restriction on the factorization energies

$$\left(\mathcal{E}_n^{-} - \epsilon_1\right)\left(\mathcal{E}_n^{-} - \epsilon_2\right) \geq 0. \tag{2.2.21}$$

Finally, since c is a real number we can classify the second-order transformations in three non-equivalent cases, depending on the $c-$value. Next we will make a brief description of each one of them.

SUBSECTION 2.2.1

Real case

In this case $c > 0$, which means that we have two different real factorization energies ϵ_1 and ϵ_2 and associated seed solutions u_1 and u_2. By substituting the corresponding β_i in the ansatz (2.2.14) we will get

$$\eta^{'} = \eta^2 + 2\beta_1\eta - (\epsilon_1 - \epsilon_2), \tag{2.2.22a}$$

$$\eta^{'} = \eta^2 + 2\beta_2\eta + (\epsilon_1 - \epsilon_2). \tag{2.2.22b}$$

Subtracting equation (2.2.22a) from (2.2.22b), after some algebra the η function will be obtained:

$$\eta = \frac{\epsilon_1 - \epsilon_2}{\beta_1 - \beta_2}. \tag{2.2.23}$$

In terms of the seed solutions it can be written as

$$\eta = -\frac{(\epsilon_1 - \epsilon_2)u_1u_2}{\mathcal{W}(u_1, u_2)} = -\frac{d}{dx}\ln\left(\mathcal{W}(u_1, u_2)\right), \tag{2.2.24}$$

where $\mathcal{W}(f, g) = fg^{'} - f^{'}g$ is the Wronskian of f and g. Notice that ϵ_1, ϵ_2 have to fulfill the condition (2.2.21), thus we can choose the factorization energies ϵ_1, ϵ_2 only as follows [14,37]:

- They can be chosen as $\epsilon_2 < \epsilon_1 < \mathcal{E}_0^-$. Then, the seed solutions u_2, u_1 are not physical eigenfunctions of H_2^-, but due to equation (2.2.20) there are two formal eigenfunctions of H_2^+ associated with ϵ_1 and ϵ_2. Since at the same time they are settled in the kernel of $\mathcal{L}_2^+$, the next relations are fulfilled

$$\psi_{\epsilon_l}^{-''} = \eta\psi_{\epsilon_l}^{-'} - (\gamma - \eta^{'})\psi_{\epsilon_l}^-, \tag{2.2.25a}$$

$$\psi_{\epsilon_l}^{-''} = (V_2^+ - \epsilon_l)\psi_{\epsilon_l}^-, \tag{2.2.25b}$$

  where $l = 1, 2$. By making equal the right-hand side of both expressions, and using equations (2.2.8a), (2.2.12) and the antzats to replace γ, V_2^+ and η^2, it turns out that:

$$\frac{\psi_{\epsilon_l}^{+'}}{\psi_{\epsilon_l}^+} = \frac{\eta^{'}}{\eta} - \frac{\psi_{\epsilon_l}^{-'}}{\psi_{\epsilon_l}^-}, \tag{2.2.26}$$

  which finally leads to

$$\psi_{\epsilon_l}^+ \propto \frac{\eta}{\psi_{\epsilon_l}^-}. \tag{2.2.27}$$

  The spectrum of H_2^+ is given by $\mathrm{Sp}(H_2^+) = \{\epsilon_2, \epsilon_1, \mathcal{E}_n^- | n = 0, 1, ...\}$, as long as the eigenfunctions (2.2.27) are normalizable, otherwise ϵ_1, ϵ_2 or both do not belong

to such spectrum. On the other hand, the normalized eigenfunctions associated with $\mathcal{E}_n^-$ are

$$\psi_n^+(x) = \frac{\mathcal{L}_2^-\psi_n^-(x)}{\sqrt{(\mathcal{E}_n^- - \epsilon_1)(\mathcal{E}_n^- - \epsilon_2)}} \quad \text{for} \quad n = 0, \dots \tag{2.2.28}$$

Finally, it must be said that the behavior of η and V_2^+ depends on the factorization energy values and the number of nodes that the seed solutions have. In Figure 2.2 we can see plots of some SUSY partner potentials for this case.

- The factorization energies can be as well located between two neighbor eigenvalues, such that $\mathcal{E}_j^- < \epsilon_2 < \epsilon_1 < \mathcal{E}_{j+1}^-$ for some value of j. In this case, the criteria to characterize the spectrum of H_2^+ are identical to the previous ones. Therefore, the eigenfunctions are given by equations (2.2.27) and (2.2.28). Nevertheless, the levels ordering will be $\mathrm{Sp}(H_2^+) = \left\{\mathcal{E}_0^-, ..., \mathcal{E}_j^-, \epsilon_2, \epsilon_1, \mathcal{E}_{j+1}^-, ...\right\}$, as long as the eigenfunction in equation (2.2.27) are normalizables, otherwise ϵ_1, ϵ_2 or both will not belong to the spectrum of H_2^+. In Figure 2.2 we can see some SUSY partner potentials for this case.

- The factorization energies can be chosen such that $\mathcal{E}_j^- = \epsilon_2 < \epsilon_1 < \mathcal{E}_{j+1}^-$ for some value of j and the seed solutions as $u_2 \equiv \psi_j^-$ and u_1. For the first factorization energy, the corresponding eigenfunction ϕ_j^+ of H_2^+ is not normalizable but $\phi_{\epsilon_1}^+$ could be, which means that $\mathrm{Sp}(H_2^+) = \left\{\mathcal{E}_0^-, ..., \mathcal{E}_{j-1}^-, \epsilon_1, \mathcal{E}_{j+1}^-, ...\right\}$ as long as $\phi_{\epsilon_1}^+$ is normalizable, otherwise ϵ_1 does not belong to the spectrum of H_2^+. The normalized eigenfunctions associated with $\mathcal{E}_n^-$ are

$$\psi_n^+(x) = \frac{\mathcal{L}_2^-\psi_n^-(x)}{\sqrt{(\mathcal{E}_n^- - \mathcal{E}_j^-)(\mathcal{E}_n^- - \epsilon_1)}} \quad \text{for} \quad n = 0, \dots, j-1, j+1, \dots \tag{2.2.29}$$

  In Figure 2.3 we can see some SUSY partner potentials for this case.

- The factorization energies can be chosen as $\epsilon_2 = \mathcal{E}_j^-$, $\epsilon_1 = \mathcal{E}_{j+1}^-$ for some value of j, and the seed solutions as $u_2 \equiv \psi_j^-$, $u_1 \equiv \psi_{j+1}^-$. The corresponding formal eigenfunctions ϕ_j^+ and ϕ_{j+1}^+ of H_2^+ are not normalizable, due to equation (2.2.21). This means that $\mathrm{Sp}(H_2^+) = \{\mathcal{E}_n^- | n = 0, ..., j-1, j+2, ...\}$, the corresponding normalized eigenfunctions are given by

$$\psi_n^+(x) = \frac{\mathcal{L}_2^-\psi_n^-(x)}{\sqrt{(\mathcal{E}_n^- - \mathcal{E}_j^-)(\mathcal{E}_n^- - \mathcal{E}_{j+1}^-)}} \quad \text{for} \quad n = 0, ..., j-1, j+2, ... \tag{2.2.30}$$

  Besides, due to the oscillation theorem it is straightforward to prove that $\mathcal{W}$ is nodeless thus η and V_2^+ are well behaved. In Figure 2.3 we can see some SUSY partner potentials for this case.

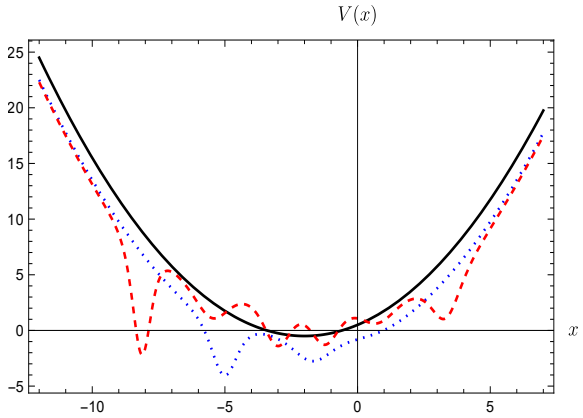

Figure 2.2: Second-order SUSY partner potentials V_2^+ of the shifted harmonic oscillator (black curve) generated by using the seed solutions (2.1.20) for $\epsilon_2 = -17\omega/10$, $\nu_2 = 1.1$, $\epsilon_1 = -15\omega/10$, $\nu_1 = 0.9$ (blue dotted curve) and $\epsilon_2 = 25\omega/10$, $\nu_2 = 1.1$, $\epsilon_1 = 27\omega/10$, $\nu_1 = 0.9$ (red dashed curve). The parameters were taken as $\omega = 1$, $k = 1$.

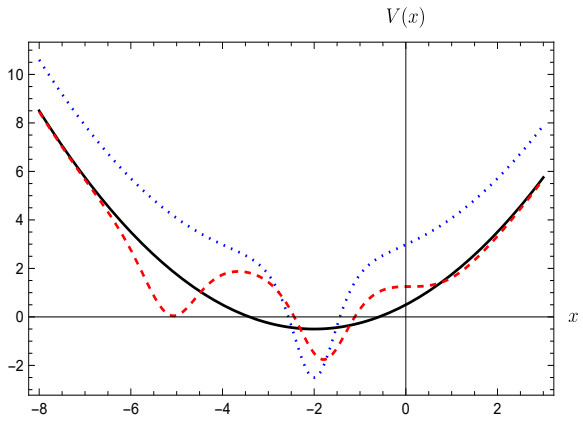

Figure 2.3: Second-order SUSY partner potentials V_2^+ of the shifted harmonic oscillator (black curve) generated by using the seed solutions (2.1.20) for $\epsilon_2 = \mathcal{E}_1^- = \omega$, $\epsilon_1 = 15\omega/10$, $\nu_1 = 1.2$ (red dashed curve) and $\epsilon_2 = \mathcal{E}_1^- = \omega$, $\epsilon_1 = \mathcal{E}_2^- = 2\omega$ (blue dotted curve). The parameters were taken as $\omega = 1$, $k = 1$.

SUBSECTION 2.2.2

Confluent case

In this case $c = 0$, which means that we have only one real factorization energy $\epsilon_1 = \epsilon_2 \equiv \epsilon$ and only one seed solution u [38–40]. This simplifies the ansatz as follows

$$\eta^{'} = \eta^2 + 2\beta\eta. \tag{2.2.31}$$

Making the change of variable $\eta = 1/y$ we get the inhomogeneous first-order linear differential equation for y:

$$y' + 2\beta y = -1. \tag{2.2.32}$$

By remembering that $\beta = u'/u$ it is straightforward to prove that the integrating factor is given by u^2, and then

$$y(x, \omega_0) = \frac{\omega_0 - \int_{x_0}^{x} u^2(t)dt}{u^2(x)}, \tag{2.2.33}$$

whence η turns out to be

$$\eta(x, \omega_0) = \frac{u^2(x)}{\omega_0 - \int_{x_0}^{x} u^2(t)dt} = -\frac{\mathrm{w}'(x)}{\mathrm{w}(x)}, \tag{2.2.34}$$

where

$$\mathrm{w}(x, \omega_0) = \omega_0 - \int_{x_0}^{x} u^2(t)dt. \tag{2.2.35}$$

In order to avoid singularities in η and V_2^+, we must ask that w has no nodes. Notice that w is a decreasing monotonic function defined in the same interval $[a, b]$ as u. Since $x_0 \in [a, b]$, if we want to avoid the nodes in w it must be required that this function is always positive or always negative. Thus, we define the next two quantities

$$I_+ = \int_{x_0}^{b} u^2(t)dt \quad \text{and} \quad I_- = \int_{a}^{x_0} u^2(t)dt, \tag{2.2.36}$$

which are non-negative, and at least one is strictly positive. Then, the singularities can be avoided if u behaves as follows:

- If u is such that $u(x \to a) = u(x \to b) = 0$, it implies that the non-singular ω_0-domain is $\omega_0 \leq -I_-$ and $\omega_0 \geq I_+$.
- If u is such that $u(x \to a) = 0$ and $u(x \to b)$ is not bounded, it implies that I_+ goes to infinity and thus $\omega_0 \leq -I_-$ for η to be nodeless.
- If u is such that $u(x \to b) = 0$ and $u(x \to a)$ is not bounded, it implies that I_- goes to infinity and thus $\omega_0 \geq I_+$ for η to be nodeless.

Note that in the three cases when the inequality for ω_0 becomes an equality, the function w will have nodes, which has to be considered as a limit case. On the other hand, analogously to the real case, the eigenfunctions turn out to be

$$\psi_n^+(x) = \frac{\mathcal{L}_2^- \psi_n^-(x)}{|\mathcal{E}_n^- - \epsilon|} \quad \text{for} \quad n = 0, ... \tag{2.2.37}$$

and

$$\psi_\epsilon^+(x) \propto \frac{\eta(x)}{u(x)} \propto \frac{u(x)}{\mathrm{w}}. \tag{2.2.38}$$

Notice that this time only two choices for the factorization energy can be made:

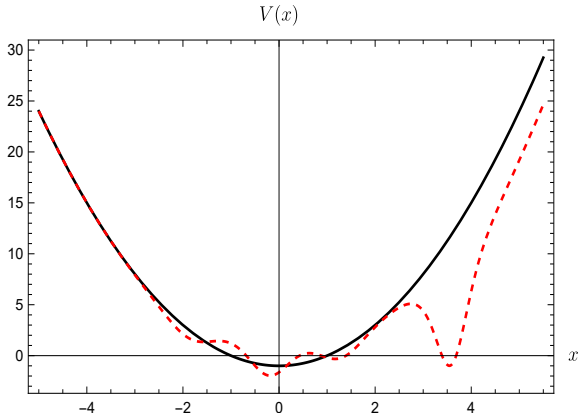

Figure 2.4: Confluent second-order SUSY partner potential V_2^+ of the shifted harmonic oscillator (black curve) generated by using the seed solution (2.1.20) for $\epsilon = 3.5$, $\nu_1 = 1$ (red dashed curve). The parameters were taken as $\omega = 2$, $k = 0$.

- If $\epsilon = \mathcal{E}_j^-$ and w is nodeless, then $Sp(H_2^+) = Sp(H_2^-)$, otherwise (limit case) $\epsilon = \mathcal{E}_j^-$ does not belong to the spectrum of H_2^+.
- If $\epsilon \neq \mathcal{E}_j^-$ and w is nodeless, then $Sp(H_2^+) = Sp(H_2^-) \cup \{\epsilon\}$, otherwise (limit case) ϵ does not belong to the spectrum of H_2^+ and both SUSY partner Hamiltonians are isospectral.

It must be stressed that in the confluent case, for a fixed factorization energy, the SUSY partner potentials are actually a one parametric family labeled by ω_0. On the other hand, an expression for η in Wronskian terms can be found in [41–44]. In Figure 2.4 a plot of the confluent SUSY partner potential of the harmonic oscillator of equation (2.1.18) is shown.

SUBSECTION 2.2.3

Complex case

In this case $c < 0$, which implies that we have two different complex but not arbitrary factorization energies, since $\epsilon_2 = \bar{\epsilon_1}$. Notice that now equation (2.2.21) becomes a strict inequality; in fact, there is no restriction on ϵ_1 as long as it is strictly complex, with a non-zero imaginary part [14, 45]. The η function can be calculated analogously to the real case by making just the following changes,

$$\epsilon_2 = \bar{\epsilon_1}, \quad u_2 = \bar{u_1}, \tag{2.2.39}$$

which leads to

$$\eta = \frac{\mathfrak{Im}(\epsilon_1)}{\mathfrak{Im}(\beta_1)} = -\frac{(\epsilon_1 - \bar{\epsilon_1})|u_1|^2}{\mathcal{W}(u_1, \bar{u_1})}. \tag{2.2.40}$$

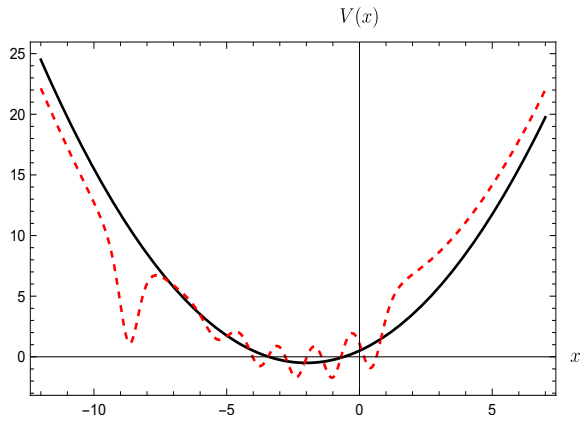

Figure 2.5: Second-order SUSY partner potential V_2^+ of the shifted harmonic oscillator (black curve) generated by using a seed solution (2.1.20) for $\epsilon_1 = (\omega/20)(98 + i)$ and $\nu_1 = -1$ (red dashed curve). The parameters were taken as $\omega = 1$, $k = 1$.

Furthermore, in this case H_2^- and H_2^+ are isospectral since the new levels can not be physical (the associated eigenfunctions are non-normalizable) but for the eigenvalues $\mathcal{E}_n^-$ the corresponding normalized eigenfunctions are given by equation (2.2.28).
We must emphasize that, by construction, the factorization energies turn out to be complex conjugate to each other. However, it is possible still to choose them as two different complex numbers, which leads to the complexification of V_2^+ and therefore to the breaking of the hermiticity of H_2^+. A plot of the SUSY partner potentials V_2^- and V_2^+ for this case is shown in Figure 2.5.

CHAPTER 3

Electronic structure of graphene

In 1946, Wallace characterized the band structure of graphene, finding something unusual: graphene behaved like a semi-metal [4]. Additionally, at low energies the charge carriers have a constant speed regardless their energy, as photons do, which is the reason why they are called Dirac electrons [5]. It was until 2004 that André Geim, Konstantin Novoselov and their collaborators managed to experimentally isolate graphene, a single atomic layer of graphite [3]. On the other hand, bilayer graphene is a material consisting of two graphene layers, one on top of the other, with an interlayer distance of 3.48Å [46]. The most common arrangement consists of two layers rotated from each other by an angle of $\pi/3$, called Bernal stacking in the literature (which we will use in this work). Bilayer graphene is receiving nowadays an increasing interest among the scientific community. As for the monolayer, bilayer graphene has a zero band gap but a quadratic dispersion relation, thus behaving like a semi-metal. On the other hand, arrangements different from Bernal stacking, known as twisted layers, lead to different conduction properties. Finally, if an external magnetic field is applied to these materials, discrete levels appear in the conduction and valence bands. In this section we will describe the Hamiltonian ruling this behavior.

SECTION 3.1

Monolayer graphene

Graphene is a two-dimensional material composed of carbon atoms arranged in a regular hexagonal pattern, also called honeycomb lattice [5]. The Bravais lattice for this material is triangular, with the lattice vectors being given by (see Figure 3.1)

$$\mathbf{a}_1 = \frac{a}{2}\left(\sqrt{3}, 1\right), \qquad \mathbf{a}_2 = \frac{a}{2}\left(\sqrt{3}, -1\right), \tag{3.1.1}$$

where $a \approx 2.46$Å is the distance between adjacent unit cells. The honeycomb lattice has two atoms per elementary cell belonging to two sub-lattices, A and B. Each atom from sub-lattice A (B) is surrounded by three atoms from sub-lattice B (A) (see Figure

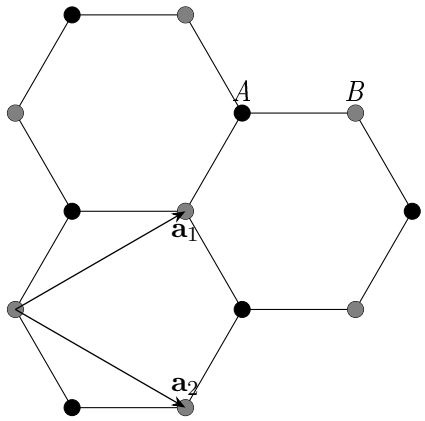

Figure 3.1: Honeycomb lattice structure of graphene, composed of two non-equivalent triangular sub-lattices A and B, represented by the black and gray circles respectively.

3.1), known as nearest-neighbors, whose vectors are given by

$$\boldsymbol{\delta}_1 = \frac{a}{2}\left(\frac{1}{\sqrt{3}}, 1\right), \qquad \boldsymbol{\delta}_2 = \frac{a}{2}\left(\frac{1}{\sqrt{3}}, -1\right), \qquad \boldsymbol{\delta}_3 = a\left(\frac{1}{\sqrt{3}}, 0\right). \tag{3.1.2}$$

On the other hand, the reciprocal lattice (which is also triangular) has vectors $\mathbf{b}_j$ defined by

$$\mathbf{a}_i \cdot \mathbf{b}_j = 2\pi\delta_{ij}, \tag{3.1.3}$$

thus

$$\mathbf{b}_1 = \frac{2\pi}{a}\left(\frac{1}{\sqrt{3}}, 1\right), \qquad \mathbf{b}_2 = \frac{2\pi}{a}\left(\frac{1}{\sqrt{3}}, -1\right). \tag{3.1.4}$$

Two special points $\mathbf{K}^+$ and $\mathbf{K}^-$ arise, known as valleys or conical points [47–49]. These points belong to the Brillouin zone (see Figure 3.2), and the vectors defining them are

$$\mathbf{K}^+ = \frac{2\pi}{a}\left(\frac{1}{\sqrt{3}}, \frac{1}{3}\right), \qquad \mathbf{K}^- = \frac{2\pi}{a}\left(\frac{1}{\sqrt{3}}, -\frac{1}{3}\right). \tag{3.1.5}$$

It is around these points that the dispersion relation becomes linear (see Figure 3.3). In the nearest-neighbor approximation, hopping processes occur only between the nearest neighbor atoms. Then, in the tight-binding model the Hamiltonian is the 2×2 matrix

$$\mathcal{H}(\mathbf{k}) = \begin{pmatrix} 0 & \gamma_0 S(\mathbf{k}) \\ \gamma_0 \bar{S}(\mathbf{k}) & 0 \end{pmatrix}, \tag{3.1.6}$$

where $\mathbf{k}$ is the wave vector, $\gamma_0 \approx 2.97eV$ is the hopping parameter between the in-plane nearest-neighbors and

$$S(\mathbf{k}) = \sum_{\boldsymbol{\delta}} e^{i\mathbf{k}\cdot\boldsymbol{\delta}} = 2\exp\left(\frac{ik_x a}{2\sqrt{3}}\right)\cos\left(\frac{k_y a}{2}\right) + \exp\left(\frac{-ik_x a}{\sqrt{3}}\right). \tag{3.1.7}$$

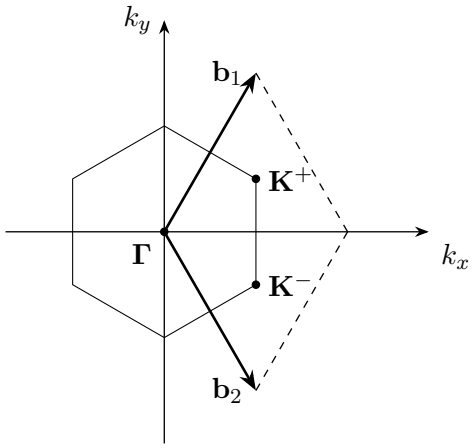

Figure 3.2: First Brillouin zone of graphene; Dirac cones lie on the conical points $\mathbf{K}^+$ and $\mathbf{K}^-$ in the reciprocal lattice.

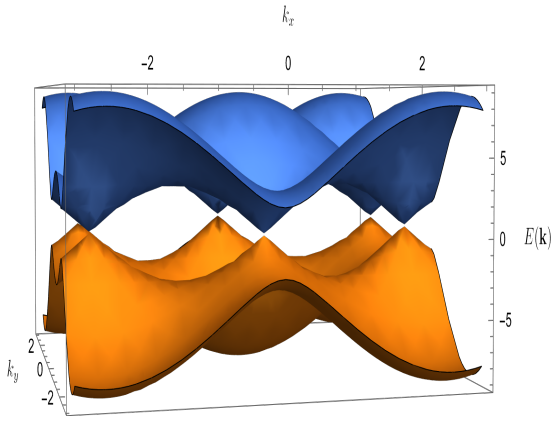

Figure 3.3: Valence and conduction bands (3.1.8) for monolayer graphene, which touch to each other at the conical point $\mathbf{K}^{\pm}$ where the dispersion relation is linear.

The eigenenergies for the Hamiltonian (3.1.6) are given by

$$E(\mathbf{k}) = \pm\gamma_0|S(\mathbf{k})| = \pm\gamma_0\sqrt{3+f(\mathbf{k})}, \tag{3.1.8}$$

with

$$f(\mathbf{k}) = 2\cos(k_y a) + 4\cos\left(\frac{k_y a}{2}\right)\cos\left(\frac{\sqrt{3}k_x a}{2}\right). \tag{3.1.9}$$

Notice that $S(\mathbf{K}^{\pm}) = 0$, indicating that the conduction and valence bands touch to each other at $\mathbf{K}^{\pm}$. The Hamiltonian can be expanded around these points as follows

$$\mathcal{H}^{\pm}(\mathbf{p}) \approx \frac{\sqrt{3}a\gamma_0}{2\hbar}\begin{pmatrix} 0 & \alpha(p_x \pm ip_y) \\ \alpha(p_x \mp ip_y) & 0 \end{pmatrix}, \tag{3.1.10}$$

where $\alpha = e^{5i\pi/6}$ and $\mathbf{p} = \hbar(\mathbf{k} - \mathbf{K}^{\pm})$. The phase factor α can be removed by a unitary transformation . Thus, the effective Hamiltonians near these points are

$$\begin{aligned}\mathcal{H}^{-}(\mathbf{p}) =& v\begin{pmatrix} 0 & p_x - ip_y \\ p_x + ip_y & 0 \end{pmatrix} = v\boldsymbol{\sigma}\cdot\mathbf{p}, \\ \mathcal{H}^{+}(\mathbf{p}) =& v\begin{pmatrix} 0 & p_x + ip_y \\ p_x - ip_y & 0 \end{pmatrix} = (v\boldsymbol{\sigma}\cdot\mathbf{p})^{T}, \end{aligned} \tag{3.1.11}$$

with $v = \sqrt{3}a\gamma_0/2\hbar \approx c/300$ being the electron velocity around the points $\mathbf{K}^{\pm}$, $\boldsymbol{\sigma}$ represents a vector whose components are the Pauli matrices and $\mathbf{p}$ is the momentum operator [50]. Finally, in order to construct an effective model describing the electron and hole states one needs to make the following replacements

$$p_x \to -i\hbar\frac{\partial}{\partial x}, \quad p_y \to -i\hbar\frac{\partial}{\partial y}. \tag{3.1.12}$$

Notice that $\mathcal{H}^{+} = (\mathcal{H}^{-})^{T}$, thus the eigenvalues of $\mathcal{H}^{+}$ and $\mathcal{H}^{-}$ are equal. From now on we will refer to the monolayer graphene effective Hamiltonian as $\mathcal{H}_{\mathcal{M}} = \mathcal{H}^{-}$, which is a Dirac-like Hamiltonian for massless particles where the speed of light has been replaced by v (the Fermi velocity of the charge carriers). That is why, at low energies $E << \gamma_0$, the electrons in graphene behave effectively as massless particles whose speed in the material is constant, regardless their energy. These charge carriers moving around the conical points (Dirac points) are sometimes called Dirac electrons, since equation (3.1.11) contains a Dirac-like Hamiltonian [51–53].

SUBSECTION 3.1.1

Monolayer graphene in external magnetic fields

If we suppose that electrons move on monolayer graphene in an external magnetic field $\mathbf{B}(x, y)$ perpendicular to the layer surface (plane $x - y$), by using the minimal coupling rule $\mathbf{p} \to \boldsymbol{\pi}$ in equation (3.1.11) the effective Hamiltonian is obtained [10, 11, 50], namely,

$$\mathcal{H}_{\mathcal{M}} = v\boldsymbol{\sigma}\cdot\boldsymbol{\pi}, \tag{3.1.13}$$

where $\boldsymbol{\pi} = \mathbf{p} + \frac{e\mathbf{A}}{c}$, $\mathbf{p}$ is the canonical momentum operator, $-e$ is the electron charge, c is the speed of light, and $\mathbf{A} = \mathbf{A}(x, y)$ is the vector potential such that $\mathbf{B}(x, y) = \nabla\times\mathbf{A}(x, y)$. If we assume that $\mathbf{B}$ is time-independent and changes only in one direction (say x), in the Landau gauge we can choose $\mathbf{A}(x) = \mathcal{A}(x)\hat{e}_y$ such that $\mathbf{B}(x) = \mathcal{B}(x)\hat{e}_z$. Then, the eigenvalue problem to be solved becomes

$$-i\hbar v_F\begin{pmatrix} 0 & \partial_x - i\partial_y + \frac{e}{c\hbar}\mathcal{A}(x) \\ \partial_x + i\partial_y - \frac{e}{c\hbar}\mathcal{A}(x) & 0 \end{pmatrix}\Psi(x, y) = E\Psi(x, y). \tag{3.1.14}$$

It is straightforward to prove that $\mathcal{H}_{\mathcal{M}}$ and p_y commute, which allows to express the eigenfunctions of the Hamiltonian as follows:

$$\Psi(x,y) = e^{iky}\begin{pmatrix}\psi^{+}(x)\\ i\psi^{-}(x)\end{pmatrix}. \tag{3.1.15}$$

By substituting them into equation (3.1.14), after some algebra it is obtained that

$$\mathcal{L}_1^{\pm}\psi^{\pm}(x) = \sqrt{\mathcal{E}}\psi^{\mp}(x), \tag{3.1.16}$$

where $\mathcal{E}$ and $\mathcal{L}_1^{\pm}$ are defined as

$$\mathcal{E} = \frac{E^2}{\hbar^2 v^2}, \qquad \mathcal{L}_1^{\pm} = \mp\frac{d}{dx} + W(x), \tag{3.1.17}$$

with the function $W(x)$ being given by

$$W(x) = \frac{e}{c\hbar}\mathcal{A}(x) + k. \tag{3.1.18}$$

By acting $\mathcal{L}_1^{\mp}$ on equation (3.1.16), in order to decouple the system, we will get

$$H_1^{\pm}\psi^{\pm}(x) = \mathcal{E}\psi^{\pm}(x), \tag{3.1.19}$$

where

$$H_1^{\pm} = \mathcal{L}_1^{\mp}\mathcal{L}_1^{\pm} = -\frac{d^2}{dx^2} + V^{\pm}, \qquad V^{\pm} = W^2 \pm W'. \tag{3.1.20}$$

Then, the functions ψ^{-} and ψ^{+} can be found by solving the eigenvalue problem for two one-dimensional Schrödinger-like Hamiltonians. Note that equation (3.1.20) ensures that the following expression holds

$$H_1^{\pm}\mathcal{L}_1^{\mp} = \mathcal{L}_1^{\mp}H_1^{\mp}. \tag{3.1.21}$$

This means that the Hamiltonians $H_1^{\pm}$ are intertwined as in equation (2.1.2), i.e., we can solve the eigenvalue problem through the first-order SUSY QM of chapter 2. In order to do that, several points must be taken into account:

- The superpotential W, and thus the intertwining operators $\mathcal{L}_1^{\pm}$, will be determined by the magnetic field since it is fulfilled that

$$\mathcal{B}(x) = \frac{c\hbar}{e}\frac{dW}{dx}. \tag{3.1.22}$$

- Equation (3.1.20) tells us that the Hamiltonians $H_1^{\pm}$ are factorized, with a null factorization energy $\epsilon = 0$.

- If for a given magnetic field $\mathcal{B}$ the potential V_1^- is solvable, with known eigenfunctions ψ_n^- and eigenvalues $\mathcal{E}_n^-$, then the solutions to the eigenvalue problem for $\mathcal{H}_\mathcal{M}$ become

$$\Psi_n(x,y) = c_n e^{iky} \begin{pmatrix} \frac{\mathcal{L}_1^- \psi_n^-(x)}{\sqrt{\mathcal{E}_n^-}} \\ i\psi_n^-(x) \end{pmatrix}, \quad E_n = \pm\hbar v\sqrt{\mathcal{E}_n^-}, \tag{3.1.23}$$

  where c_n is a normalization constant and the sign $+$ $(-)$ characterizes the eigenenergies for electrons (holes).

- For an arbitrary state $\Psi(x,y)$, the probability and current densities are given by

$$\rho_\mathcal{M}(x,y) = \Psi^\dagger(x,y)\Psi(x,y), \quad \mathcal{J}_\mathcal{M} = v\Psi^\dagger(x,y)\boldsymbol{\sigma}\Psi(x,y). \tag{3.1.24}$$

Although theoretically ψ_n^- and ψ_n^+ are intertwined, the problem stays still not trivial, since in general the magnetic field profile determines if $V_1^\pm$ are either solvable or not. Some authors have found several electromagnetic fields leading to exact analytical solutions for other gauges and/or configurations [26, 54–57]. An example of SUSY partner potentials obtained for a constant magnetic field is shown in Figure 3.4.

SECTION 3.2

Bilayer graphene

In Bernal stacking, bilayer graphene structure consists of two layers of graphene, each one having a honeycomb crystal structure, where the sub-lattices A of each layer lie exactly on top of one another (see Figure 3.5), with a hopping parameter γ_1 between them. At first-order we consider that there are no hopping processes between the sub-lattices B [58]. The parameter γ_1 is usually taken as $\gamma_1 = 0.4$ eV, which is one order of magnitude lower than the nearest-neighbor in-plane hopping parameter γ_0. This simple model is described by the Hamiltonian

$$\mathcal{H}(\mathbf{k}) = \begin{pmatrix} 0 & \gamma_0 S(\mathbf{k}) & \gamma_1 & 0 \\ \gamma_0 \bar{S}(\mathbf{k}) & 0 & 0 & 0 \\ \gamma_1 & 0 & 0 & \gamma_0 \bar{S}(\mathbf{k}) \\ 0 & 0 & \gamma_0 S(\mathbf{k}) & 0 \end{pmatrix}, \tag{3.2.1}$$

with $S(\mathbf{k})$ being given in equation (3.1.7); then, the eigenvalues are

$$E(\mathbf{k}) = \pm\frac{1}{2}\gamma_1 \pm \sqrt{\frac{1}{4}\gamma_1^2 + \gamma_0^2|S(\mathbf{k})|^2}, \tag{3.2.2}$$

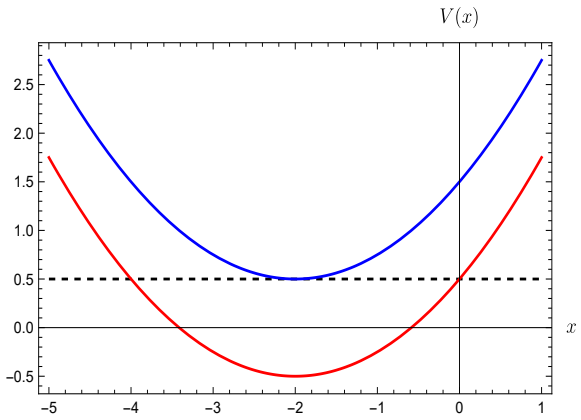

Figure 3.4: Plot of a constant magnetic field (black dashed line) and its associated SUSY partner potentials: the red line represents V^- and the blue line to V^+.

with two independent $\pm$ signs. Since S is zero at $\mathbf{K}^+$ and $\mathbf{K}^-$, two bands touch to each other at zero energy in these points (see Figure 3.6). For these two energies we have

$$E(\mathbf{k})_{1,2} \approx \pm\frac{\gamma_0^2|S(\mathbf{k})|^2}{\gamma_1} \approx \pm\frac{\mathbf{p}^2}{2m^*}. \tag{3.2.3}$$

The other two bands are separated by a gap of size $2\gamma_1$, and they are irrelevant at low-energies ($2v|\mathbf{p}|/\gamma_1 << 1$). In this approximation the effective Hamiltonian describing the bilayer graphene around the conical point $\mathbf{K}^-$ turns out to be

$$\mathcal{H}_{\mathbf{K}^-} = \frac{1}{2m^*}\begin{pmatrix} 0 & (p_x - ip_y)^2 \\ (p_x + ip_y)^2 & 0 \end{pmatrix}, \tag{3.2.4}$$

where $m^* = \gamma_1/2v^2$ is the electron effective mass. Like in monolayer graphene, once again we have that $\mathcal{H}_{\mathbf{K}^-} = (\mathcal{H}_{\mathbf{K}^+})^T$, which implies that the eigenvalues of $\mathcal{H}_{\mathbf{K}^\pm}$ are equal. From now on we will refer to the bilayer graphene effective Hamiltonian as $\mathcal{H}_{\mathfrak{B}} = \mathcal{H}_{\mathbf{K}^-}$. Note that this is a new kind of Hamiltonian, neither a Dirac-like (relativistic) Hamiltonian nor a Schrödinger-like (non-relativistic) one [5, 6].

SUBSECTION 3.2.1

Bilayer graphene in external magnetic fields

We are going to suppose now that bilayer graphene is placed in an external magnetic field as the one described in the previous section ($\mathcal{B}(x)\hat{e}_z$). The Landau gauge and the minimal coupling rule still hold, but now we will consider an additional term proportional to σ_x that only depends on x, which could be interpreted as a potential term, as the result of trigonal warping effect or a deformation by strain, and so on

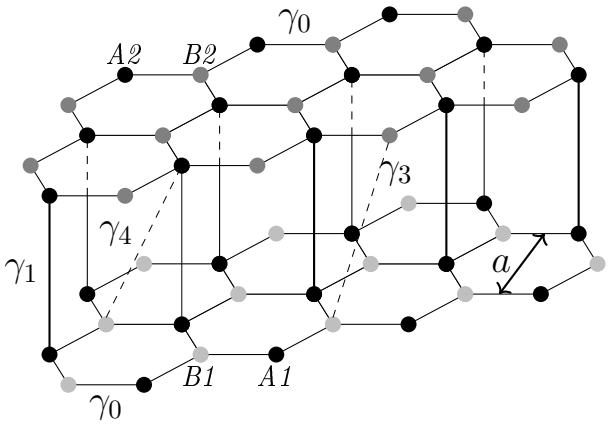

Figure 3.5: Side view of bilayer graphene, where the atoms *A1*, *B1* on the lower layer are represented as the black and light gray circles while the atoms *A2*, *B2* on the upper layer are drawn as the black and gray circles, respectively.

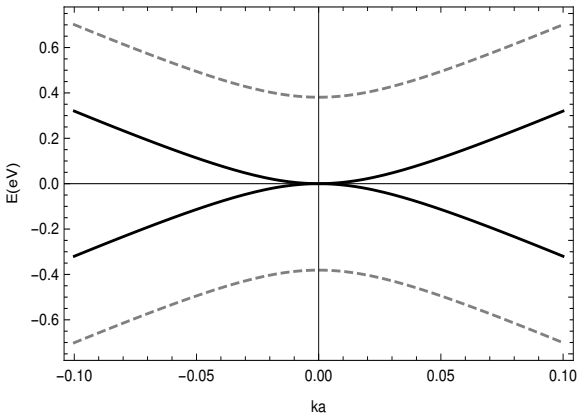

Figure 3.6: The band structure of bilayer graphene around the points $\mathbf{K}^{\pm}$ within the tight-binding model.

[6, 59–61]. Under these conditions the effective Hamiltonian becomes

$$\mathcal{H}_{\mathfrak{B}} = \frac{1}{2m^*}\begin{pmatrix} 0 & (\pi_x - i\pi_y)^2 \\ (\pi_x + i\pi_y)^2 & 0 \end{pmatrix} - \frac{\hbar^2}{2m^*} f(x)\sigma_x. \tag{3.2.5}$$

Once again, $\mathcal{H}_{\mathfrak{B}}$ commutes with p_y, then the eigenfunctions $\Psi(x, y)$ admit the following form

$$\Psi(x, y) = e^{iky}\begin{pmatrix} \psi^+(x) \\ \psi^-(x) \end{pmatrix}, \tag{3.2.6}$$

with k being the wavenumber in y-direction. Hence, the eigenvalue problem $\mathcal{H}_{\mathfrak{B}}\Psi(x,y) = E\Psi(x,y)$ leads to

$$\left[\frac{d^2}{dx^2} \pm \eta(x)\frac{d}{dx} \pm \left(\frac{\eta^{'}}{2} + \frac{\eta^2}{4} + f(x)\right)\right]\psi^{\mp}(x) = -\frac{2m^*}{\hbar^2}E\psi^{\pm}(x), \tag{3.2.7}$$

where η is given by:

$$\eta(x) = 2\left(k + \frac{e}{c\hbar}\mathcal{A}(x)\right). \tag{3.2.8}$$

If f is chosen in the way

$$f(x) = -\frac{\eta^{''}}{2\eta} + \left(\frac{\eta^{'}}{2\eta}\right)^2 - \left(\frac{\epsilon_1 - \epsilon_2}{2\eta}\right)^2, \tag{3.2.9}$$

where ϵ_1, ϵ_2 are two arbitrary real constants, then the system of equations (3.2.7) can be rewritten as follows:

$$\mathcal{L}_2^{\mp}\psi^{\mp}(x) = -\frac{2m^*E}{\hbar^2}\psi^{\pm}(x), \tag{3.2.10}$$

with the operators $\mathcal{L}_2^-$, $\mathcal{L}_2^+$ being given by

$$\mathcal{L}_2^- = \frac{d^2}{dx^2} + \eta(x)\frac{d}{dx} + \gamma(x), \quad \mathcal{L}_2^+ = \left(\mathcal{L}_2^-\right)^{\dagger}, \tag{3.2.11}$$

and

$$\gamma(x) = -\frac{\eta^{''}}{2\eta} + \left(\frac{\eta^{'}}{2\eta}\right)^2 + \frac{\eta^{'}}{2} + \frac{\eta^2}{4} - \left(\frac{\epsilon_1 - \epsilon_2}{2\eta}\right)^2. \tag{3.2.12}$$

The system of equations (3.2.10) can be decoupled by acting $\mathcal{L}_2^{\pm}$ to the left, which leads to:

$$\mathcal{L}_2^{\pm}\mathcal{L}_2^{\mp}\psi^{\mp}(x) = \left(\frac{2m^*E}{\hbar^2}\right)^2\psi^{\mp}(x). \tag{3.2.13}$$

Equation (3.2.10) means that ψ^- and ψ^+ are intertwined by a second-order differential operator, thus it seems natural to assume that they are formal eigenfunctions of two Schrödinger-like Hamiltonians H_2^-, H_2^+ fulfilling the following intertwining relation

$$H_2^+\mathcal{L}_2^- = \mathcal{L}_2^-H_2^-. \tag{3.2.14}$$

Although the previous proposal allows to implement straightforwardly the second-order SUSY QM, it is necessary to clarify some points.

- The constants ϵ_1 and ϵ_2 play the role of factorization energies, thus they must be understood as fixed but with arbitrary values.
- Since the SUSY partner potentials depend explicitly on ϵ_1, ϵ_2 and η, they will be actually determined by the magnetic field (see equation (3.2.8)).

- If we compare equations (2.2.19) and (3.2.13), the eigenenergies for the effective Hamiltonian (3.2.5) will be given by

$$E_n = \pm\frac{\hbar^2}{2m^*}\sqrt{(\mathcal{E}_n^- - \epsilon_1)\,(\mathcal{E}_n^- - \epsilon_2)}, \tag{3.2.15}$$

  where $\mathcal{E}_n^-$ are the eigenvalues of H_2^- and the $+$ $(-)$ sign is associated with electrons (holes). Note that, although the index n orders the energies $\mathcal{E}_n^-$ in increasing way, this does not necessarily happen for E_n. The corresponding eigenstates are

$$\Psi_n(x,y) = c_n e^{iky}\begin{pmatrix} \frac{\mathcal{L}_2^-\psi_n^-(x)}{\sqrt{(\mathcal{E}_n^- - \epsilon_1)(\mathcal{E}_n^- - \epsilon_2)}} \\ \psi_n^-(x) \end{pmatrix}, \tag{3.2.16}$$

  with c_n being a normalization constant.

- The probability and current densities in this case are

$$\rho_{\mathfrak{B}}(x,y) = \Psi^\dagger(x,y)\Psi(x,y), \quad \mathcal{J}_{\mathfrak{B}}(x,y) = \frac{\hbar}{m^*}\mathfrak{Im}\left[\Psi^\dagger(x,y)\mathbf{j}\Psi(x,y)\right], \tag{3.2.17}$$

  where the components of $\mathbf{j}$ are

$$j_x = \boldsymbol{\sigma}\cdot\boldsymbol{\pi}, \tag{3.2.18a}$$

$$j_y = \boldsymbol{\chi}\cdot\boldsymbol{\pi}, \tag{3.2.18b}$$

  with $\boldsymbol{\sigma} = (\sigma_x, \sigma_y)$ and $\boldsymbol{\chi} = (\sigma_y, -\sigma_x)$.

Note that the minimal coupling rule modifies the current as compared with the free case [62]. However, the modification is proportional to the change induced by the vector potential $\mathcal{A}$ (see appendix A). We must remark as well that, when working with strained graphene, some terms called pseudomagnetic fields appear, whose mathematical description is identical to the one presented here, but they are from a completely different nature [63,64]. In the next chapter we are going to discuss some kinds of SUSY partner potentials, characterized by some particular choices of factorization energies.

CHAPTER 4

Solvable cases

As we said previously, the magnetic field and the values of ϵ_1 and ϵ_2 unequivocally determine the SUSY partners $H_2^{\pm}$, but in this process it is assumed that V_2^- (or V_2^+) is a known solvable potential, a requirement that is not easy to satisfy. However, one can proceed in the opposite direction, assuming that V_2^- is given, the factorization energies and associated seed solutions fixed and reconstructing the magnetic field by means of expression (3.2.8) and the equations determining η according to the particular case under study (see chapter 2). Proceeding in this way, we will show next some interesting kinds of SUSY partner potentials.

SECTION 4.1

Shape-invariant potentials

Given two SUSY partners V_2^-, V_2^+, they are said to be shape-invariant potentials if V_2^- can be obtained from V_2^+ by changing its parameters, plus a constant term. This can be expressed as follows

$$V_2^+(x;\lambda_1) = V_2^-(x;\lambda_0) + R(\lambda_1), \tag{4.1.1}$$

where λ_1, λ_0 represent the two sets of parameters with λ_1 being a function of λ_0 [33,65–67]. The previous statement means essentially that the two potentials are shape-invariant if they are functionally similar. In order to get shape-invariant potentials in a second-order SUSY transformation we need to set $\epsilon_2 = \mathcal{E}_0^-$, $\epsilon_1 = \mathcal{E}_1^-$ and take V_2^- as a known member of the shape-invariant family of potentials (see e.g. [68]).

SUBSECTION 4.1.1

Shifted harmonic oscillator potential

As first example let us consider the shifted harmonic oscillator

$$V_2^-(x;\omega,\kappa) = \frac{\omega^2}{4}\left(x + \frac{2\kappa}{\omega}\right)^2 - \frac{\omega}{2}, \tag{4.1.2}$$

whose eigenfunctions and eigenvalues are given by

$$\psi_n^-(\zeta) = c_n e^{-\frac{1}{2}\zeta^2} \mathrm{H}_n(\zeta), \quad \mathcal{E}_n^- = n\omega, \quad n = 0, \dots \tag{4.1.3}$$

where H_n are the Hermite polynomials, $\zeta = \sqrt{\omega/2}\left(x + \frac{2\kappa}{\omega}\right)$, and c_n is a normalization constant.

Taking now the seed solutions and factorization energies as the ground and the first excited states, the η function turns out to be

$$\eta(x) = 2\kappa + \omega x. \tag{4.1.4}$$

Then, according to equation (3.2.8), we will get the magnetic field

$$\mathcal{B}(x) = \mathcal{B}_0 = \frac{c\hbar}{2e}\omega, \tag{4.1.5}$$

which is constant. On the other hand, the relationship between the wavenumber k and the parameter κ turns out to be $k = \kappa$ (see appendix B). By plugging equation (4.1.4) into (2.2.7b), the SUSY partner of V_2^- becomes:

$$V_2^+(x;\omega,\kappa) = \frac{\omega^2}{4}\left(x + \frac{2\kappa}{\omega}\right)^2 + \frac{3}{2}\omega. \tag{4.1.6}$$

It is straightforward to see that $V_2^+(x;\omega,\kappa) = V_2^-(x;\omega,\kappa) + 2\omega$, thus they are shape-invariant potentials (see Figure 4.1). Besides, the eigenfunctions of V_2^+ are given by:

$$\psi_n^+(\zeta) = \psi_{n-2}^-(\zeta) = c_{n-2} e^{-\frac{1}{2}\zeta^2} \mathrm{H}_{n-2}(\zeta), \quad n = 2, ... \tag{4.1.7}$$

with the corresponding eigenenergies

$$\mathcal{E}_n^+ = \mathcal{E}_n^- = n\omega, \quad n = 2, \dots \tag{4.1.8}$$

From equation (3.2.15) the energies of electrons (holes) in bilayer graphene under a constant magnetic field turn out to be

$$E_n = \pm\frac{\hbar^2}{2m^*}\sqrt{n(n-1)}, \quad n = 0, ... \tag{4.1.9}$$

which do not depend on the wavenumber k, as can be seen in Figure 4.2. On the other hand, for $n = 0, 1$ the value for E_n is the same (zero), meaning that the ground state energy is two-fold degenerate. Since there are no restrictions on the eigenfunctions, the spectrum is infinite discrete, with eigenfunctions given by

$$\Psi_0(x,y) = e^{iky}\begin{pmatrix} 0 \\ \psi_0^-(x) \end{pmatrix}, \quad \Psi_1(x,y) = e^{iky}\begin{pmatrix} 0 \\ \psi_1^-(x) \end{pmatrix},$$
$$\Psi_n(x,y) = \frac{e^{iky}}{\sqrt{2}}\begin{pmatrix} \psi_{n-2}^-(x) \\ \psi_n^-(x) \end{pmatrix}, \quad \text{for} \quad n = 2, 3, \dots \tag{4.1.10}$$

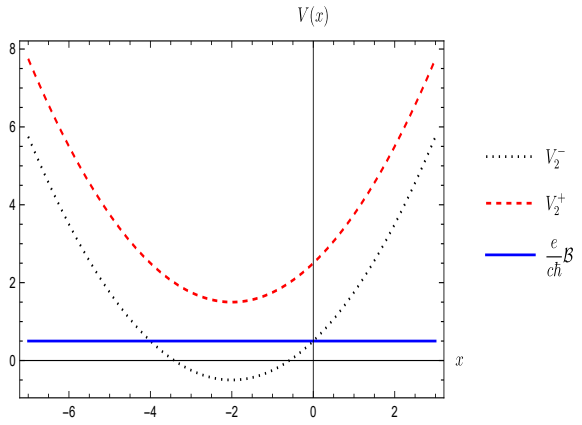

Figure 4.1: Plot of the shifted harmonic oscillator V_2^- (black), its shape-invariant SUSY partner potential V_2^+ (red) and the constant magnetic field (blue). The parameters were taken as $\omega = 1$ and $k = 1$.

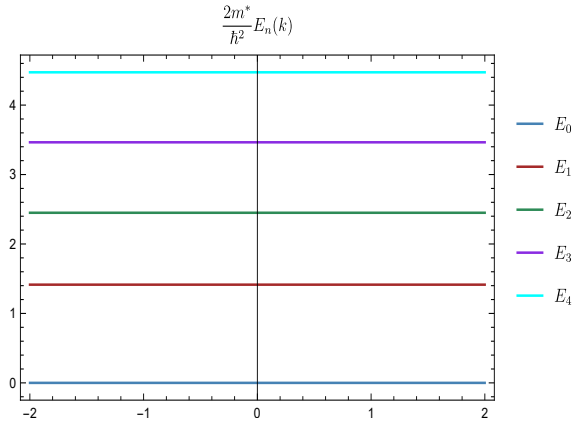

Figure 4.2: Plot of the first electron energies for bilayer graphene in a constant magnetic field as functions of the wavenumber k taking $\omega = 1$.

where ψ_n^- is given in equation (4.1.3). Finally, the probability and y-component current densities for these states are plotted in Figure 4.3. Note that the x-component current density is always zero for stationary states (see Appendix A).

SUBSECTION 4.1.2

Hyperbolic Rosen-Morse potential

The second example to be considered is the hyperbolic Rosen-Morse potential (Rosen-Morse II) given by

$$V_2^-(x; D, \kappa, \alpha) = D^2 + \kappa^2 - D(D + \alpha)\text{sech}^2(\alpha x) + 2\kappa D\tanh(\alpha x). \tag{4.1.11}$$

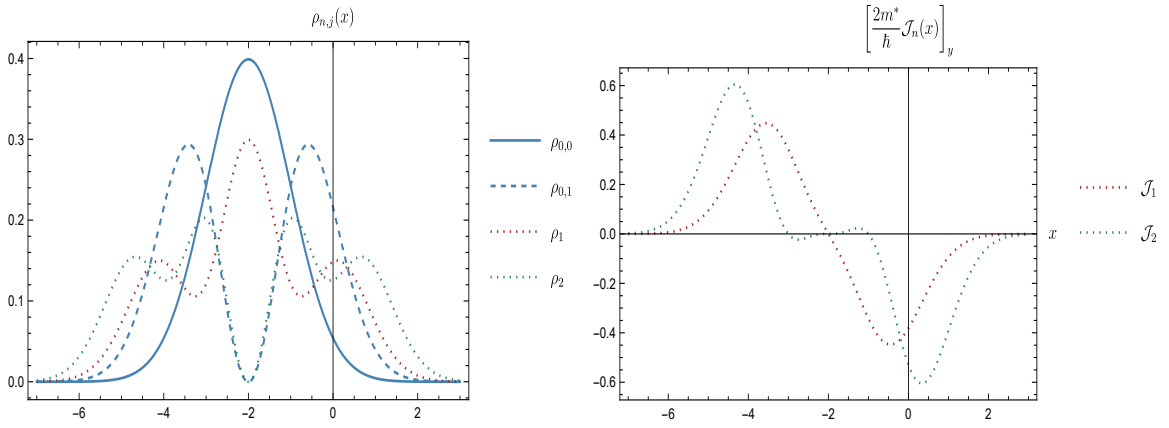

(a) (b)

Figure 4.3: Plot of the probability density (a) and current density in y-direction (b) for bilayer graphene in a constant magnetic field. Note that the two ground states Ψ_0 and Ψ_1 do not produce any current. The parameters were taken as $\omega = k = 1$.

This potential will have a finite discrete spectrum for $|\kappa| < D$, whose eigenvalues are

$$\mathcal{E}_n^- = D^2 + \kappa^2 - (D - n\alpha)^2 - \frac{\kappa^2 D^2}{(D - n\alpha)^2}, \quad n = 0, \ldots, N, \tag{4.1.12}$$

where $N\alpha < D$. The corresponding eigenfunctions become

$$\psi_n^-(\zeta) = c_n (1-\zeta)^{\frac{s^- - n + a^-}{2}} (1+\zeta)^{\frac{s^- - n - a^-}{2}} \mathrm{P}_n^{(s^- - n + a^-, s^- - n - a^-)}(\zeta), \qquad n = 0, \ldots, N. \tag{4.1.13}$$

In this expression c_n is a normalization factor, $\zeta = \tanh(\alpha x)$, $s^- = \frac{D}{\alpha}$, $a^- = \frac{D\kappa}{\alpha(D - n\alpha)}$ and $\mathrm{P}_n^{(a,b)}(\zeta)$ are the Jacobi polynomials [69]. In order to fulfill the square-integrability condition, the exponents of the first two factors in equation (4.1.13) need to be greater than zero.

Once again, taking the factorization energies and corresponding seed solutions as the ground and first excited states, the η function becomes

$$\eta(x) = (2D - \alpha)\left(\frac{\kappa}{D - \alpha} + \tanh(\alpha x)\right). \tag{4.1.14}$$

According to equation (3.2.8), the magnetic field will be

$$\mathbf{B} = \left(0, 0, \mathcal{B}_0 \mathrm{sech}^2(\alpha x)\right) \tag{4.1.15}$$

where $\mathcal{B}_0 = \frac{\hbar c \alpha}{2e}(2D - \alpha)$. From equation (A.6) of Appendix A the parameter κ as function of the wavenumber k becomes

$$\kappa = 2k\left(\frac{D - \alpha}{2D - \alpha}\right). \tag{4.1.16}$$

Equation (2.2.8a) and the expression (4.1.14) for η lead to the following SUSY partner potential V_2^+:

$$V_2^+(x;D,\kappa,\alpha) = D^2+\kappa^2-(D-\alpha)(D-2\alpha)\text{sech}^2(\alpha x)+2\kappa D\tanh(\alpha x). \quad (4.1.17)$$

Note that the potential V_2^- in equation (4.1.11) is related to $V_2^+(x;D,\kappa,\alpha)$ in the way

$$V_2^+(x;D+2\alpha,\frac{D\kappa}{D+2\alpha},\alpha) = V_2^-(x;D,\kappa,\alpha)+(D+2\alpha)^2+\left(\frac{D\kappa}{D+2\alpha}\right)^2-D^2-\kappa^2, \quad (4.1.18)$$

i.e., they are shape-invariant potentials. A plot of both potentials is drawn in Figure 4.4. The eigenfunctions and eigenvalues of V_2^+ turn out to be

$$\begin{aligned}\psi_n^+(\zeta) &= c_n\,(1-\zeta)^{\frac{s^+-n+a^+}{2}}\,(1+\zeta)^{\frac{s^+-n-a^+}{2}}\,\mathrm{P}_n^{(s^+-n+a^+,s^+-n-a^+)}(\zeta), \quad n=0,\dots,N-2,\\ \mathcal{E}_n^+ &= \mathcal{E}_{n+2}^- = D^2+\kappa^2-(D-n\alpha-2\alpha)^2-\frac{\kappa^2D^2}{(D-n\alpha-2\alpha)^2}, \quad n=0,\dots,N-2,\end{aligned} \quad (4.1.19)$$

with $s^+=\frac{D}{\alpha}-2$ and $a^+=\frac{D\kappa}{\alpha(D-(n+2)\alpha)}$. Thus, the discrete eigenvalues for electrons (holes) in this case are

$$E_0=E_1=0, \quad E_n=\frac{\hbar^2}{2m^*}\mathcal{E}_n^{(0)}\sqrt{1-\gamma_n},\ n=2,\dots,N, \quad (4.1.20)$$

where

$$\gamma_n=\frac{D^2+\kappa^2-(D-\alpha)^2-\frac{\kappa^2D^2}{(D-\alpha)^2}}{D^2+\kappa^2-(D-n\alpha)^2-\frac{\kappa^2D^2}{(D-n\alpha)^2}}. \quad (4.1.21)$$

The corresponding eigenfunctions are

$$\begin{aligned}\Psi_0(x,y) &= e^{iky}\begin{pmatrix}0\\ \psi_0^-(x)\end{pmatrix}, \quad \Psi_1(x,y)=e^{iky}\begin{pmatrix}0\\ \psi_1^-(x)\end{pmatrix},\\ \Psi_n(x,y) &= \frac{e^{iky}}{\sqrt{2}}\begin{pmatrix}\psi_n^+(x)\\ \psi_n^-(x)\end{pmatrix}, \quad \text{for} \quad n=2,3,\dots\end{aligned} \quad (4.1.22)$$

where ψ_n^-, ψ_n^+ are given in equations (4.1.13), (4.1.19). Once again, the ground state energy is two-fold degenerate. Let us remark that now these eigenvalues form a bounded finite discrete spectrum depending on the wavenumber k, as can be seen in Figure 4.5. For these energies an enveloping quadratic curve ak^2+bk+c can be found, whose first derivative is proportional to the group velocity in y-direction and the second derivative is a constant related to the component $[M_{inert}]_{2,2}$ of the effective mass tensor [12], i.e.,

$$[M_{inert}]_{2,2}=\frac{m^*}{a}, \quad v_g=v^2\left(\frac{\hbar}{\gamma_1}\right)(2ak+b). \quad (4.1.23)$$

For this specific example we have that $a=4D(D-\alpha)/(2D-\alpha)^2$, $b=2\alpha-4D^2/(2D-\alpha)$ and $c=D(D-\alpha)$. Finally, in Figure 4.6 the probability density and probability current in y-direction are sketched.

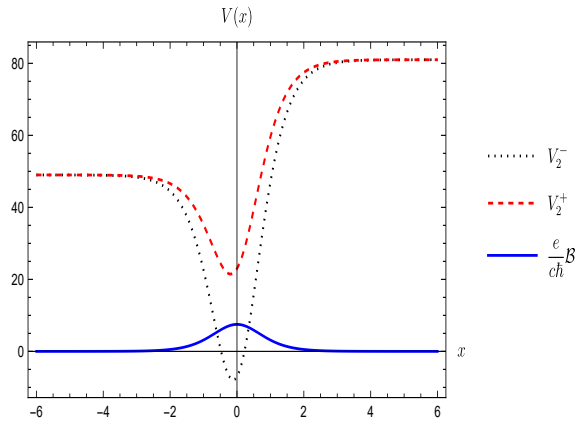

Figure 4.4: Plot of the Rosen-Morse II potential V_2^- (black), its shape-invariant SUSY partner V_2^+ (red) and the hyperbolic magnetic field (blue). The parameters were taken as $D = 8$, $\kappa = 1$ and $\alpha = 1$.

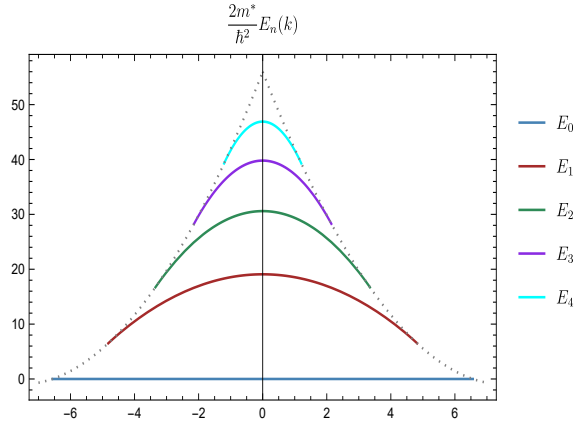

Figure 4.5: Plot of some eigenvalues E_n as functions of the wavenumber k for the hyperbolic magnetic field with $D = 8$ and $\alpha = 1$.

SECTION 4.2

Rational extensions

The SUSY partner potential V_2^+ is said to be a rational extension of V_2^- if it can be decomposed in two terms: one is the initial potential with modified parameters (a shape-invariant part) and the other is a rational function of another variable which depends on the original one. If $V_2^- = V_2^-(x;\lambda_0)$ then its rational extension takes the form:

$$V_2^+(x;\lambda_0) = V_2^-(x;\lambda_1) + \frac{P(\zeta)}{Q(\zeta)}, \tag{4.2.1}$$

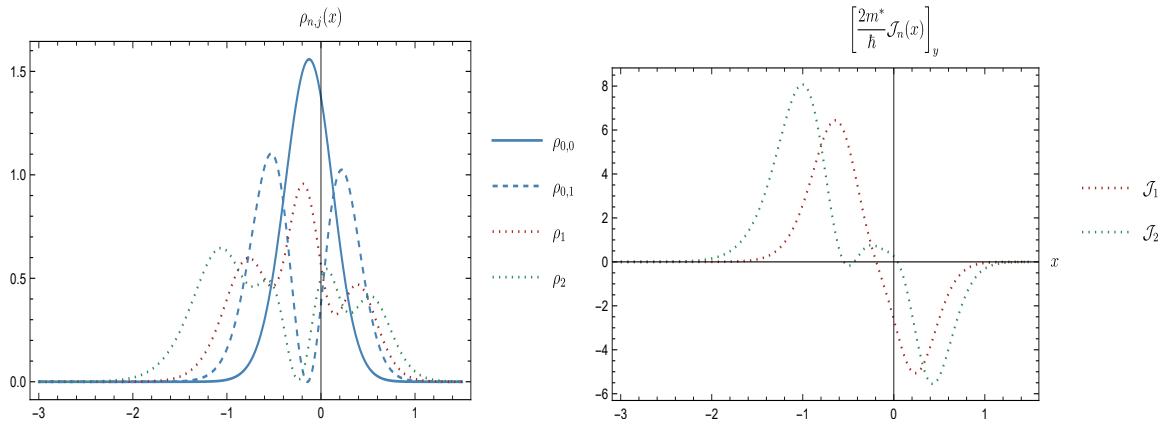

(a) (b)

Figure 4.6: Plot of some probability densities (a) and the y-component currents (b) for the hyperbolic magnetic field with $D = 8$, $k = 15/14$ and $\alpha = 1$.

where λ_0 represents the set of parameters of V_2^-, λ_1 denotes a new set which depends on λ_0, ζ is a function of x, and Q, P are polynomials [70–73]. In order to achieve this kind of potentials in a second-order SUSY transformation, we need to choose $\epsilon_2 = \mathcal{E}_j^-$ and $\epsilon_1 = \mathcal{E}_{j+1}^-$. Notice that by taking $j = 0$ (shape-invariant case) ones arrives to a trivial rational extension, therefore in the following examples we will consider $j = 1$.

SUBSECTION 4.2.1

Shifted harmonic oscillator potential

Let us start by taking V_2^- as the shifted harmonic oscillator of equation (4.1.2). According to our choice of factorization energies, the seed solutions ψ_1^- and ψ_2^- are given by equation (4.1.3) with $n = 1$ and $n = 2$. By using them to calculate η it is straightforward to find that

$$V_2^+(x) = V_2^-(x) + 2\omega\frac{4\zeta^4 + 8\zeta^2 - 1}{\left(1 + 2\zeta^2\right)^2}, \tag{4.2.2a}$$

$$\mathcal{B}(x) = \mathcal{B}_{SI}\left[1 + \frac{4\zeta^2 - 2}{\left(1 + 2\zeta^2\right)^2}\right], \tag{4.2.2b}$$

where $\zeta = \sqrt{\omega/2}(x + 2\kappa/\omega)$ and $\mathcal{B}_{SI} = c\hbar\omega/2e$ is the constant magnetic field of the shape-invariant case. Thus, we conclude that V_2^+ represents a rational extension of V_2^-. Both potentials have been plotted in Figure 4.7. Note that, in contrast with the shape-invariant case, the magnetic field now is non-constant, although asymptotically it is, which can be seen in Figure 4.8. In this case the relationship between the parameter κ and the wavenumber is k is simply $k = \kappa$.

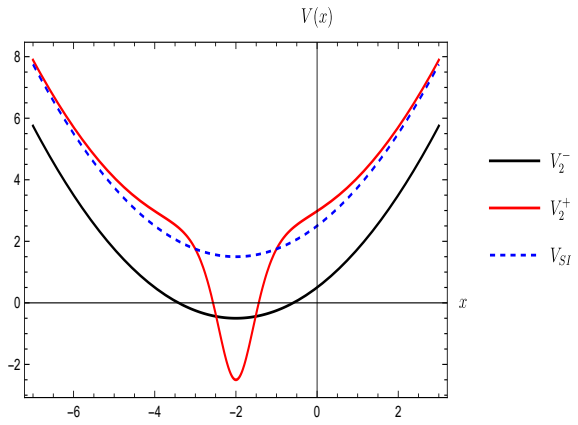

Figure 4.7: Plot of the shifted harmonic oscillator V_2^- and its rational extension V_2^+ for $\omega = \kappa = 1$.

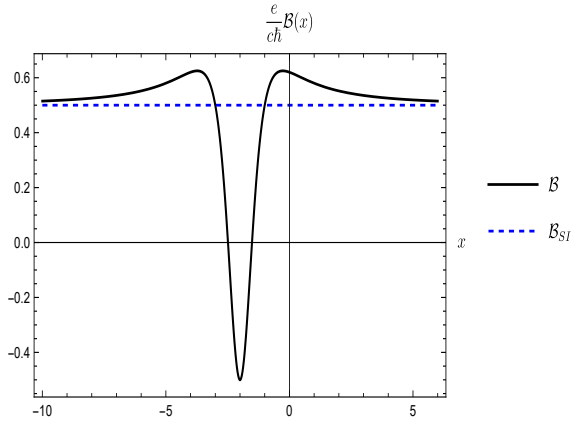

Figure 4.8: Plot of the magnetic field for the rational extension of the shifted harmonic oscillator (black line) and for the shape-invariant case (blue-dashed line). The parameters were taken as $\kappa = \omega = 1$.

On the other hand, the electron (hole) energies for bilayer graphene in the external magnetic field (4.2.2b) are

$$E_n = \pm\frac{\hbar^2}{2m^*}\sqrt{(n-1)(n-2)}, \quad \text{for} \quad n = 0, \dots \tag{4.2.3}$$

while the corresponding eigenfunctions are

$$\Psi_1(x,y) = e^{iky}\begin{pmatrix} 0 \\ \psi_1^-(x) \end{pmatrix}, \quad \Psi_2(x,y) = e^{iky}\begin{pmatrix} 0 \\ \psi_2^-(x) \end{pmatrix},$$
$$\Psi_n(x,y) = \frac{e^{iky}}{\sqrt{2}}\begin{pmatrix} \psi_n^+(x) \\ \psi_n^-(x) \end{pmatrix}, \quad \text{for} \quad n = 0, 3, 4, \dots \tag{4.2.4}$$

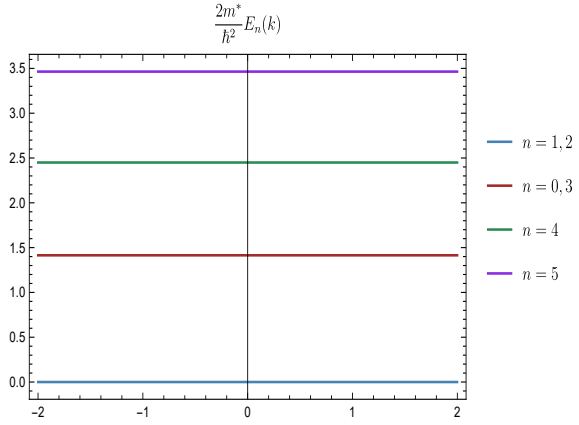

Figure 4.9: Plot of some energies for electrons (holes) in bilayer graphene under the magnetic field (4.2.2b). The parameters were taken as $\kappa = \omega = 1$.

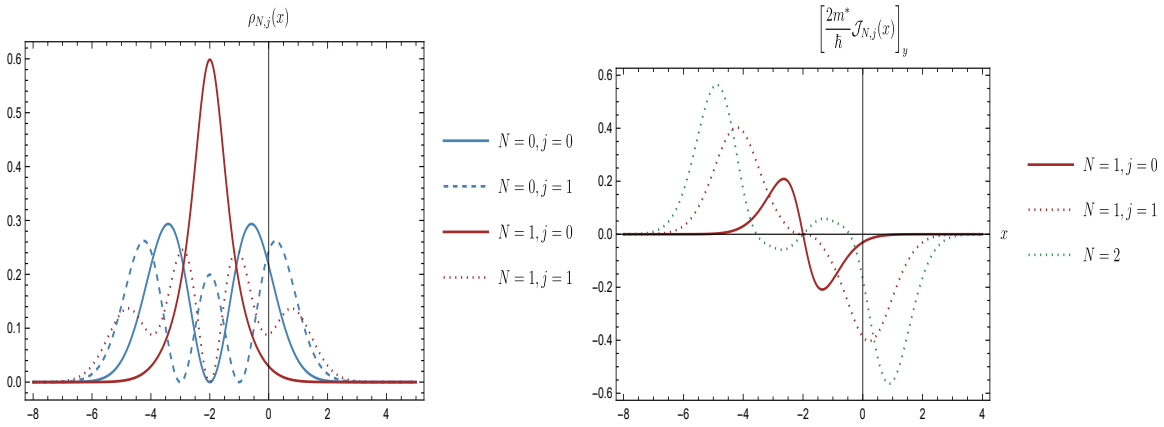

(a) (b)

Figure 4.10: Plot of some probability (a) and current densities in y-direction (b) for the rational extension of the shifted harmonic oscillator. The parameters were taken as $\kappa = \omega = 1$.

where ψ_n^+ are determined from equation (2.2.30). Note that now the index n does not supply the standard ordering for the energies (4.2.3) of the electron (hole). On the other hand, as in the shape-invariant case, the energies do not depend on k (see Figure 4.9), but now they have a different behavior since there is a double degeneracy for the first excited state ($n = 0$, $n = 3$) in addition to the two-fold degeneracy for the ground state ($n = 1$, $n = 2$). Although $j = 1$ has been chosen to exemplify this type of potentials, we can ensure that if j is an arbitrary non-negative integer, the number of doubly degenerate eigenvalues will be $j+1$, which correspond to the pairs of eigenstates $\{(\Psi_j, \Psi_{j+1}), (\Psi_{j-1}, \Psi_{j+2}), ..., (\Psi_0, \Psi_{2j+1})\}$, the first pair is associated with

the ground state energy, the second one to the first excited state energy and so on [13]. Finally, some probability and current densities are plotted in Figure 4.10.

SUBSECTION 4.2.2

Hyperbolic Rosen-Morse potential

As a second example let us consider the hyperbolic Rosen-Morse potential V_2^- of equation (4.1.11). The seed solutions ψ_1^-, ψ_2^- are given in equation (4.1.13) for $n = 1, 2$ (with the square integrability conditions described there). Then, we get

$$V_2^+(x) = V_2^-\left(x; D-2\alpha, \frac{\kappa D}{D-2\alpha}\right) + (1-\zeta^2)\Bigg\{\left(4\alpha D - 2\alpha^2\right) + \alpha^2\left[(D-2\alpha)^2 - \kappa^2\right]$$
$$\times \frac{2(\kappa + D\zeta)^2 - (D + 6\kappa\zeta + 5D\zeta^2)\alpha + (1+3\zeta^2)\alpha^2}{(2\kappa^2 + (D-2\alpha)((2D-3\alpha)\zeta^2 + \alpha) + \kappa(4D-6\alpha)\zeta)^2}\Bigg\}, \tag{4.2.5a}$$

$$\mathcal{B}(x) = \mathcal{B}_{SI}\left[1 + \frac{4\alpha\left[(D-2\alpha)^2 - \kappa^2\right]\left[2(D\zeta+\kappa)^2 - (5D\zeta^2 + 6\kappa\zeta + D)\alpha + (3\zeta^2+1)\alpha^2\right]}{(2D-\alpha)\left[2\kappa^2 + (D-2\alpha)\left(\zeta^2(2D-3\alpha) + \alpha\right) + 2\kappa\zeta(2D-3\alpha)\right]^2}\right], \tag{4.2.5b}$$

where $\zeta = \tanh(\alpha x)$ and $\mathcal{B}_{SI} = \frac{c\hbar\alpha}{2e}(2D-\alpha)(1-\zeta^2)$ is the magnetic field (4.1.15) of the shape-invariant case. From equation (4.2.5a) it follows that V_2^+ is a rational extension of V_2^-. In Figure 4.11 a plot of these potentials is shown. Note that the magnetic field (4.2.5b) is also a rational extension of the field (4.1.15) of the shape-invariant case, which can be seen in Figure 4.12. In this case the relationship between the wavenumber k and the parameter κ is not lineal, since now

$$k = \frac{(2D-3\alpha)\left[D\kappa^3 + \kappa(D^3 - 5\alpha D^2 + 8\alpha^2 D - 4\alpha^3)\right]}{2(D-2\alpha)(D-\alpha)\left[\kappa^2 + (D^2 - 3\alpha D + 2\alpha^2)\right]}. \tag{4.2.6}$$

This expression can be seen in the plot of Figure 4.13. The energies for the electron (hole) in bilayer graphene under the external magnetic field (4.2.5b) are given by $E_n = \pm\frac{\hbar^2}{2m^*}\sqrt{\Delta_{n,1}\Delta_{n,2}}$, where

$$\Delta_{n,1} = D^2\kappa^2\left(\frac{1}{(D-\alpha)^2} - \frac{1}{(D-\alpha n)^2}\right) + \alpha(n-1)[2D - \alpha(n+1)], \tag{4.2.7}$$

$$\Delta_{n,2} = D^2\kappa^2\left(\frac{1}{(D-2\alpha)^2} - \frac{1}{(D-\alpha n)^2}\right) + \alpha(n-2)[2D - \alpha(n+2)]. \tag{4.2.8}$$

Note that, due to equations (4.2.6), (4.2.7), (4.2.8), these energies are functions of the wavenumber k, which can be seen in Figure 4.14. The corresponding eigenfunctions are constructed as indicated in equation (4.2.4). It is important to stress that the standard ordering for E_n and the possible degeneracies will depend on the election of the parameters D, α and k (see Figure 4.14). We are showing as well the probability and $y-$component current density in Figure 4.15 for a fixed value of k, in order to identify the standard ordering for the non-degenerate excited state levels [13].

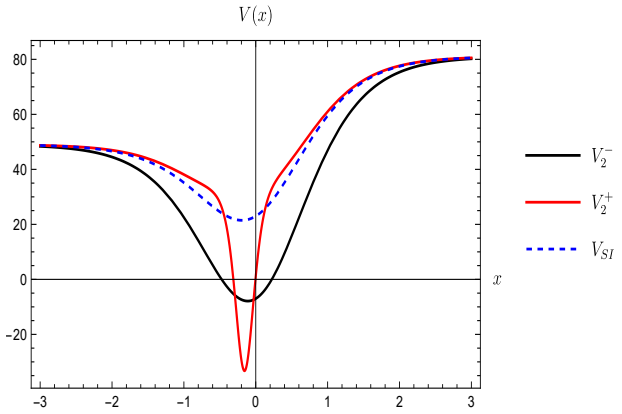

Figure 4.11: Plot of the hyperbolic Rosen-Morse potential V_2^- and its rational extension V_2^+ for $D = 8$, $\kappa = \alpha = 1$.

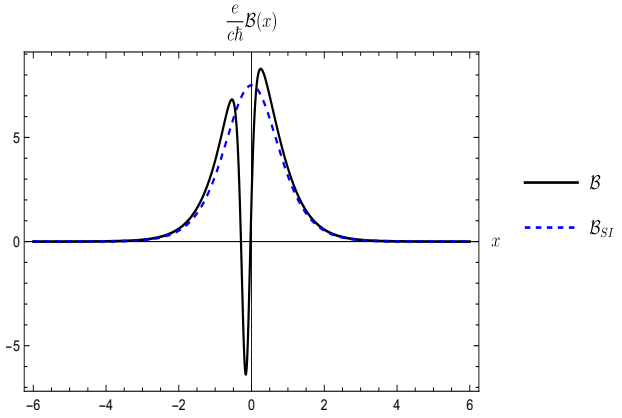

Figure 4.12: Plot of the magnetic field for the rational extension of the hyperbolic Rosen-Morse potential (black line) and for the shape-invariant case (blue-dashed line). The parameters were taken as $D = 8$, $\kappa = \alpha = 1$.

SECTION 4.3

The confluent algorithm

Finally, the confluent algorithm discussed in chapter 2 consists of a transformation whose key peculiarity is that the factorization energies are equal, $\epsilon_1 = \epsilon_2 = \epsilon$. In addition, it turns out that the η function depends on a free parameter w_0 (see equation (2.2.34)), in the same way as the magnetic field does. In this case it is convenient to express V_2^+ as follows

$$V_2^+(x;\mathrm{w}_0) = V_2^-(x) + \frac{4e}{c\hbar}\mathcal{B}(x;\mathrm{w}_0). \tag{4.3.1}$$

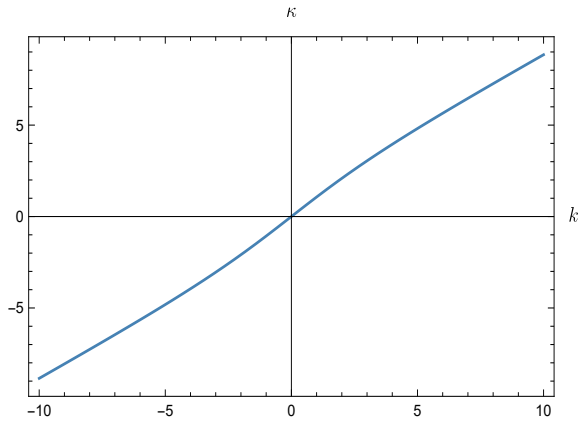

Figure 4.13: Plot of k versus κ for the rational extension of the hyperbolic Rosen-Morse potential with $D = 8$, $\alpha = 1$.

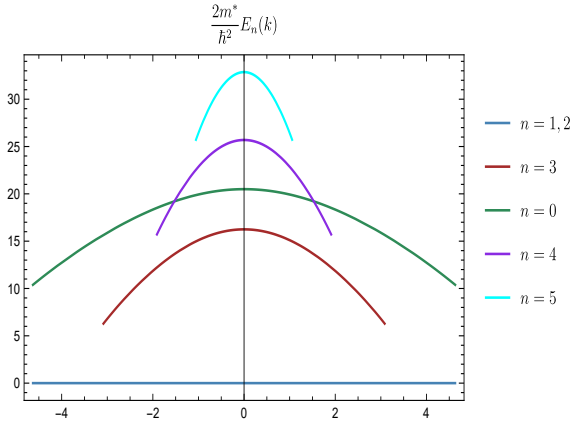

Figure 4.14: Plot of some energies for electrons (holes) in bilayer graphene under the magnetic field (4.2.5b). The parameters were taken as $D = 8$ $\kappa = \alpha = 1$.

The spectra of V_2^- and V_2^+ could be the same, or differ by the factorization energy ϵ in the limit case of the confluent algorithm. On the other hand, for the electron (hole) the energies are given by

$$E_n = \pm \frac{\hbar^2}{2m^*} |\mathcal{E}_n^- - \epsilon|, \tag{4.3.2}$$

whose eigenfunctions are

$$\Psi_n(x, y) = \frac{e^{iky}}{\sqrt{2}} \begin{pmatrix} \psi_n^+(x) \\ \psi_n^-(x) \end{pmatrix}, \qquad \text{for } n = 0, 1, \ldots \tag{4.3.3}$$

where ψ_n^+ are given by equations (2.2.37) and (2.2.38). In the limit case we will take $\psi_0^+ = 0$ and will drop the factor $1/\sqrt{2}$ in Ψ_0. In the next examples we will illustrate the confluent algorithm by taking $\epsilon = \mathcal{E}_0^-$.

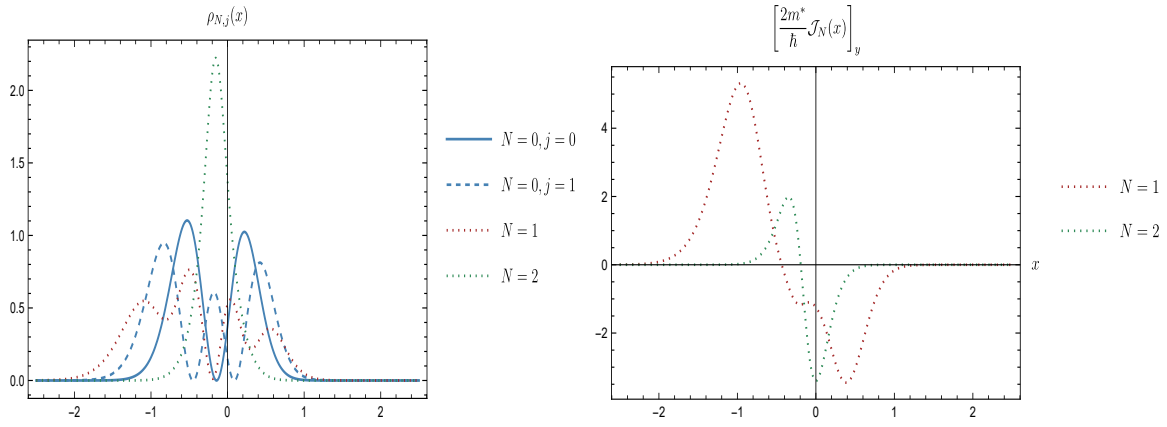

Figure 4.15: Plot of some probability (a) and current densities in y-direction (b) for the rational extension of the hyperbolic Rosen-Morse potential. The parameters were taken as $D = 8$, $\kappa = \alpha = 1$.

SUBSECTION 4.3.1

Shifted harmonic oscillator potential

If we consider V_2^- as the shifted harmonic oscillator of equation (4.1.2), the seed solution ψ_0^- is given by equation (4.1.3) with $n = 0$, which is used to find η and thus it is straightforward to see that

$$\mathcal{B}(x; \mathrm{w}_0) = \frac{c\hbar\omega}{e}\left\{\frac{e^{-2\zeta^2}}{\pi\left[\mathrm{erfc}\left(\zeta\right) - 2 + 2\mathrm{w}_0\right]^2} - \frac{\zeta e^{-\zeta^2}}{\sqrt{\pi}\left[\mathrm{erfc}\left(\zeta\right) - 2 + 2\mathrm{w}_0\right]}\right\}, \tag{4.3.4}$$

where $\mathrm{erfc}(x)$ is the complementary error function. In Figure 4.16 we can see the SUSY partner potentials V_2^-, $V_2^+(x;-1)$, and $V_2^+(x;0)$ (limit case). The associated magnetic fields are shown in Figure 4.17.

From equation (A.6), the parameter κ and the wavenumber k turn out to be independent to each other (see Figure 4.18). Thus, the energy eigenvalues for electrons (holes) in bilayer graphene under the magnetic field (4.3.4) do not depend on k, neither the magnetic field does (see Figure 4.19). Thus, the energies are given by

$$E_n = \frac{\hbar^2\omega}{2m^*}n, \qquad n = 0, 1, \ldots \tag{4.3.5}$$

An interesting fact about these eigenvalues is that they are equidistant. Moreover, since $j = 0$ all of them are non-degenerate. However, if we would take $j \geq 1$, despite the spectrum would remain equidistant the first j excited state energies would be two-fold degenerate [13]. Finally, the probability and the $y-$component current density are

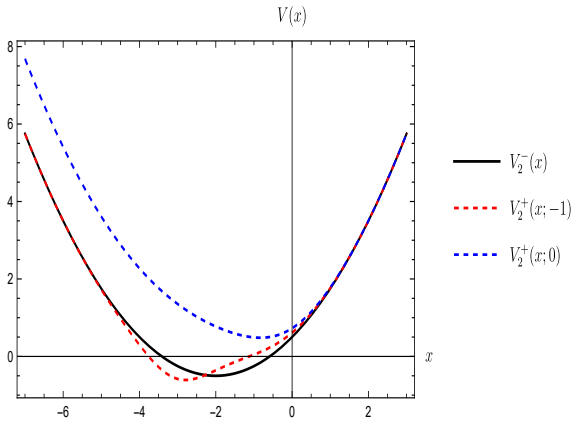

Figure 4.16: Plot of the shifted harmonic oscillator V_2^- and its confluent SUSY partners $V_2^+(x;-1)$ (isospectral case) and $V_2^+(x;0)$ (limit case). The parameters were taken as $\kappa = \omega = 1$.

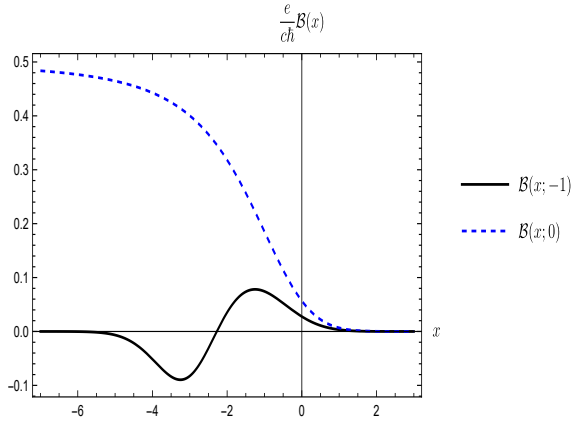

Figure 4.17: Plot of the magnetic fields in the limit case $\mathcal{B}(x;0)$ and the isospectral case $\mathcal{B}(x;-1)$ for the confluent algorithm applied to the shifted harmonic oscillator. The parameters were taken as $\kappa = \omega = 1$.

plotted in Figure 4.20. Once again, these quantities do not depend explicitly on the wavenumber k.

SUBSECTION 4.3.2

Hyperbolic Rosen-Morse potential

Finally, let us consider the hyperbolic Rosen-Morse potential V_2^- of equation (4.1.11) [74]. If we choose as seed solution the ground state ψ_0^- of equation (4.1.13) for $n = 0$,

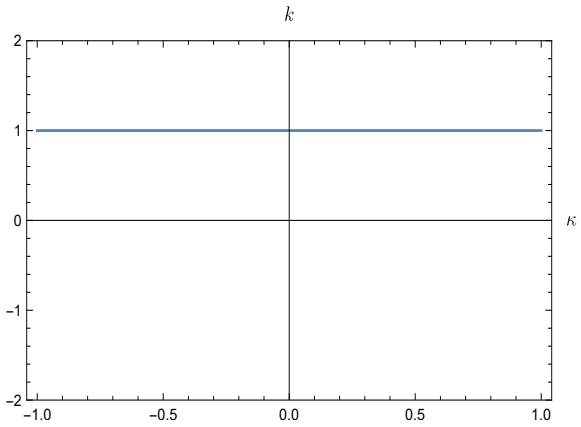

Figure 4.18: Plot of k versus κ for the confluent algorithm applied to the shifted harmonic oscillator with $\omega = 1$.

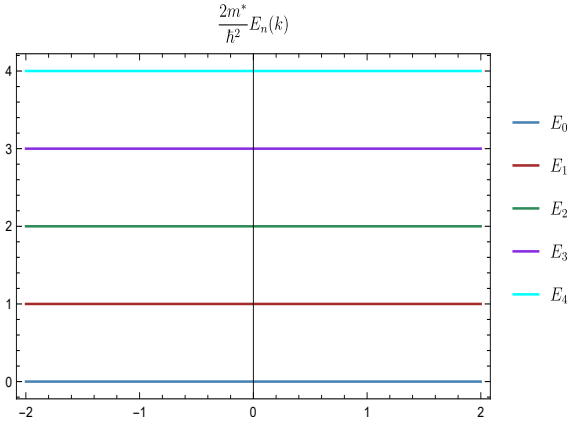

Figure 4.19: Plot of some energies for electrons (holes) in bilayer graphene under the magnetic field (4.3.4). The parameters were taken as $\kappa = \omega = 1$.

after some calculations the magnetic field turns out to be

$$\mathcal{B}(x;\mathrm{w}_0) = \frac{c\hbar}{e}\alpha^2 pq(1-\zeta)^p(1+\zeta)^q\Bigg\{q(1-\zeta)^p(1+\zeta)^q + (\mathrm{w}_0-1)(p+q) - 2^{p+q}\Bigg[pq(1-2\mathrm{w}_0)\mathrm{B}(q,p)$$
$$+ (p+q)\Bigg(q\mathrm{B}\left(\frac{\zeta+1}{2};q,p+1\right) + (\mathrm{w}_0-1)\left(p\mathrm{B}\left(\frac{1}{2};p,q+1\right) + q\mathrm{B}\left(\frac{1}{2};q,p+1\right)\right)\Bigg)\Bigg]\Bigg\}^{-2}\Bigg\{(p+q)$$
$$\times\Big(q(1-\zeta)^{1+p}(1+\zeta)^q - (p-q+(p+q)\zeta)(-1+\mathrm{w}_0)\Big) + 2^{p+q}\big(p-q+(p+q)\zeta\big)\Bigg[pq(1-2\mathrm{w}_0)\mathrm{B}(q,p)$$
$$+ (p+q)\left((-1+\mathrm{w}_0)\left(p\mathrm{B}\left(\frac{1}{2};p,1+q\right) + q\mathrm{B}\left(\frac{1}{2};q,1+p\right)\right) + q\mathrm{B}\left(\frac{1+\zeta}{2};q,1+p\right)\right)\Bigg]\Bigg\}, \tag{4.3.6}$$

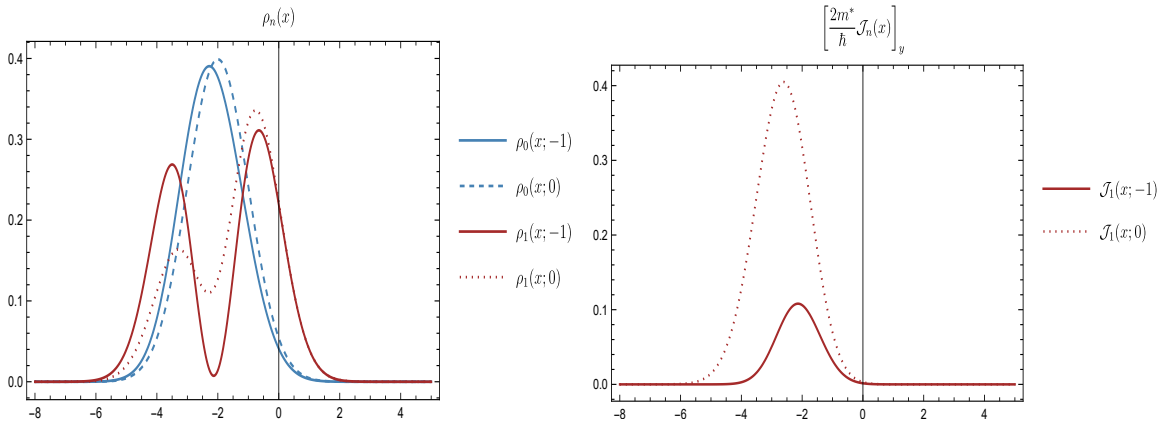

(a) (b)

Figure 4.20: Plot of some probability (a) and currents densities in y-direction (b) for the confluent algorithm applied to the shifted harmonic oscillator. The parameters were taken as $\kappa = \omega = 1$.

where $\zeta = \tanh(\alpha x)$, $s = \frac{D}{\alpha}$, $p = s + \frac{\kappa}{\alpha D}$, $q = s - \frac{\kappa}{\alpha D}$ and $\mathrm{B}(x; a, b)$ is the incomplete beta function. Plots of such magnetic fields for the limit case and the isospectral one are shown in Figure 4.21, the corresponding SUSY partner potentials arise in Figure 4.22.

As in the previous case, k and κ are independent to each other but now k depends on w_0 (see Figure 4.23). The energies for the electron in bilayer graphene under these magnetic fields become

$$E_n = \frac{\hbar^2}{2m^*}\left[D^2 + \kappa^2 - (D - n\alpha)^2 - \frac{\kappa^2 D^2}{(D - n\alpha)^2}\right], \quad n = 0, 1, \ldots, N. \tag{4.3.7}$$

Once again, all these eigenvalues are non-degenerate, proportional to the auxiliary energies of equation (4.1.12), and the index n supplies the standard ordering for this set. Such electron energies do not depend on k (see Figure 4.24), but they are still functions on κ. In this case, it is non-trivial to calculate $k(\kappa)$ for arbitrary values of D and α. However, for $D = 8$ and $\alpha = 1$ we have found that $k = 15/(4\mathrm{w}_0 - 2)$ [13]. Finally, the probability and $y-$direction current densities are drawn in Figure 4.25.

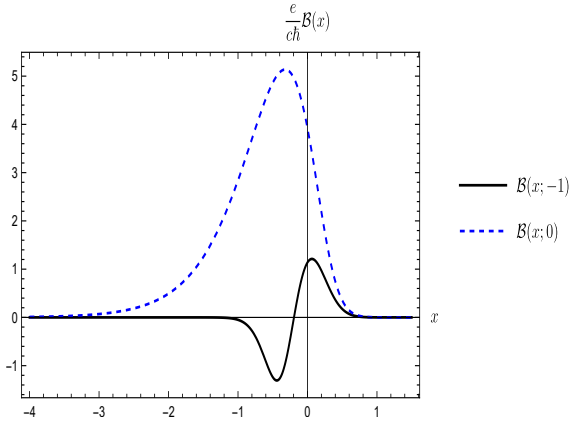

Figure 4.21: Plot of the magnetic field in the limit case $\mathcal{B}(x;0)$ and in the isospectral case $\mathcal{B}(x;-1)$ for the confluent algorithm applied to the hyperbolic Rosen-Morse potential. The parameters were taken as $D=8$, $\kappa=\alpha=1$.

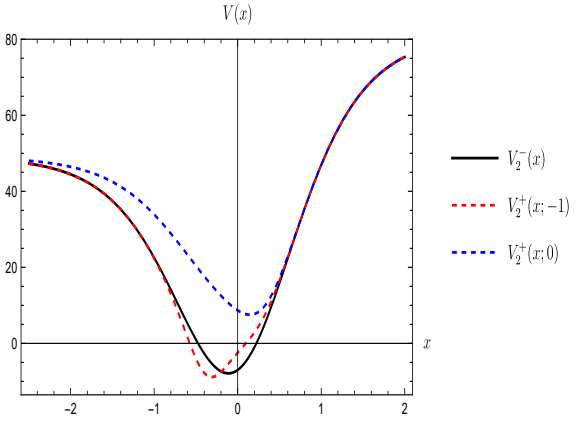

Figure 4.22: Plot of the hyperbolic Rosen-Morse potential V_2^- and its confluent SUSY partners $V_2^+(x;-1)$ (isospectral case) and $V_2^+(x;0)$ (limit case). The parameters were taken as $D=8$, $\kappa=\alpha=1$.

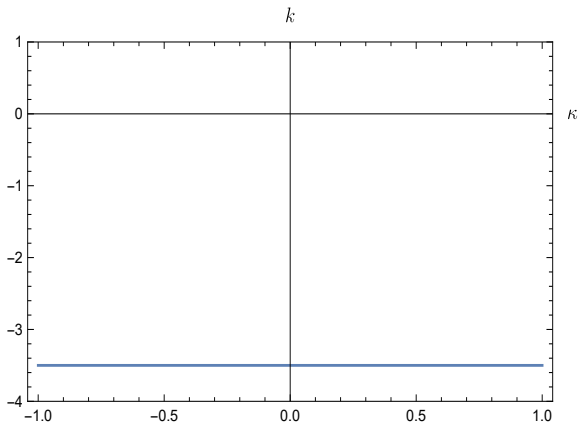

Figure 4.23: Plot of k versus κ for the confluent algorithm applied to the hyperbolic Rosen-Morse potential with $D = 8$, $\alpha = 1$ and $\mathrm{w}_0 = 0$

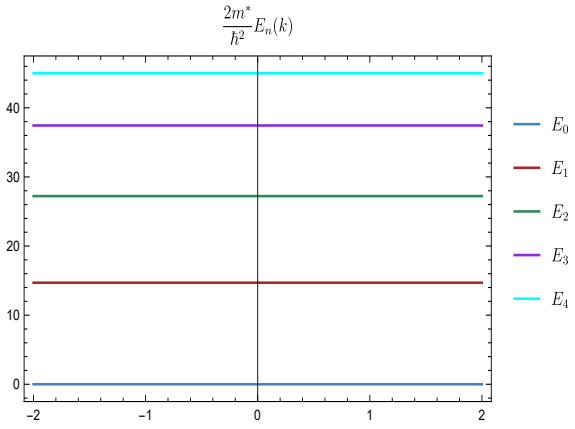

Figure 4.24: Plot of some energies for electrons (holes) in bilayer graphene under the magnetic field (4.3.6). The parameters were taken as $D = 8$, $\kappa = \alpha = 1$.

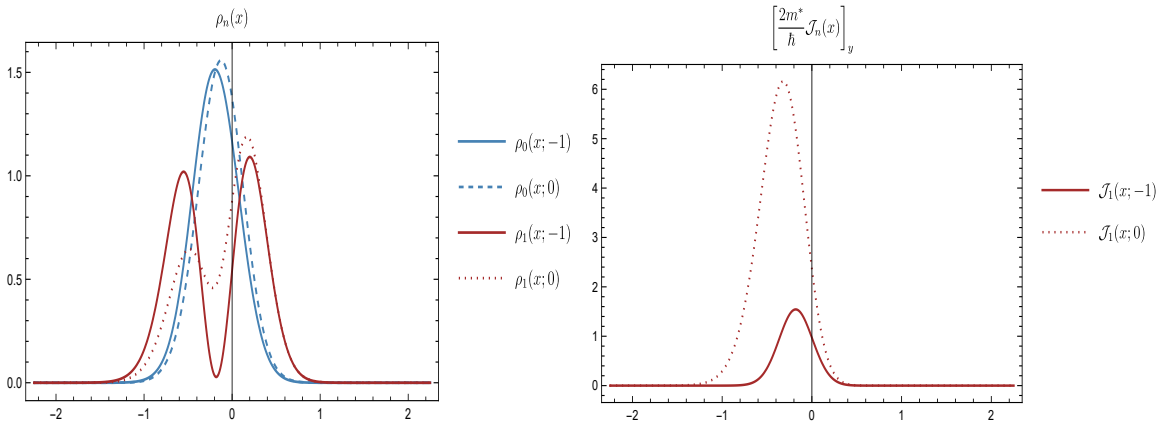

(a) (b)

Figure 4.25: Plot of some probability (a) and currents densities in y-direction (b) for the confluent algorithm applied to the hyperbolic Rosen-Morse potential. The parameters were taken as $D = 8$, $\kappa = \alpha = 1$.

CHAPTER 5

Graphene generalized coherent states

The subjecto of coherent states, associated initially with the harmonic oscillator, is widely known. These states fulfill mutually equivalent properties/definitions. Thus, they are known as canonical coherent states (CCS). However, trying to extend the concept of CS to another systems does not seem trivial. The coherent states have been generalized by different authors, departing from some of the CCS properties and using them as CS definitions, but each of them leads to sets of states that in general are non-equivalent. Next let us describe these definitions of generalized coherent states.

- Generalized coherent states as eigenstates of the annihilation operator. This definition was promoted initially by Barut and Girardello [75]. To construct these states it is necessary to find an annihilation operator acting appropriately on the eigenstates of the system Hamiltonian. However, for systems described by finite-dimensional Hilbert spaces the CS family becomes trivial (composed by a finite set of states).

- Generalized coherent states obtained from a displacement operator. For an arbitrary system with defined ladder operators, the coherent states can be obtained as the result of acting a generalized displacement operator onto an extremal state (an eigenstate of the Hamiltonian which is annihilated by the annihilation operator). This generalization was originally introduced by Gilmore and Perelomov [76–78].

- Generalized coherent states as minimum uncertainty states. The coherent states minimize the uncertainty relation for the quadratures. This generalization was pushed forward by Aragone, Nieto and Simmons, and it was the original approach used by Schrödinger [79–83]. To build these states it is also necessary to have the ladder operators. However, in the most general context this definition includes as well the so-called squeezed coherent states, thus it is required to add an extra condition in order to recover the harmonic oscillator CCS.

SECTION 5.1

Ladder operators

For each one of the two graphene systems previously discussed we will determine appropriate ladder operators. Let us start by assuming that we know proper annihilation and creation operators $\{\Theta^-, \Theta^+\}$ for the ψ_n^- of equations (3.1.23, 3.2.16), such that

$$\begin{aligned} \Theta^- \psi_n^- &= \sqrt{p_n}\psi_{n-1}^-, \\ \Theta^+ \psi_n^- &= \sqrt{q_n}\psi_{n+1}^-, \end{aligned} \tag{5.1.1a}$$

where $\Theta^+ \equiv (\Theta^-)^\dagger$ and the generalized number operator is defined by $N \equiv \Theta^+\Theta^-$. We also assume that these operators supply a global ladder relationship, i.e., the ground state is the only one annihilated by Θ^- and $q_n \neq 0 \; \forall \; n$. Note that, in general, Θ^-, Θ^+ are not ladder operators for ψ_n^+.

SUBSECTION 5.1.1

Ladder operators for monolayer graphene

By taking advantage of the intertwining operators $\mathcal{L}_1^\pm$, let us introduce an annihilation operator for the monolayer graphene eigenfunctions (3.1.23) in a way similar to the proposal made in [22, 23, 25, 26, 54] as follows

$$A_{\mathcal{M}}^- = \begin{pmatrix} \mathcal{L}_1^- \frac{1}{\sqrt{H_1^-}} \Theta^- \frac{f_1(H_1^-)}{\sqrt{H_1^-}} \mathcal{L}_1^+ & -i\mathcal{L}_1^- \frac{1}{\sqrt{H_1^-}} \Theta^- f_1(H_1^-) \\ i\Theta^- \frac{f_1(H_1^-)}{\sqrt{H_1^-}} \mathcal{L}_1^+ & \Theta^- f_1(H_1^-) \end{pmatrix}, \tag{5.1.2}$$

where f_1 is an auxiliary real function. Then, the action of $A_{\mathcal{M}}^-$ onto Ψ_n turns out to be

$$A_{\mathcal{M}}^- \Psi_n(x,y) = 2\sqrt{p_n} f_1(\mathcal{E}_n^-) \Psi_{n-1}(x,y) \times \begin{cases} 0 & \text{for} \quad n = 0, \\ \frac{1}{\sqrt{2}} & \text{for} \quad n = 1, \\ 1 & \text{for} \quad n \geq 2. \end{cases} \tag{5.1.3}$$

The associated creation operator $A_{\mathcal{M}}^+ \equiv \left(A_{\mathcal{M}}^-\right)^\dagger$ is given by

$$A_{\mathcal{M}}^+ = \begin{pmatrix} \mathcal{L}_1^- \frac{f_1(H_1^-)}{\sqrt{H_1^-}} \Theta^+ \frac{1}{\sqrt{H_1^-}} \mathcal{L}_1^+ & -i\mathcal{L}_1^- \frac{f_1(H_1^-)}{\sqrt{H_1^-}} \Theta^+ \\ i f_1(H_1^-) \Theta^+ \frac{1}{\sqrt{H_1^-}} \mathcal{L}_1^+ & f_1(H_1^-) \Theta^+ \end{pmatrix}, \tag{5.1.4}$$

whose action onto Ψ_n becomes

$$A^+_{\mathcal{M}}\Psi_n(x,y) = 2\sqrt{q_n}f_1(\mathcal{E}^-_{n+1})\Psi_{n+1}(x,y) \times \begin{cases} \frac{1}{\sqrt{2}} & \text{for} \quad n=0, \\ \\ 1 & \text{for} \quad n \geq 1. \end{cases} \tag{5.1.5}$$

This equation allows us to construct the n-th eigenstate through the successive application of $A^+_{\mathcal{M}}$ over Ψ_0, as long as $f_1(\mathcal{E}^-_m) \neq 0$ for $m \in [1,n]$.

SUBSECTION 5.1.2

Ladder operators for bilayer graphene

Since different choices of factorization energies and associated seed solutions lead us to different eigenfunctions of the Hamiltonian $\mathcal{H}_{\mathfrak{B}}$, from now on we will always consider that $\epsilon_2 = \mathcal{E}^-_0$ and $\epsilon_1 = \mathcal{E}^-_1$. However, some minor changes would allow us to address the case for arbitrary factorization energies.

Let us introduce now the following annihilation operator

$$A^-_{\mathfrak{B}} = \begin{pmatrix} \mathcal{L}^-_2 \frac{1}{\sqrt{(H^-_2-\mathcal{E}^-_0)(H^-_2-\mathcal{E}^-_1)}}\Theta^- \frac{f_2(H^-_2)}{\sqrt{(H^-_2-\mathcal{E}^-_0)(H^-_2-\mathcal{E}^-_1)}}\mathcal{L}^+_2 & \mathcal{L}^-_2 \frac{1}{\sqrt{(H^-_2-\mathcal{E}^-_0)(H^-_2-\mathcal{E}^-_1)}}\Theta^- f_2(H^-_2) \\ \\ \Theta^- \frac{f_2(H^-_2)}{\sqrt{(H^-_2-\mathcal{E}^-_0)(H^-_2-\mathcal{E}^-_1)}}\mathcal{L}^+_2 & \Theta^- f_2(H^-_2) \end{pmatrix}, \tag{5.1.6}$$

where f_2 is a real function.Then, the action of $A^-_{\mathfrak{B}}$ over the eigenstates (3.2.16) is ruled by

$$A^-_{\mathfrak{B}}\Psi_n(x,y) = 2\sqrt{p_n}f_2(\mathcal{E}^-_n)\Psi_{n-1}(x,y) \times \begin{cases} 0 & \text{for} \quad n=0, \\ \\ \frac{1}{2} & \text{for} \quad n=1, \\ \\ \frac{1}{\sqrt{2}} & \text{for} \quad n=2, \\ \\ 1 & \text{for} \quad n \geq 3. \end{cases} \tag{5.1.7}$$

The corresponding creation operator $A^+_{\mathfrak{B}} \equiv \left(A^-_{\mathcal{B}}\right)^\dagger$ reads

$$A^+_{\mathfrak{B}} = \begin{pmatrix} \mathcal{L}^-_2 \frac{f_2(H^-_2)}{\sqrt{(H^-_2-\mathcal{E}^-_0)(H^-_2-\mathcal{E}^-_1)}}\Theta^+ \frac{1}{\sqrt{(H^-_2-\mathcal{E}^-_0)(H^-_2-\mathcal{E}^-_1)}}\mathcal{L}^+_2 & \mathcal{L}^-_2 \frac{f_2(H^-_2)}{\sqrt{(H^-_2-\mathcal{E}^-_0)(H^-_2-\mathcal{E}^-_1)}}\Theta^+ \\ \\ f_2(H^-_2)\Theta^+ \frac{1}{\sqrt{(H^-_2-\mathcal{E}^-_0)(H^-_2-\mathcal{E}^-_1)}}\mathcal{L}^+_2 & f_2(H^-_2)\Theta^+ \end{pmatrix}, \tag{5.1.8}$$

which is such that

$$A^{+}_{\mathfrak{B}}\Psi_n(x,y) = 2\sqrt{q_n}f_2(\mathcal{E}^{-}_{n+1})\Psi_{n+1}(x,y) \times \begin{cases} \frac{1}{2} & \text{for} \quad n=0, \\ \frac{1}{\sqrt{2}} & \text{for} \quad n=1, \\ 1 & \text{for} \quad n \geq 2. \end{cases} \tag{5.1.9}$$

Once again, we are able to construct the n-th eigenstate Ψ_n through the repeated action of $A^{+}_{\mathcal{B}}$ over Ψ_0, as long as $f_2(\mathcal{E}^{-}_{m}) \neq 0$ for $m \in [1,n]$.

SUBSECTION 5.1.3

Algebraic equality between the ladder operators

In order to work with both graphene cases simultaneously, let us suppose that the functions f_1 and f_2 introduced in equations (5.1.2), (5.1.6) are given by

$$f_1(\mathcal{E}^{-}_{n}) = f(n) \times \begin{cases} \frac{1}{\sqrt{2}} & \text{for} \quad n=1, \\ \frac{1}{2} & \text{for} \quad n \geq 2, \end{cases} \tag{5.1.10}$$

and

$$f_2(\mathcal{E}^{-}_{n}) = f(n) \times \begin{cases} 1 & \text{for} \quad n=1, \\ \frac{1}{\sqrt{2}} & \text{for} \quad n=2, \\ \frac{1}{2} & \text{for} \quad n \geq 3. \end{cases} \tag{5.1.11}$$

Thus, equations (5.1.3), (5.1.5), (5.1.7) and (5.1.9) can be written in the compact form

$$A^{-}_{\mathcal{G}}\Psi_n(x,y;\mathcal{G}) = \sqrt{p_n}f(n)\Psi_{n-1}(x,y;\mathcal{G}) \quad \forall\, n, \tag{5.1.12a}$$
$$A^{+}_{\mathcal{G}}\Psi_n(x,y;\mathcal{G}) = \sqrt{q_n}f(n+1)\Psi_{n+1}(x,y;\mathcal{G}) \quad \forall\, n, \tag{5.1.12b}$$

where $\mathcal{G} = \mathcal{M}, \mathfrak{B}$ and $\Psi_n(x,y;\mathcal{G})$ represents the monolayer or bilayer graphene eigenfunctions. We must emphasize that although algebraically this relation is similar for both systems, the involved eigenfunctions describe completely different physical situations. Next, we will work with the generalized coherent states, making use of the relationships (5.1.12a) and (5.1.12b).

SECTION 5.2

Barut–Girardello coherent states

The Barut-Girardello coherent states (BGCS) are defined as eigenstates of the annihilation operator [75], namely,

$$A_{\mathcal{G}}^{-}\Psi_{\alpha}^{\mathrm{BG}}(x,y;\mathcal{G}) = \alpha\Psi_{\alpha}^{\mathrm{BG}}(x,y;\mathcal{G}), \tag{5.2.1}$$

where α is a complex eigenvalue. They can be represented in the basis of Hamiltonian eigenfunctions as follows

$$\Psi_{\alpha}^{\mathrm{BG}}(x,y;\mathcal{G}) = \sum_{n=0}^{\infty} a_n \Psi_n(x,y;\mathcal{G}). \tag{5.2.2}$$

By substituting this expression into equation (5.2.1), after some algebra we get that

$$\alpha a_n = f(n+1)\sqrt{p_{n+1}}a_{n+1} \qquad \text{for} \qquad n = 0,1,... \tag{5.2.3}$$

In the previous recurrence relationship f plays an important role. In fact, two different cases appear, according to the values that $f(n)$ can take.

Case with $f(n) \neq 0$

If $f(n) \neq 0$ for $n = 1,2,...$, the recurrence relationship (5.2.3) leads to

$$a_n = \frac{\alpha^n a_0}{\sqrt{[p_n]!}\,[f(n)]!}, \tag{5.2.4}$$

where the generalized factorial function is defined by

$$[f(k)]! \equiv \begin{cases} 1 \quad \text{for} \quad k = 0, \\ \\ f(1)f(2)\cdots f(k) \quad \text{for} \quad k = 1,2,... \end{cases} \tag{5.2.5}$$

Thus, the normalized BGCS in this case turn out to be

$$\Psi_{\alpha}^{\mathrm{BG}}(x,y;\mathcal{G}) = \left[\sum_{n=0}^{\infty} \frac{|\alpha|^{2n}}{[p_n]!\,([f(n)]!)^2}\right]^{-\frac{1}{2}} \left[\sum_{n=0}^{\infty} \frac{\alpha^n}{\sqrt{[p_n]!}\,[f(n)]!}\Psi_n(x,y;\mathcal{G})\right]. \tag{5.2.6}$$

Note that although f is an arbitrary function, we must restrict ourselves to functions allowing the convergence of expression (5.2.6).

Case with $f(n) = 0$ for some n

In this case we suppose that f has roots for some $n \in \mathbb{N}$, we denote by m the maximum value of n for which there is a root, $m \geq 1$. It can be proven that it does not matter for our analysis if either there are more roots or not, equation (5.2.3) leads to

$$a_n = 0 \quad \text{for} \quad 0 \leq n \leq m-1, \tag{5.2.7a}$$

$$a_{n+1} = \frac{\alpha a_n}{\sqrt{p_{n+1}} f(n+1)} \quad \text{for} \quad n \geq m. \tag{5.2.7b}$$

Finally, the normalized BGCS become

$$\Psi_\alpha^{\mathrm{BG}}(x,y;\mathcal{G}) = \left[\sum_{n=0}^{\infty} \frac{|\alpha|^{2n}}{[\hat{p}_n]! \left(\left[\hat{f}(n)\right]!\right)^2}\right]^{-\frac{1}{2}} \left[\sum_{n=0}^{\infty} \frac{\alpha^n}{\sqrt{[\hat{p}_n]!}\left[\hat{f}(n)\right]!} \Psi_{n+m}(x,y;\mathcal{G})\right]. \tag{5.2.8}$$

Note that this linear combination starts from $\Psi_m(x,y;\mathcal{G})$ and the coefficients in such decomposition have changed compared with the CS (5.2.6), since now $\hat{p}_n \equiv p_{n+m}$ and $\hat{f}(n) \equiv f(n+m)$.

SECTION 5.3

Gilmore-Perelomov coherent states

Gilmore-Perelomov coherent states (GPCS) are obtained by acting a generalized displacement operator onto an extremal state of the system [77, 84]. In order to address the GPCS, we will carry out next the analysis of the commutator $\left[A_{\mathcal{G}}^-, A_{\mathcal{G}}^+\right]$.

Let us begin by assuming that equations (5.1.12a) and (5.1.12b) are fulfilled. For an arbitrary state expressed as a linear combination of the basis vectors, $\Psi(x,y;\mathcal{G}) = \sum_{n=0}^{\infty} a_n \Psi_n(x,y;\mathcal{G})$, we have that

$$\left[A_{\mathcal{G}}^-, A_{\mathcal{G}}^+\right] \Psi(x,y;\mathcal{G}) = \sum_{n=0}^{\infty} a_n \left(\gamma_{n+1} - \gamma_n\right) \Psi_n(x,y;\mathcal{G}), \tag{5.3.1}$$

where γ_n is a real non-negative function of n defined by

$$\gamma_n = \sqrt{q_{n-1} p_n} f^2(n). \tag{5.3.2}$$

We are interested in knowing if we can get the commutation relationship $\left[A_{\mathcal{G}}^-, A_{\mathcal{G}}^+\right] = 1$, as for the harmonic oscillator. Once again two different cases arise, according to the values taken by f.

Case with $f(n) \neq 0$

In this case, f has no roots for $n \in \mathbb{N}$, therefore the only extremal state is $\Psi_0(x, y; \mathcal{G})$. The ladder operators commute to the identity if the following conditions are fulfilled

$$f(1) = (q_0 p_1)^{-\frac{1}{4}}, \tag{5.3.3a}$$

$$f(n+1) = \left(\frac{1 + \sqrt{q_{n-1} p_n} f^2(n)}{\sqrt{q_n p_{n+1}}} \right)^{\frac{1}{2}} \quad \text{for} \quad n \geq 1. \tag{5.3.3b}$$

Equations (5.3.3a), (5.3.3b) imply that $\left[A_{\mathcal{G}}^-, A_{\mathcal{G}}^+\right] = 1$, i.e., the operators $A_{\mathcal{G}}^-$ and $A_{\mathcal{G}}^+$ fulfill the Heisenberg-Weyl algebra. The displacement operator defined by $D_{\mathcal{G}}(\alpha) = \exp\left(\alpha A_{\mathcal{G}}^+ - \alpha^* A_{\mathcal{G}}^-\right)$ can be factorized using the Baker-Hausdorff formula in the way $D_{\mathcal{G}}(\alpha) = e^{-\frac{1}{2}|\alpha|^2} e^{\alpha A_{\mathcal{G}}^+} e^{-\alpha^* A_{\mathcal{G}}^-}$.

The GPCS $\Psi_\alpha^{\mathrm{GP}}(x, y; \mathcal{G})$ in this case are the result of acting $D_{\mathcal{G}}(\alpha)$ over the extremal state Ψ_0, thus we have

$$\Psi_\alpha^{\mathrm{GP}}(x, y; \mathcal{G}) = e^{-\frac{1}{2}|\alpha|^2} \sum_{n=0}^{\infty} \frac{\alpha^n \sqrt{[\hat{q}_n]!}\, [f(n)]!}{n!} \Psi_n(x, y; \mathcal{G}), \tag{5.3.4}$$

where $\hat{q}_n = q_{n-1}$. It is important to stress that we do not need to normalize the Gilmore-Perelomov coherent states, since $D_{\mathcal{G}}(\alpha)$ is a unitary operator.

Case with $f(n) = 0$ for some n

Let us consider the ordered set of integers $\{m_i | f(m_i) = 0 \quad \text{for} \quad i = 1, 2, ..., l\}$, then $\Psi_{m_i}(x, y; \mathcal{G})$ are the extremal states. Notice that $\gamma_{m_i} = 0$ when $f(m_i) = 0$, which implies that the coefficients multiplying $\Psi_{m_i}(x, y; \mathcal{G})$ and $\Psi_{m_i - 1}(x, y; \mathcal{G})$ in equation (5.3.1) reduce to $a_{m_i} \gamma_{m_i + 1}$ and $-a_{m_i - 1} \gamma_{m_i - 1}$ respectively. Since γ_n is non-negative, for a particular election of f the coefficient of $\Psi_{m_i}(x, y; \mathcal{G})$ can be made equal to a_{m_i} while the one for $\Psi_{m_i - 1}(x, y; \mathcal{G})$ can not, regardless the choice of f. As a consequence, $\left[A_{\mathcal{G}}^-, A_{\mathcal{G}}^+\right]$ can not be made equal to the identity operator in this case, under any circumstances.

Although now $\left[A_{\mathcal{G}}^-, A_{\mathcal{G}}^+\right] \neq 1$, there are still some cases that may be worth of some discussion.

a) If $m_{i+1} - m_i \geq 2$ for $i = 1, 2, ...$ all the roots of f are non-consecutive. Thus, under an appropriate choice of f equation (5.3.1) produces a slight modification on the initial contribution of $\Psi_{m_i}(x, y; \mathcal{G})$ to the linear combination, i.e., the commutator could be made very close to the identity.

b) If $m_{i+1} - m_i = 1$ for some i, at least two roots of f are consecutive which implies that the term $\Psi_{m_i}(x, y; \mathcal{G})$ will disappear from the linear combination (5.3.1). Then, the commutator is very close to the identity minus the projector onto the subspace generated by $\Psi_{m_i}(x, y; \mathcal{G})$.

Any other configuration of roots will be achieved by combining the previous cases. However, the most important implication of having roots in $f(n)$ is that the Baker-Hausdorff factorization formula can not be applied anymore. Nevertheless, we can use an alternative non-unitary displacement operator defined by $D_{\mathcal{G}}(\alpha) = e^{\alpha A_{\mathcal{G}}^{+}}$. The Gilmore-Perelomov coherent states will appear from acting $D_{\mathcal{G}}(\alpha)$ over the extremal states $\Psi_{m_i}(x, y; \mathcal{G})$. By remembering that there are l roots for f, the coherent states are thus given by

$$\Psi_{\alpha}^{\mathrm{GP}}(x, y, m_i; \mathcal{G}) = \sum_{n=0}^{m_{i+1}-m_i-1} \frac{\alpha^n \sqrt{[\tilde{q}(n)]![\tilde{f}(n)]!}}{n!} \Psi_{n+m_i}(x, y; \mathcal{G}), \quad i = 0, 1, ..., l, \quad (5.3.5)$$

where $m_0 = 0$, $m_{l+1} = \infty$, $\tilde{q}(n) = q(n + m_i - 1)$ and $\tilde{f}(n) = f(n + m_i)$. Some points must be stressed: in this case, the GPCS have two labels, namely, the complex number α and the extremal state label m_i from which they are generated; these states are orthogonal with respect to the last label. In addition, since the displacement operator used is non-unitary, the coherent states of equation (5.3.5) should still be normalized.

SECTION 5.4

Minimum uncertainty coherent states

In this definition, the so-called minimum uncertainty coherent states (MUCS) $\Psi^{\mathrm{MU}}(x, y; \mathcal{G})$ must saturate the uncertainty product for the quadratures $Q_{\mathcal{G}}$ and $P_{\mathcal{G}}$ [81, 82], defined by

$$Q_{\mathcal{G}} = \frac{1}{\sqrt{2}} \left(A_{\mathcal{G}}^{+} + A_{\mathcal{G}}^{-} \right), \qquad P_{\mathcal{G}} = \frac{i}{\sqrt{2}} \left(A_{\mathcal{G}}^{+} - A_{\mathcal{G}}^{-} \right). \quad (5.4.1)$$

Note that, for any two arbitrary hermitian operators F and G, their commutator $[F, G] = K$ should be antihermitian, i.e., $K^{\dagger} = -K$. Thus, for an arbitrary state $|\Psi\rangle$ it must hold that

$$\Delta F \Delta G \geq \frac{1}{2} |\langle K \rangle|, \quad (5.4.2)$$

where $\langle K \rangle = \langle \Psi | K | \Psi \rangle$ and $(\Delta K)^2 \equiv \langle \Psi | K^2 | \Psi \rangle - \langle \Psi | K | \Psi \rangle^2$. Equation (5.4.2) will be saturated if it is fulfilled

$$\left(F + i \frac{\Delta F}{\Delta G} G \right) \Psi = \left(\langle F \rangle + i \frac{\Delta F}{\Delta G} \langle G \rangle \right) \Psi. \quad (5.4.3)$$

If we consider now the quadratures $F = Q_{\mathcal{G}}$ and $G = P_{\mathcal{G}}$, after some algebra the previous condition becomes

$$\left[\frac{(1-\lambda)}{(1+\lambda)}A_{\mathcal{G}}^{+} + A_{\mathcal{G}}^{-}\right]\Psi = \alpha\Psi, \tag{5.4.4}$$

where $\lambda = \Delta Q_{\mathcal{G}}/\Delta P_{\mathcal{G}}$ and $\alpha = \left[\frac{(1-\lambda)}{(1+\lambda)}\langle A_{\mathcal{G}}^{+}\rangle + \langle A_{\mathcal{G}}^{-}\rangle\right]$.

Some points must be taken into account: for this treatment the quadratures $Q_{\mathcal{G}}$ and $P_{\mathcal{G}}$ are not, in general, the position and moment operators. Furthermore, equation (5.4.4) is the eigenvalue problem for the so-called squeezed coherent states, which saturate the Heisenberg uncertainty product $\Delta Q_{\mathcal{G}}\Delta P_{\mathcal{G}}$ but the uncertainty in one of its quadratures is less than the other one. However, if $\lambda = 1$ expression (5.4.4) reduces to an equation of eigenvalues for $A_{\mathcal{G}}^{-}$, therefore the minimum uncertainty coherent states turn out to be equal to the Barut-Girardello coherent states in this case, $\Psi^{\mathrm{MU}}(x, y; \mathcal{G}) = \Psi^{\mathrm{BG}}(x, y; \mathcal{G})$. From now on we will refer to this particular case as the minimum uncertainty coherent states.

CHAPTER 6

Example: constant magnetic field

In this chapter we are going to analyze the simplest coherent states for the monolayer and bilayer graphene previously discussed. In order to do that, we will take the external magnetic field to be constant, in the framework of shape-invariant potentials for bilayer graphene studied in chapter 4 and in [10].

Let us consider the constant magnetic field $\mathbf{B} = \mathcal{B}_0\hat{e}_z$ with $\mathcal{B}_0 > 0$, thus the vector potential amplitude is $\mathcal{A}(x) = \mathcal{B}_0 x$. The eigenfunctions $\psi_n^-(x)$ of H_i^-, $i = 1, 2$ for both monolayer and bilayer graphene are given by:

$$\psi_n^-(x) = \sqrt{\frac{1}{2^n n!}\left(\frac{\omega}{2\pi}\right)^{\frac{1}{2}}}\mathrm{H}_n\left[\sqrt{\frac{\omega}{2}}\left(x + \frac{2k}{\omega}\right)\right] e^{-\frac{\omega}{4}\left(x+\frac{2k}{\omega}\right)^2}, \qquad n = 0, 1... \tag{6.1}$$

where $\omega \equiv 2e\mathcal{B}_0/c\hbar$ and k is the wave number in y direction (see [10–13]). The corresponding eigenvalues are $\mathcal{E}_n^- = n\omega$. Thus, the eigenfunctions and eigenvalues for monolayer graphene become

$$\Psi_n(x, y; \mathcal{M}) = \frac{e^{iky}}{\sqrt{2^{1-\delta_{n0}}}}\begin{pmatrix}(1-\delta_{n0})\psi_{n-1}^-(x)\\ i\psi_n^-(x)\end{pmatrix}, \quad E_n = \hbar v_F\sqrt{n\omega}, \quad n = 0, 1, ... \tag{6.2}$$

while for bilayer graphene are

$$\Psi_n(x, y; \mathfrak{B}) = \frac{e^{iky}}{\sqrt{2^{1-\delta_{n0}-\delta_{n1}}}}\begin{pmatrix}(1-\delta_{n0}-\delta_{n1})\psi_{n-2}^-(x)\\ \psi_n^-(x)\end{pmatrix}, \; E_n = \frac{\hbar^2\omega}{2m^*}\sqrt{n(n-1)}, \; n = 0, ... \tag{6.3}$$

Notice that the eigenfunctions ψ_n^- correspond to the shifted harmonic oscillator, for which the well known one-dimensional ladder operators are given by

$$\begin{aligned}\Theta^- &= \frac{1}{\sqrt{2}}\left(\zeta + \frac{d}{d\zeta}\right),\\ \Theta^+ &= \frac{1}{\sqrt{2}}\left(\zeta - \frac{d}{d\zeta}\right),\end{aligned} \tag{6.4}$$

where $\zeta = \sqrt{\frac{\omega}{2}}\left(x + \frac{2k}{\omega}\right)$. Thus

$$\begin{aligned} \Theta^{-}\psi_n^{-} &= \sqrt{n}\psi_{n-1}^{-}, \\ \Theta^{+}\psi_n^{-} &= \sqrt{n+1}\psi_{n+1}^{-}, \qquad n = 0, 1, .. \end{aligned} \tag{6.5}$$

Equations (5.1.1a, 6.5) are all we need to determine the generalized coherent states. From now on we will restrict ourselves to the case where f has no roots, in particular we will choose $f(n) = 1$ for the BGCS (5.2.6).

SECTION 6.1

Equivalent generalized coherent states

Since we have chosen $f(n) = 1$, looking at equations (5.1.1a, 6.5) we can simplify the BGCS of equation (5.2.6), which coincide with the MUCS,

$$\begin{aligned} \Psi_{\alpha}^{\mathrm{BG}}(x, y; \mathcal{G}) &= \Psi_{\alpha}^{\mathrm{MU}}(x, y; \mathcal{G}) \\ &= e^{-\frac{1}{2}|\alpha|^2} \sum_{n=0}^{\infty} \frac{\alpha^n}{\sqrt{n!}} \Psi_n(x, y; \mathcal{G}), \end{aligned} \tag{6.1.1}$$

where the index $\mathcal{G} = \mathcal{M}, \mathfrak{B}$ indicates monolayer or bilayer graphene, respectively.

Focusing now on the the GPCS, after some algebra we can simplify equation (5.3.4) to obtain:

$$\begin{aligned} \Psi_{\alpha}^{\mathrm{GP}}(x, y; \mathcal{G}) &= e^{-\frac{1}{2}|\alpha|^2} \sum_{n=0}^{\infty} \frac{\alpha^n}{\sqrt{n!}} \Psi_n(x, y; \mathcal{G}) \\ &= \Psi_{\alpha}^{\mathrm{BG}}(x, y; \mathcal{G}) = \Psi_{\alpha}^{\mathrm{MU}}(x, y; \mathcal{G}). \end{aligned} \tag{6.1.2}$$

Equations (6.1.1) and (6.1.2) indicate the existence of a family of coherent states for which the three definitions are mutually equivalent. Such a family is determined by the function $f(n) = 1$, $n = 1, 2, ...$

Note that $f(n) = 1$ does not mean necessarily that $f(x) = 1, \forall\ x \in \mathbb{R}$. It is enough that such a function takes the unit value for any positive integer. Due to the mutual equivalence between these three definitions from now on we will call the states $\Psi_{\alpha}(x, y; \mathcal{G})$ (6.1.2) just coherent states. Besides, it must be stressed that these states constitute an overcomplete set of vectors in the Hilbert space fulfilling a resolution of the identity as follows

$$\mathbb{I} = \frac{1}{\pi} \int_{\mathbb{C}} |\Psi_{\alpha}\rangle \langle\Psi_{\alpha}| \, d\mu(\alpha), \tag{6.1.3}$$

where $d\mu(\alpha) = \frac{r dr d\theta}{\pi}$ and $\alpha = re^{i\theta}$. In the following sections we will calculate some physical quantities associated with these coherent states.

SECTION 6.2

Probability density

The probability density for the CS (6.1.2) is calculated as follows

$$\rho_{\mathcal{G}}(x,y;\alpha) = \Psi^{\dagger}_{\alpha}(x,y;\mathcal{G})\Psi_{\alpha}(x,y;\mathcal{G}). \tag{6.2.1}$$

This expression can be simplified by defining

$$a_n(\alpha) \equiv e^{-\frac{1}{2}|\alpha|^2}\frac{\alpha^n}{\sqrt{n!}}, \qquad \rho_{n,m}(x,y;\mathcal{G}) \equiv \Psi_m(x,y;\mathcal{G})^{\dagger}\Psi_n(x,y;\mathcal{G}),$$
$$C_{m,n}(x,y,\alpha;\mathcal{G}) = a^*_m(\alpha)a_n(\alpha)\rho_{n,m}(x,y;\mathcal{G}), \tag{6.2.2}$$

with a_n being a complex function of α. Due to the functions ψ_n^- in equation (6.2.1),(6.2.2) are real, $\rho_{n,m}$ is symmetric under the exchange of indexes. On the other hand, $\rho_{n,m}(x,y;\mathcal{G}) = \rho_{n,m}(x;\mathcal{G})$. Thus, the probability density depends only on x and can be written as

$$\rho_{\mathcal{G}}(x;\alpha) = \sum_{n,m=0}^{\infty} \mathfrak{Re}\left(C_{m,n}(x,\alpha;\mathcal{G})\right). \tag{6.2.3}$$

By defining

$$\rho_n(x;\mathcal{G}) \equiv \rho_{n,n}(x;\mathcal{G}), \tag{6.2.4}$$

and taking into account equations (6.2) and (6.3), respectively, the probability density for monolayer graphene coherent states is given by

$$\begin{aligned}\rho_{\mathcal{M}}(x,\alpha) =& e^{-r^2}\left\{\rho_0(x;\mathcal{M}) + 2\sum_{n=1}^{\infty}\frac{r^n\cos(n\theta)}{\sqrt{n!}}\rho_{n,0}(x;\mathcal{M})\right.\\ &\left.+\sum_{n,m=1}^{\infty}\frac{r^{n+m}\cos\left[(n-m)\theta\right]}{\sqrt{n!m!}}\rho_{n,m}(x;\mathcal{M})\right\},\end{aligned} \tag{6.2.5}$$

while for the bilayer graphene coherent states we have that

$$\begin{aligned}\rho_{\mathfrak{B}}(x,\alpha) =& e^{-r^2}\left\{\sum_{n,m=2}^{\infty}\frac{r^{n+m}\cos\left[(n-m)\theta\right]}{\sqrt{n!m!}}\rho_{n,m}(x;\mathfrak{B}) + \rho_0(x;\mathfrak{B})\right.\\ &+ r^2\rho_1(x;\mathfrak{B}) + 2r\cos(\theta)\rho_{1,0}(x;\mathfrak{B})\\ &\left.+2\sum_{n=2}^{\infty}\frac{r^n}{\sqrt{n!}}\left[\cos(n\theta)\rho_{n,0}(x;\mathfrak{B}) + r\cos\left[(n-1)\theta\right]\rho_{n,1}(x;\mathfrak{B})\right]\right\}.\end{aligned} \tag{6.2.6}$$

Note that in both cases the change $\theta \to -\theta$ keeps invariant the probability density, which can be expressed as $\rho_{\mathcal{G}}(x,\alpha) = \rho_{\mathcal{G}}(x,\bar{\alpha})$. In addition, by keeping fixed r it is observed that the amplitude and the position of the probability density maximum depends on the value of θ, as it is shown in Figure 6.1 for monolayer graphene and in Figure 6.2 for bilayer graphene.

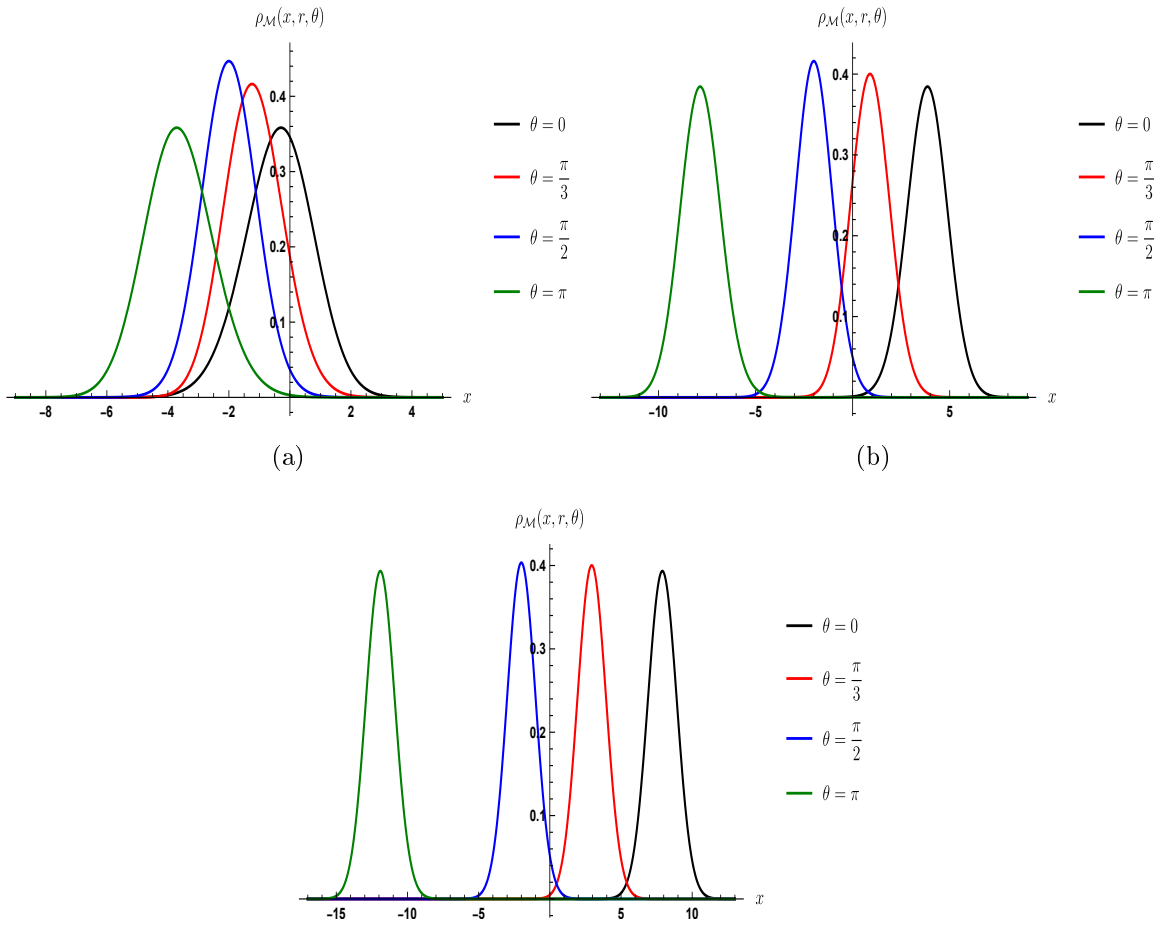

Figure 6.1: Plots of the probability density for the monolayer graphene coherent states (6.1.2) as functions of x and θ, for fixed values of $\omega = k = 1$ and different values of r: (a) $r = 1$; (b) $r = 3$; (c) $r = 5$. We can see that the maximum shifts to the left as θ increases.

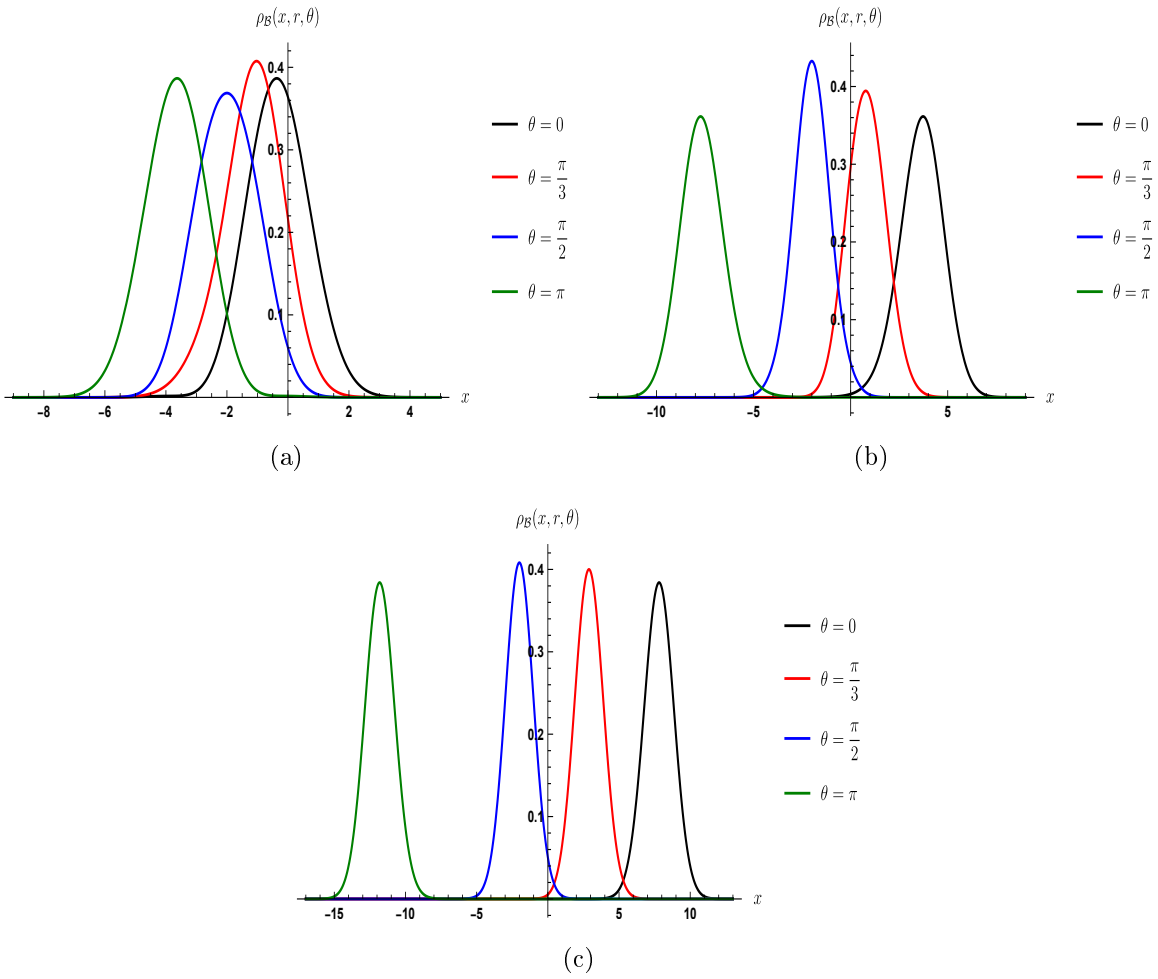

Figure 6.2: Plots of the probability density for the bilayer graphene coherent states (6.1.2) as functions of x and θ, for fixed values of $\omega = k = 1$ and different values of r: (a) $r = 1$; (b) $r = 3$; (c) $r = 5$. We can see that the maximum shifts to the left as θ increases.

SECTION 6.3

Current density

The expressions for the current density are given in equations (3.1.24) and (3.2.17) for monolayer and bilayer graphene respectively. Due to their different structure we will treat them separately.

For monolayer graphene the current components for the coherent states (6.1.2) are given by

$$\begin{aligned}
\left[\mathcal{J}_{\mathcal{M}}\right]_x &= v_F e^{-r^2}\left\{\sum_{n,m=0}^{\infty}\frac{r^{n+m}\sin\left[(n-m)\theta\right]}{\sqrt{n!m!}}j^{-}_{n,m}(x)\right\},\\
\left[\mathcal{J}_{\mathcal{M}}\right]_y &= v_F e^{-r^2}\left\{\sum_{n,m=0}^{\infty}\frac{r^{n+m}\cos\left[(n-m)\theta\right]}{\sqrt{n!m!}}j^{+}_{n,m}(x)\right\},
\end{aligned} \tag{6.3.1}$$

where

$$j^{\pm}_{n,m}(x)=\frac{\left(1-\delta_{n,0}\right)\psi^{-}_{n-1}(x)\psi^{-}_{m}(x)\pm\left(1-\delta_{m,0}\right)\psi^{-}_{n}(x)\psi^{-}_{m-1}(x)}{\sqrt{2^{2-\delta_{n,0}-\delta_{m,0}}}}. \tag{6.3.2}$$

It is worth noting that by making $\theta\to-\theta$ ($\alpha\to\bar{\alpha}$) the current density $y-$component keeps invariant while the $x-$component $\left[\mathcal{J}_{\mathcal{M}}\right]_x$ goes to $-\left[\mathcal{J}_{\mathcal{M}}\right]_x$. In Figures 6.3 and 6.4 we have plots of the current density x and $y-$components for a monolayer graphene coherent state, respectively.

On the other hand, for bilayer graphene after some algebra the components (3.2.18a), (3.2.18b) of the operator current $\mathbf{j}$ become

$$\begin{aligned}
j_x &= \begin{pmatrix}0 & \mathcal{L}_1^{-}\\ -\mathcal{L}_1^{+} & 0\end{pmatrix}=\sqrt{\omega}\begin{pmatrix}0 & \Theta^{-}\\ -\Theta^{+} & 0\end{pmatrix},\\
j_y &= -i\begin{pmatrix}0 & \mathcal{L}_1^{-}\\ \mathcal{L}_1^{+} & 0\end{pmatrix}=-i\sqrt{\omega}\begin{pmatrix}0 & \Theta^{-}\\ \Theta^{+} & 0\end{pmatrix}.
\end{aligned} \tag{6.3.3}$$

Thus, the current density components are now:

$$\begin{aligned}
\left[\mathcal{J}_{\mathfrak{B}}\right]_x &= \frac{\hbar}{m^*}\sqrt{\omega}e^{-r^2}\left\{\sum_{n,m=0}^{\infty}\frac{r^{n+m}\sin\left[(n-m)\theta\right]}{\sqrt{n!m!}}\mathrm{j}^{-}_{n,m}(x)\right\},\\
\left[\mathcal{J}_{\mathfrak{B}}\right]_y &= -\frac{\hbar}{m^*}\sqrt{\omega}e^{-r^2}\left\{\sum_{n,m=0}^{\infty}\frac{r^{n+m}\cos\left[(n-m)\theta\right]}{\sqrt{n!m!}}\mathrm{j}^{+}_{n,m}(x)\right\},
\end{aligned} \tag{6.3.4}$$

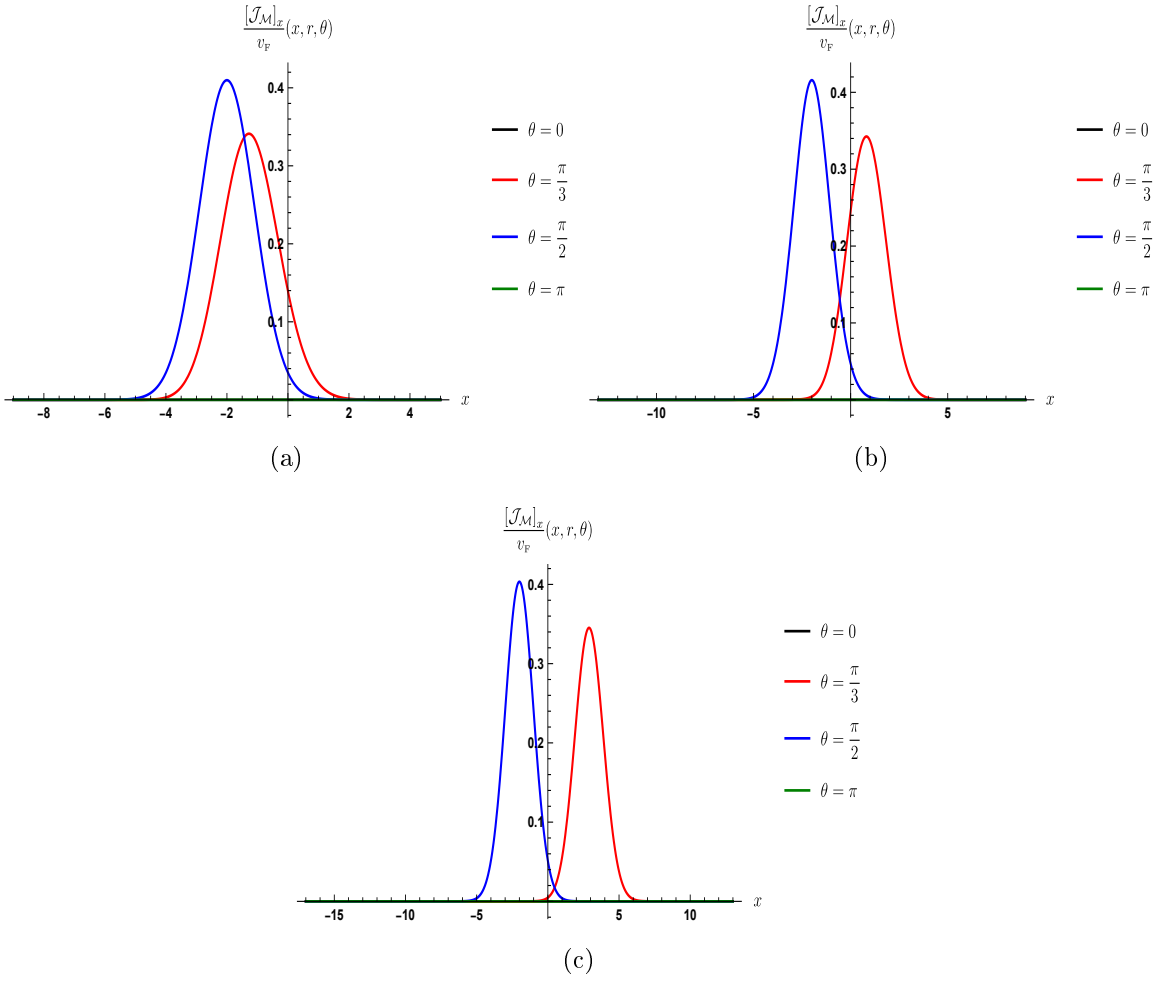

Figure 6.3: Plots of the current density $x-$component $[\mathcal{J}_{\mathcal{M}}]_x$ for the monolayer graphene coherent states (6.1.2) as function of x and θ, for fixed values of $\omega = k = 1$ and different values of r: (a) $r = 1$; (b) $r = 3$; (c) $r = 5$.

where

$$\mathrm{j}^{\pm}_{n,m}(x) = \frac{(1-\delta_{m,0}-\delta_{m,1})\sqrt{n}\psi^{-}_{m-2}(x)\psi^{-}_{n-1}(x) \pm (1-\delta_{n,0}-\delta_{n,1})\sqrt{n-1}\psi^{-}_{m}(x)\psi^{-}_{n-1}(x)}{\sqrt{2^{2-\delta_{n,0}-\delta_{n,1}-\delta_{m,0}-\delta_{m,1}}}}. \tag{6.3.5}$$

As for monolayer graphene, if $\theta \to -\theta$ ($\alpha \to \bar{\alpha}$) the current density $y-$component keeps invariant while the $x-$component $[\mathcal{J}_{\mathfrak{B}}]_x$ goes to $-[\mathcal{J}_{\mathfrak{B}}]_x$. In Figures 6.5 and 6.6 we can see plots of the current density x and $y-$components for bilayer graphene coherent states, respectively.

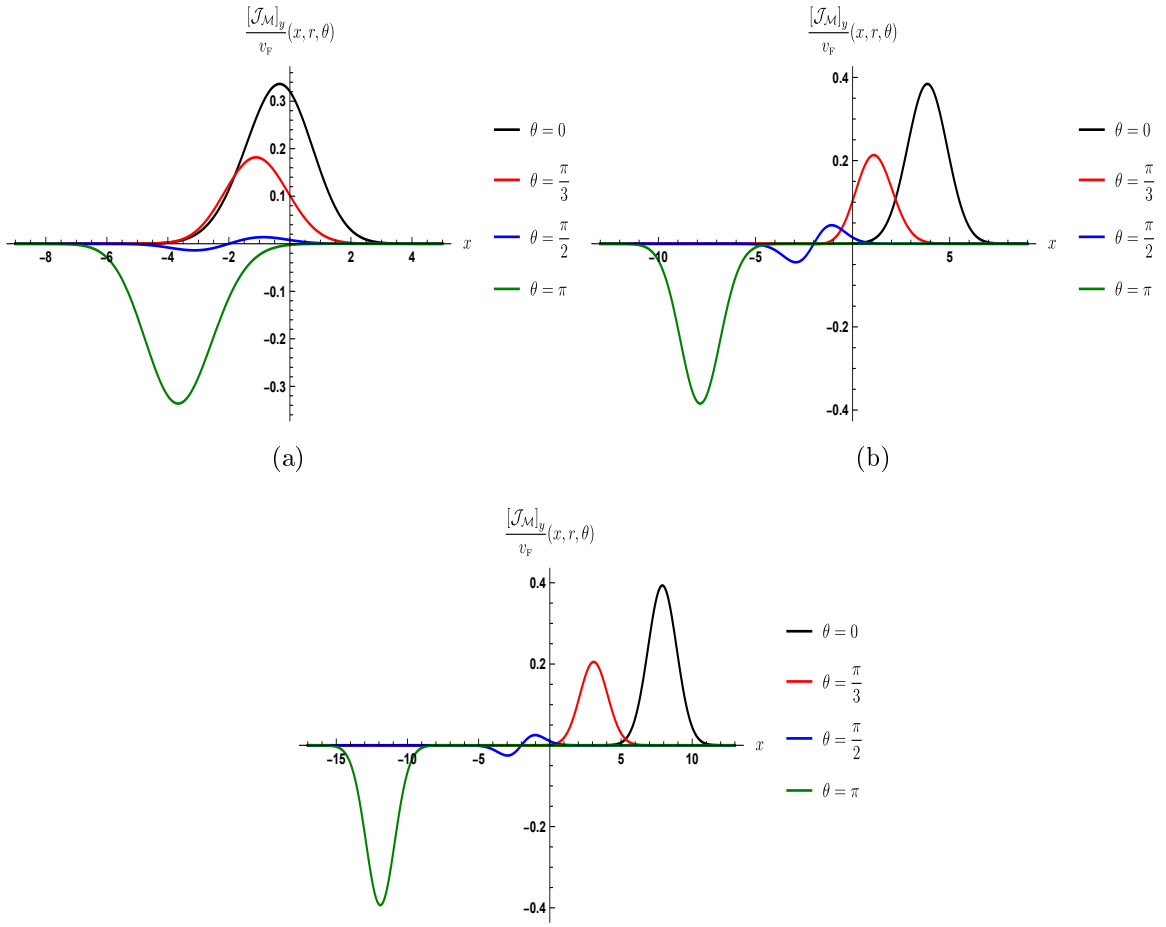

Figure 6.4: Plots of the current density $y-$component $[\mathcal{J}_\mathcal{M}]_y$ for the monolayer graphene coherent states (6.1.2) as function of x and θ, for fixed values of $\omega = k = 1$ and different values of r: (a) $r = 1$; (b) $r = 3$; (c) $r = 5$.

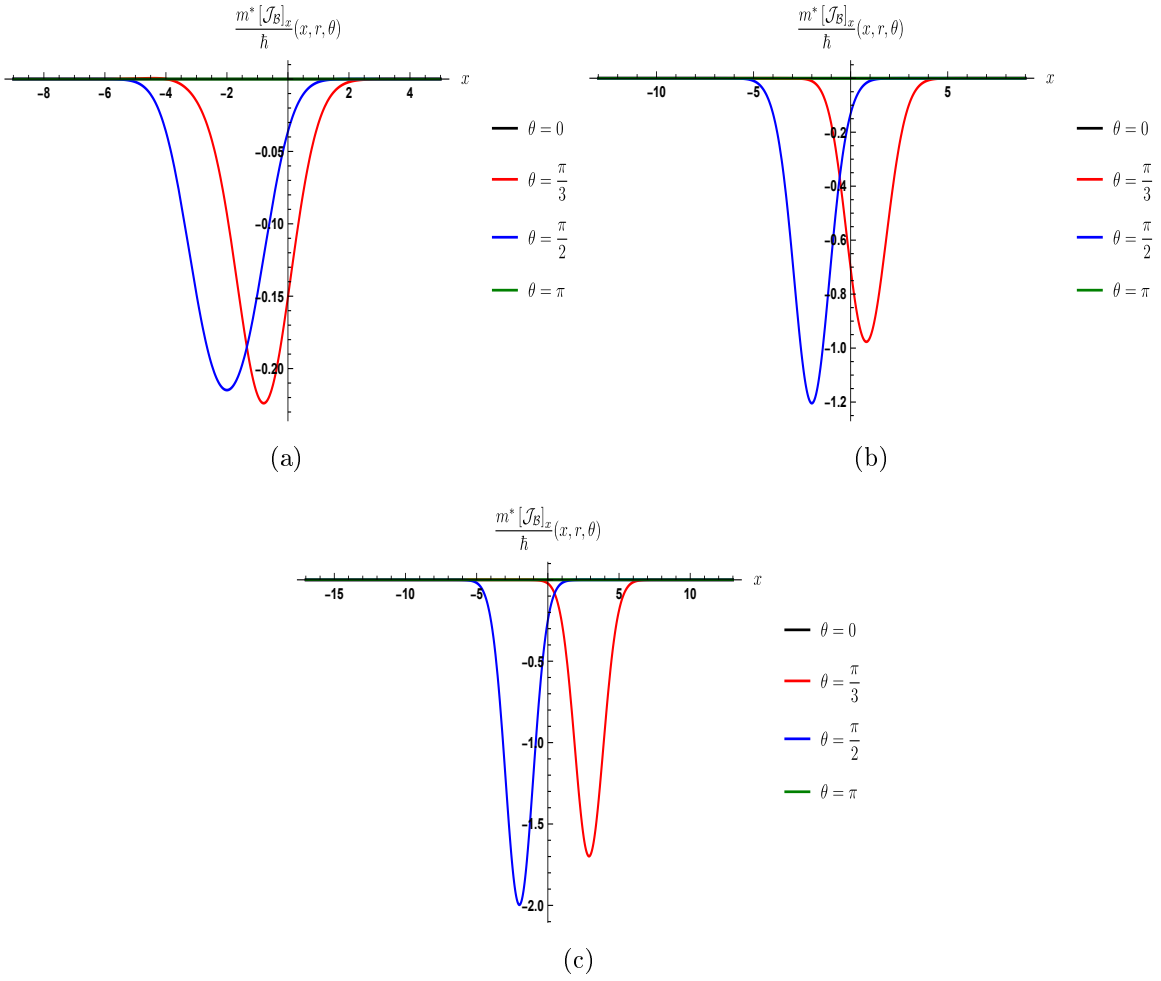

Figure 6.5: Plots of the current density $x-$component $[\mathcal{J}_{\mathcal{B}}]_x$ for the bilayer graphene coherent states (6.1.2) as function of x and θ, for fixed values of $\omega = k = 1$ and different values of r: (a) $r = 1$; (b) $r = 3$; (c) $r = 5$.

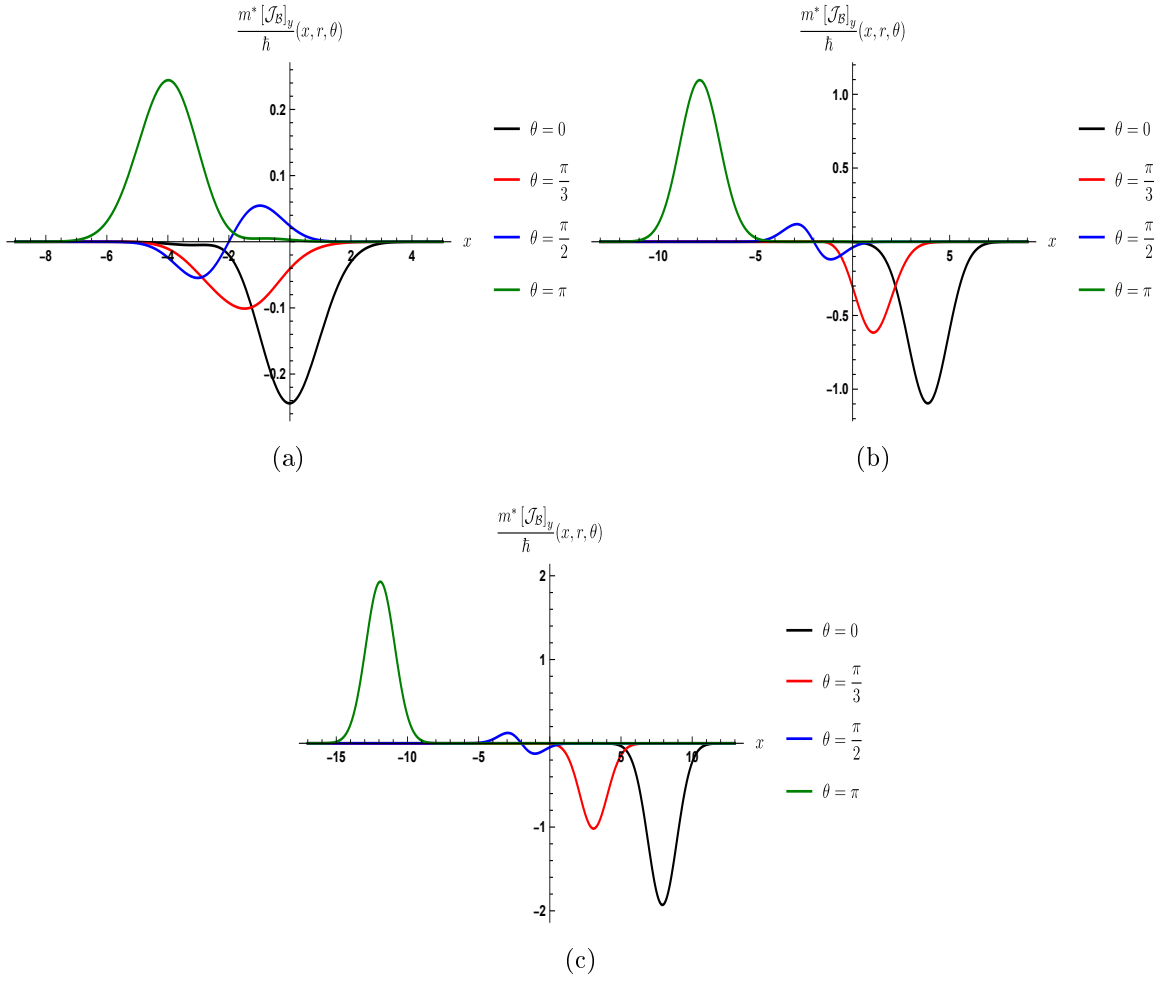

Figure 6.6: Plots of the current density $y-$component $[\mathcal{J}_\mathfrak{B}]_y$ for the bilayer graphene coherent states (6.1.2) as function of x and θ, for fixed values of $\omega = k = 1$ and different values of r: (a) $r = 1$; (b) $r = 3$; (c) $r = 5$.

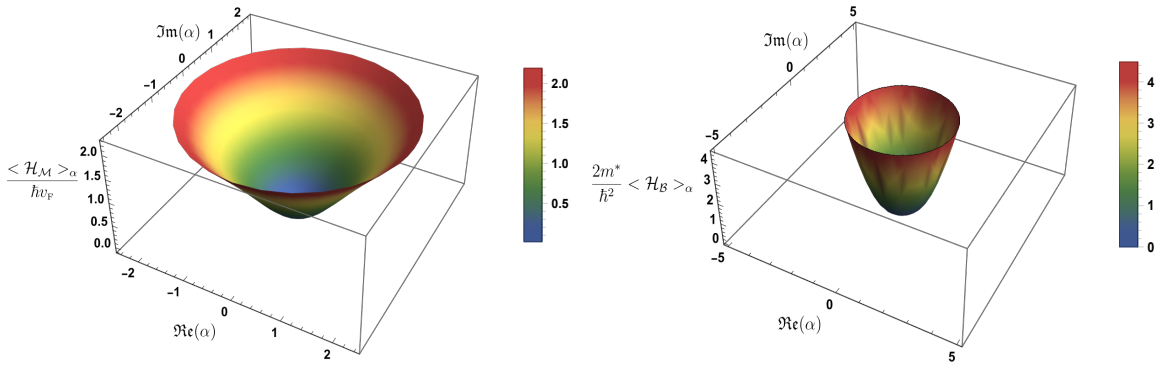

(a) (b)

Figure 6.7: Mean energy value for the monolayer graphene coherent states (a) and the bilayer graphene coherent states (6.1.2) (b). In both cases the parameters were fixed as $\omega = k = 1$. The reflexion symmetry with respect to θ can be seen.

SECTION 6.4

Mean energy value

The mean energy value is defined as $\langle \mathcal{H}_{\mathcal{G}} \rangle_\alpha = \langle \Psi_\alpha | \mathcal{H}_{\mathcal{G}} | \Psi_\alpha \rangle$ for the coherent states (6.1.2). Taking into account the eigenstates and energy eigenvalues (6.2) and (6.3) for monolayer and bilayer respectively, we have that

$$\begin{aligned} \langle \mathcal{H}_{\mathcal{M}} \rangle_\alpha &= \hbar v_F \sqrt{\omega} e^{-r^2} r^2 \sum_{n=0}^{\infty} \frac{r^{2n}}{\sqrt{n+1}(n)!}, \\ \langle \mathcal{H}_{\mathcal{B}} \rangle_\alpha &= \frac{\hbar^2 \omega}{2m^*} e^{-r^2} r^4 \sum_{n=0}^{\infty} \frac{r^{2n}}{\sqrt{(n+2)(n+1)}(n)!}. \end{aligned} \tag{6.4.1}$$

In both cases the mean energy value does not depend on the phase θ, but only on the norm $|\alpha| = r$ of the complex number. A plot of the mean energy value for monolayer graphene coherent states is shown in Figure 6.7(a), while for bilayer graphene coherent states it is shown in Figure 6.7(b).

SECTION 6.5

Heisenberg uncertainty principle

The quadratures defined in equation (5.4.1) saturate the uncertainty product $\Delta Q_{\mathcal{G}} \Delta P_{\mathcal{G}}$ for the coherent states (6.1.2), but they do not correspond to the position and canonical

momentum. Thus, we will calculate next the Heisenberg uncertainty relationship for the canonical position and momentum operators in the coherent states (6.1.2).

The Heisenberg uncertainty principle for the position x and canonical momentum p_x reads as

$$\Delta x \Delta p_x = \hbar \Delta\zeta \Delta p_\zeta \geq \frac{\hbar}{2}, \tag{6.5.1}$$

where ζ and p_ζ are dimensionless position and momentum operators defined in terms of the one-dimensional ladder operators by

$$\begin{aligned} \zeta =& \frac{\Theta^+ + \Theta^-}{\sqrt{2}}, \\ p_\zeta =& i\frac{\Theta^+ - \Theta^-}{\sqrt{2}}. \end{aligned} \tag{6.5.2}$$

Taking first the expression for the monolayer graphene coherent states (6.1.2) it is straightforward to prove that the mean values of ζ, p_ζ, and their squares, are given by

$$\begin{aligned} \langle\zeta\rangle_\alpha =& \frac{e^{-r^2}\mathfrak{Re}(\alpha)}{\sqrt{2}}\left(e^{r^2}+\sqrt{2}-1+\sum_{n=0}^{\infty}\frac{r^{2n+2}}{\sqrt{n!(n+2)!}}\right), \\ \langle\zeta^2\rangle_\alpha =& \frac{e^{-r^2}}{2}\left[1+2r^2e^{r^2}+\mathfrak{Re}(\alpha^2)\left(e^{r^2}+\sqrt{2}-1+\sum_{n=0}^{\infty}\frac{\sqrt{n+2}r^{2n+2}}{\sqrt{n!(n+3)!}}\right)\right], \\ \langle p_\zeta\rangle_\alpha =& \frac{e^{-r^2}\mathfrak{Im}(\alpha)}{\sqrt{2}}\left(e^{r^2}+\sqrt{2}-1+\sum_{n=0}^{\infty}\frac{r^{2n+2}}{\sqrt{n!(n+2)!}}\right), \\ \langle p_\zeta^2\rangle_\alpha =& \frac{e^{-r^2}}{2}\left[1+2r^2e^{r^2}-\mathfrak{Re}(\alpha^2)\left(e^{r^2}+\sqrt{2}-1+\sum_{n=0}^{\infty}\frac{\sqrt{n+2}r^{2n+2}}{\sqrt{n!(n+3)!}}\right)\right]. \end{aligned} \tag{6.5.3}$$

In Figure 6.8 we can see that for $\alpha \to 0$ it turns out that $\Delta\zeta = \Delta p_\zeta = 1/\sqrt{2}$ and thus $\Delta x \Delta p_x = 1/2$, in units of $\hbar$. Now, for bilayer graphene coherent states the

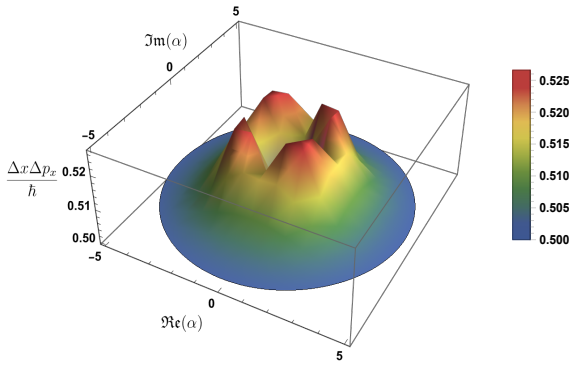

Figure 6.8: Plot of the uncertainty product $\Delta x \Delta p_x$ for the monolayer graphene coherent sates (6.1.2) as function of α, in units of $\hbar$. It can be seen that for $r \to 0$ and $r \to \infty$ the uncertainty product is saturated (tends to 1/2).

corresponding mean values turn out to be

$$
\begin{aligned}
\langle \zeta \rangle_\alpha =& \frac{e^{-r^2} \mathfrak{Re}(\alpha)}{\sqrt{2}} \left[e^{r^2} + 1 + \left(\sqrt{2} - 1\right) r^2 + \sum_{n=0}^{\infty} \frac{\sqrt{n+1} r^{2n+4}}{\sqrt{(n+2)!(n+3)!}} \right], \\
\langle \zeta^2 \rangle_\alpha =& \frac{e^{-r^2}}{2} \left[2(r^2+1) + (2r^2-1)e^{r^2} + \mathfrak{Re}(\alpha^2) \left(e^{r^2} + (\sqrt{2}-1)(1+r^2) \right.\right. \\
& \left.\left. + \sum_{n=0}^{\infty} \frac{r^{2n+4}}{\sqrt{n!(n+4)!}} \right) \right], \\
\langle p_\zeta \rangle_\alpha =& \frac{e^{-r^2} \mathfrak{Im}(\alpha)}{\sqrt{2}} \left[e^{r^2} + 1 + \left(\sqrt{2} - 1\right) r^2 + \sum_{n=0}^{\infty} \frac{\sqrt{n+1} r^{2n+4}}{\sqrt{(n+2)!(n+3)!}} \right], \\
\langle p_\zeta^2 \rangle_\alpha =& \frac{e^{-r^2}}{2} \left[2(r^2+1) + (2r^2-1)e^{r^2} - \mathfrak{Re}(\alpha^2) \left(e^{r^2} + (\sqrt{2}-1)(1+r^2) \right.\right. \\
& \left.\left. + \sum_{n=0}^{\infty} \frac{r^{2n+4}}{\sqrt{n!(n+4)!}} \right) \right].
\end{aligned}
\tag{6.5.4}
$$

Once again, if $\alpha \to 0$ thus $\Delta\zeta = \Delta p_\zeta = 1/\sqrt{2}$ and thus $\Delta x \Delta p_x = 1/2$, in units of $\hbar$ (see Figure 6.9).

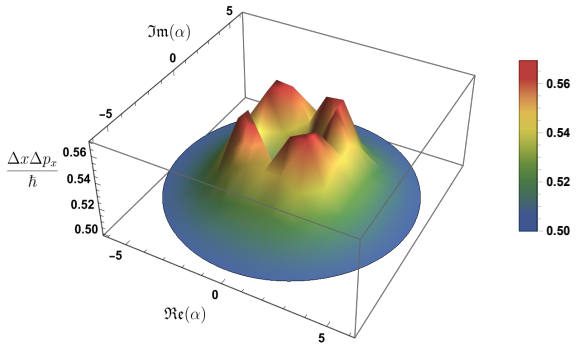

Figure 6.9: Plot of the uncertainty product $\Delta x \Delta p_x$ for the bilayer graphene coherent sates (6.1.2) as function of α, in units of $\hbar$. It can be seen that for $r \to 0$ and $r \to \infty$ the uncertainty product is saturated (tends to 1/2).

SECTION 6.6

Quantum fidelity

The stability in time of the canonical coherent states is expressed as

$$U(t, t_0) \left|\alpha\right\rangle = e^{-i\phi} \left|\alpha(t)\right\rangle, \tag{6.6.1}$$

with ϕ being a phase and $U(t, t_0)$ the time-evolution operator. This behavior is tightly related to the equidistance of the energy levels of the harmonic oscillator. However, such condition is not fulfilled exactly by the eigenvalues for monolayer and bilayer graphene of equations (6.2) and (6.3), respectively, which prevents to obtain in general a time evolution similar to the harmonic oscillator one. Despite this, in both cases it is possible to analyze the dynamics through the quantum fidelity, particularly for bilayer graphene where quasi-periods of oscillation will be found (see also [25]).

Let us begin by applying the evolution operator $U(t, t_0) = e^{-i\mathcal{H}_\mathcal{G}(t-t_0)/\hbar}$ to the monolayer graphene coherent states (6.1.2), thus we get:

$$\Psi_\alpha(x, y, t; \mathcal{M}) = e^{-\frac{1}{2}r^2} \sum_{n=0}^{\infty} \frac{\alpha^n}{\sqrt{n!}} e^{-i\sqrt{n}t_1} \Psi_n(x, y; \mathcal{M}), \tag{6.6.2}$$

with $t_1 = v_F\sqrt{\omega}t$ being a dimensionless time. On the other hand, for the bilayer graphene CS it turns out that

$$\Psi_\alpha(x, y, t; \mathcal{B}) = e^{-\frac{1}{2}r^2} \sum_{n=0}^{\infty} \frac{\alpha^n}{\sqrt{n!}} e^{-i\sqrt{n(n-1)}t_2} \Psi_n(x, y; \mathcal{B}), \tag{6.6.3}$$

where $t_2 = \hbar\omega t/2m^*$ is another dimensionless time; in both cases we have fixed $t_0 = 0$. We know that the quantum fidelity gives us a measure of the closeness between two states, which is defined by

$$F(\phi, \xi) \equiv |\langle\phi|\xi\rangle|^2. \tag{6.6.4}$$

Thus, if $F(\phi, \xi) = 1$ it can be said that $|\phi\rangle, |\xi\rangle$ differ at most by a global phase factor and both represent the same quantum state. Keeping this in in mind, one can look for the time τ such that the initial and evolved states tend to be the same, so that we can call τ a quasiperiod (if it exists).

Now, by considering the states (6.1.2), (6.6.2) and (6.6.3), the quantum fidelity is given by

$$F(\Psi_\alpha, \Psi_\alpha(t)) = e^{-2r^2} \sum_{n,m=0}^{\infty} \frac{r^{2(n+m)}}{n!m!} \cos\left[(h(n) - h(m))\, t_{\mathcal{G}}\right], \tag{6.6.5}$$

where $t_{\mathcal{G}} = \{t_{\mathcal{M}} \equiv t_1, t_{\mathcal{B}} \equiv t_2\}$ and

$$h(n) = \begin{cases} \sqrt{n} & \text{for monolayer graphene,} \\ \sqrt{n(n-1)} & \text{for bilayer graphene.} \end{cases} \tag{6.6.6}$$

In Figure 6.10 we can see the quantum fidelity (6.6.5) between the initial and evolved states at time t for monolayer and bilayer graphene coherent states. In both cases such a quantity depends only on r and time (t_1 or t_2). We can identify as well the values of t_1, t_2 which make $F(\Psi_\alpha, \Psi_\alpha(t))$ to be close to 1, which can be considered as the quasiperiods τ.

Discussion

The energy eigenvalues for bilayer graphene can be written as follows

$$E_n = \frac{\hbar^2\omega}{2m^*} \begin{cases} 0 & \text{for } n = 0, 1, \\ n - \frac{1}{2} + \mathcal{O}(\frac{1}{n}) & \text{for } n \geq 2. \end{cases} \tag{6.6.7}$$

Thus, there is a certain value N for which the approximation equation (6.6.7) can be considered linear, then we will have that

$$\Psi_\alpha(x, y, t) = \Psi'_\alpha(x, y, t) + \gamma_\alpha(x, y, t, N), \tag{6.6.8}$$

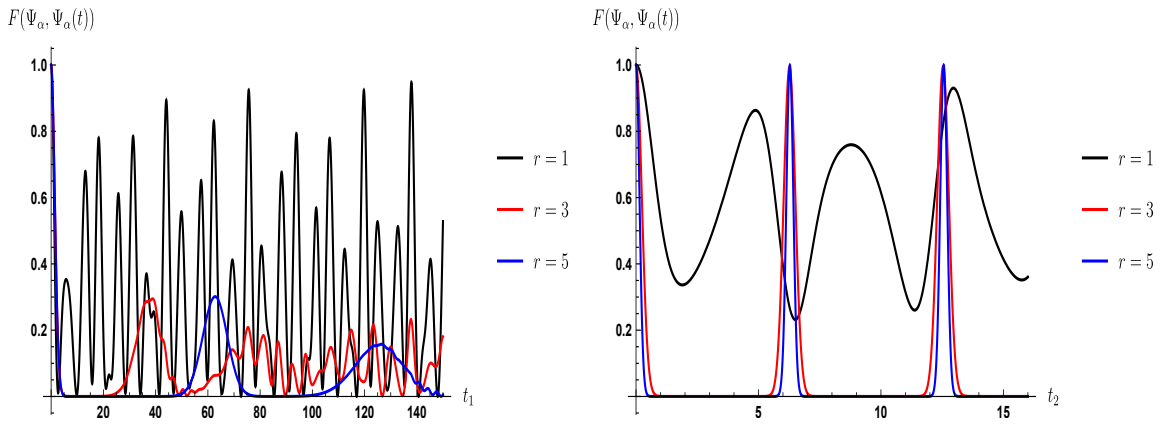

(a) (b)

Figure 6.10: (a) Plot of the fidelity between the initial and the evolving state (6.6.2) for monolayer graphene coherent states as function of the dimensionless time t_1. (b) Plot of the fidelity between the initial and the evolving state (6.6.3) for bilayer graphene coherent states as function of the dimensionless time t_2. In both cases the fidelity is independent of θ.

where

$$\Psi'_\alpha(x,y,t) = e^{it_2/2}\left(e^{-\frac{r^2}{2}}\sum_{n=0}^{\infty}\frac{\alpha(t)^n}{\sqrt{n!}}\Psi_n(x,y)\right),$$
$$\gamma_\alpha(x,y,t;N) = e^{-\frac{r^2}{2}}\sum_{n=0}^{N-1}\frac{\alpha^n}{\sqrt{n!}}\left(e^{-i\sqrt{n(n-1)}t_2} - e^{-i(n-1/2)t_2}\right)\Psi_n(x,y), \tag{6.6.9}$$

and $\alpha(t) = \alpha e^{-it_2}$ (remember that t_2 is proportional to t). Then, the quantum fidelity can be expressed as follows:

$$\begin{aligned} F(\Psi_\alpha, \Psi_\alpha(t)) &= F(\Psi_\alpha, \Psi'_\alpha(t)) + F(\Psi_\alpha, \gamma_\alpha(t;N)) + 2\mathfrak{Re}\left(\langle\Psi'_\alpha(t)|P_\alpha|\gamma_\alpha(t;N)\rangle\right) \\ &= e^{-4r^2\sin^2(\frac{t_2}{2})} + F(\Psi_\alpha, \gamma_\alpha(t;N)) + 2\mathfrak{Re}\left(\langle\Psi'_\alpha(t)|P_\alpha|\gamma_\alpha(t;N)\rangle\right), \end{aligned} \tag{6.6.10}$$

with P_α being the projector onto the subspace generated by the initial coherent state. Given equation (6.6.10), the process to find the quasiperiods is the following: the fidelity must be approximately equal to 1, thus a value of N is fixed and the equation is solved for t_2. We must emphasize that $\gamma_\alpha \to 0$ for $r \to \infty$. This means that in this limit $F(\Psi_\alpha, \Psi_\alpha(t)) = e^{-4r^2\sin^2(\frac{t_2}{2})}$, which implies that the quasiperiods are $\tau = 2\pi$ and its integer multiples, regardless the value of N. We can see that this approximation is

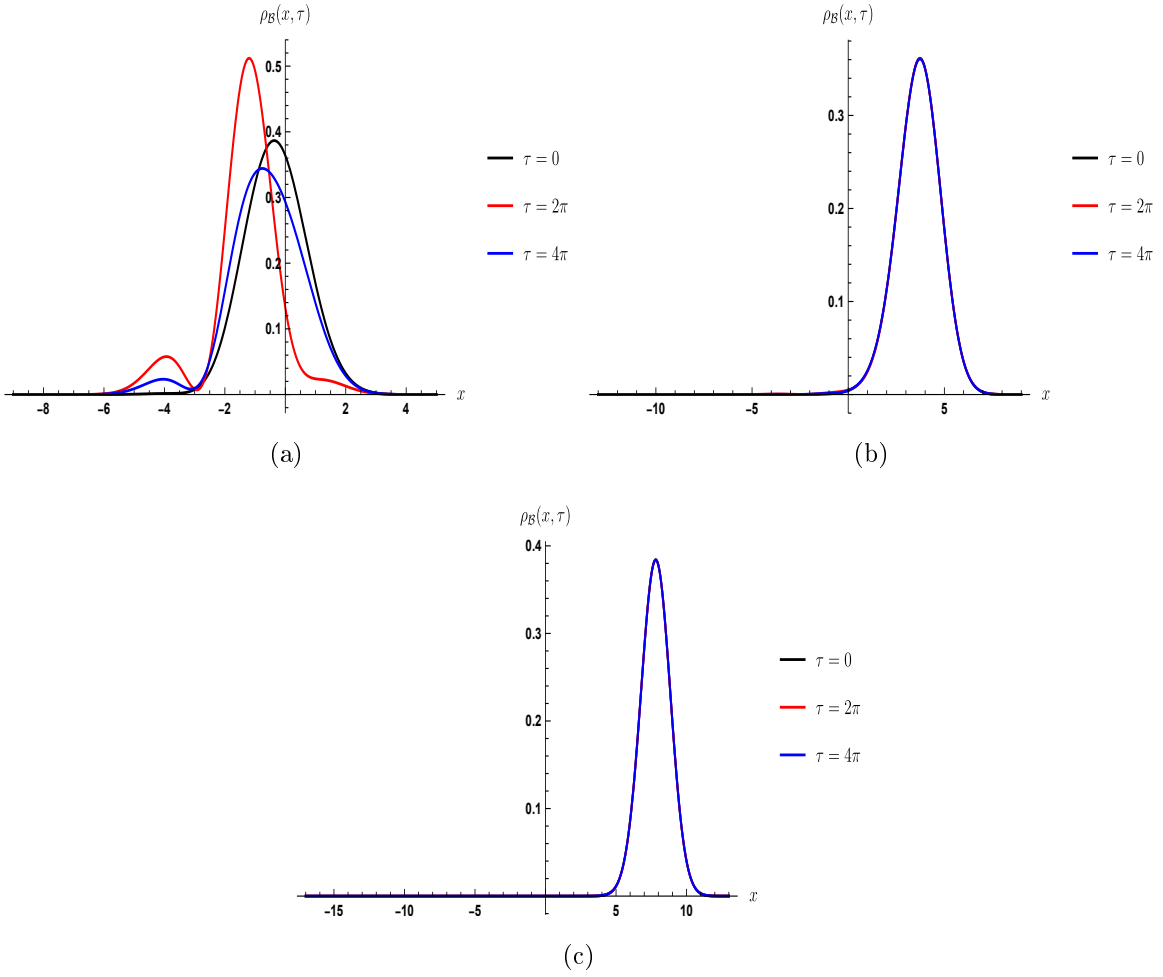

Figure 6.11: Plots of the probability density for bilayer graphene coherent states at several multiples of the quasiperiod $\tau = 2\pi$ and different values of r: (a) $r = 1$; (b) $r = 3$; (c) $r = 5$. We can see that the different curves tend to coincide as r increases. We have fixed $\theta = 0$ and $\omega = k = 1$.

consistent as well with the points observed in Figure 6.10(b) for $r > 1$. A plot of the probability density at such quasiperiods is shown in Figure 6.11.

CHAPTER 7

Conclusions

In this work we have studied the effective Hamiltonians $\mathcal{H}_{\mathcal{M}}$, $\mathcal{H}_{\mathfrak{B}}$ for monolayer and bilayer graphene under an external magnetic field $\mathbf{B}$ orthogonal to the surface of the material. It has been proven that for those cases where the magnetic field $\mathbf{B} = \nabla \times \mathcal{A}(x)$ is described using the Landau gauge, supersymmetric quantum mechanics is the simplest tool allowing to determine exactly the energy levels of the electrons (holes), as well as their associated eigenfunctions. For bilayer graphene three different supersymmetry transformations were carried out: the first one led to shape-invariant potentials, the second to rational extensions and the last one was the so-called confluent algorithm. All these transformations were applied to the shifted harmonic oscillator and the hyperbolic Rosen-Morse potentials. For each of them the magnetic field giving place to the specific transformation was reconstructed.

In the shape-invariant case it was found that the ground state energy has a two-fold degeneracy. However, the main difference lies in the energy dependence on the wave number k for the Rosen-Morse potential, while for the oscillator such a dependence does not arise. For the second case, which leads to rational extensions in the potentials, the same behavior of the energy eigenvalues for both potentials was observed. However, in contrast with the shape-invariant case, now some excited state energies could be degenerated, which in the oscillator case depends on the factorization energies chosen while for the hyperbolic Rosen-Morse potential of the wavenumber selected. Finally, for the confluent case the degeneracy of the ground state disappears. However, degeneracies associated with the excited state levels could arise, which will depend on the factorization energy used. Surprisingly, in this case the energy levels for electrons (holes) do not depend on the wavenumber for both potentials.

On the other hand, we have analyzed the different definitions of coherent states for monolayer and bilayer graphene. For doing this, we made use of the intertwining operators $\mathcal{L}_1^{\pm}$ and $\mathcal{L}_2^{\pm}$ to find out a family of well-behaved ladder operators, and the commutation relationship between them was studied. Then, we determined the

sufficiency conditions for the commutator of the ladder operators to be equal to the identity, to be able to use the Baker-Hausdorff formula. Therefore, the associated displacement operator will be unitary, which represents one of our most important results of this work, in contrast with the operators defined by other authors [85]. For the shape-invariant transformation applied to the harmonic oscillator it was found that these three definitions can be made equivalent, for a suitable choice of the function f, which represents a big difference with the graphene coherent states previously derived in the same Landau gauge [22, 25]. Finally, by using the quantum fidelity it was shown that the bilayer graphene coherent states have quasiperiods of evolution which are multiples of 2π (a result previously reported in [25]).

SECTION 7.1

Perspectives

Last but not least, we would like to mention the outlook for the future:

- In this work, the complex case of the second-order supersymmetric quantum mechanics has been left aside. However, like its real and confluent counterpart, it is expected that such a choice of factorization energies will lead to unexpected behavior of the bilayer graphene energy levels and corresponding eigenfunctions.

- In the construction of coherent states we have restricted ourselves to the shape-invariant case. However, it must be emphasized that in the confluent case the energy levels are equidistant. In particular, when the factorization energy is taken as the ground state for H_2^- they are non-degenerate. Therefore, it seems that for the magnetic field configuration leading to non-degenerate equidistant energy levels the coherent states could have temporal stability similar to the one for the canonical coherent states.

- The graphene coherent states also appear for systems where the magnetic field is not expressed in the Landau gauge [26], but the energy levels are not found through supersymmetric quantum mechanics. However, given the relationship between the components of the spinor, it is possible to define intertwining-like operators. Therefore, it seems suggestive to use a process similar to the one described here for constructing the corresponding coherent states.

Wavenumber k and parameter κ

The introduction of the parameter κ allows us to have a wider range of values of k for which we will get stationary states. Both quantities are connected, and the relationship between them is calculated next.
Let us start by remembering that

$$k = \frac{1}{2}\left(\eta(x) - \frac{2e}{c\hbar}\mathcal{A}(x)\right). \tag{A.1}$$

Since η depends on some other parameters, denoted by the symbol γ that includes κ, let us to express η as follows

$$\eta(x) = f(x;\gamma) + C_1(\gamma), \tag{A.2}$$

with C_1 being the constant part and f the variable one that depends on x and γ. Thus we get

$$k = \frac{1}{2}\left(f(x;\gamma) + C_1(\gamma) - \frac{2e}{c\hbar}\mathcal{A}(x)\right). \tag{A.3}$$

At the same time, the magnetic field $\mathcal{B}$ and η' are proportional

$$\mathcal{B}(x) = \frac{c\hbar}{2e}\eta'(x) = \frac{c\hbar}{2e}f'(x;\gamma). \tag{A.4}$$

Now, remembering that we are working in the Landau gauge, $\mathcal{A}(x)$ can be calculated by integrating $\mathcal{B}(x)$ in the way

$$\mathcal{A}(x) = \int \mathcal{B}(x)dx = \frac{c\hbar}{2e}\int f'(x;\gamma)dx = \frac{c\hbar}{2e}\left(f(x;\gamma) + C_2\right), \tag{A.5}$$

where C_2 is an arbitrary integration constant. By plugging equations (A.5), (A.2) into (A.1) we get

$$k = \frac{1}{2}\left(C_1(\gamma) - C_2\right). \tag{A.6}$$

Thus, if we fix the integration constant C_2 it will suffice to find the constant part of η to obtain k. However, in general this is not an easy task.

Bilayer graphene probability current

In order to get the expression for the probability current, let us remember that for the free case ($\mathcal{B}(x) = 0$)

$$\mathcal{J}_{\mathfrak{B}} = \frac{\hbar}{m^*} \left[\mathfrak{Im} \left(\Psi^\dagger \mathbf{j} \Psi \right) \right], \tag{B.1}$$

where

$$j_x = \sigma_x \partial_x + \sigma_y \partial_y, \tag{B.2a}$$
$$j_y = \sigma_y \partial_x - \sigma_x \partial_y. \tag{B.2b}$$

If we define $\boldsymbol{\sigma} = (\sigma_x, \sigma_y)$ and $\boldsymbol{\chi} = (\sigma_y, -\sigma_x)$, the components become

$$j_x = \frac{i}{\hbar} \boldsymbol{\sigma} \cdot \nabla = \boldsymbol{\sigma} \cdot \mathbf{p}, \tag{B.3a}$$
$$j_y = \frac{i}{\hbar} \boldsymbol{\chi} \cdot \nabla = \boldsymbol{\chi} \cdot \mathbf{p}, \tag{B.3b}$$

with $\mathbf{p}$ being simultaneously the kinematic and canonical momentum operator. Now, if there is a magnetic field described by the vector potential $\mathbf{A}$, by making use of the minimal coupling rule we get

$$j_x \to \boldsymbol{\sigma} \cdot \boldsymbol{\pi}, \tag{B.4a}$$
$$j_y \to \boldsymbol{\chi} \cdot \boldsymbol{\pi}, \tag{B.4b}$$

where $\boldsymbol{\pi} = \mathbf{p} + (e/c)\mathcal{A}$ is the kinematic momentum operator and $\mathbf{p}$ the canonical momentum operator. Note that the change in each component depends on the changes in all directions of the momentum due to the magnetic field. Moreover, the probability current (B.1) is gauge independent. It is worth mentioning that the same result can be obtained using the continuity equation derived in terms of the Hamiltonian, namely,

$$\frac{\partial \rho_{\mathfrak{B}}}{\partial t} + \frac{i}{\hbar} \left[\Psi^\dagger (\mathcal{H}_{\mathfrak{B}} \Psi) - (\mathcal{H}_{\mathfrak{B}} \Psi)^\dagger \Psi \right] = 0. \tag{B.5}$$

More arduous work will be needed, however we will obtain an identical result, as expected.

Bibliography

[1] H. P. Boehm, A. Clauss, G. O. Fischer, and U. Hofmann. Das adsorptionsverhalten sehr dünner kohlenstoff-folien. *Z Anorg Allg Chem.*, 316(3-4):119–127, 1962.

[2] Riichiro Saito, Mitsutaka Fujita, G. Dresselhaus, and M. S. Dresselhaus. Electronic structure of graphene tubules based on c_{60}. *Phys. Rev. B*, 46:1804–1811, 1992.

[3] K. S. Novoselov, A. K. Geim, S. V. Morozov, D. Jiang, Y. Zhang, S. V. Dubonos, I. V. Grigorieva, and A. A. Firsov. Electric field effect in atomically thin carbon films. *Science*, 306(5696):666–669, 2004.

[4] P. R. Wallace. The band theory of graphite. *Phys. Rev.*, 71:622–634, 1947.

[5] Mikhail I. Katsnelson. *Graphene: Carbon in Two Dimensions*. Cambridge University Press, 2012.

[6] Edward McCann and Mikito Koshino. The electronic properties of bilayer graphene. *Rep. Prog. Phys.*, 76(5):056503, 2013.

[7] V. P. Gusynin and S. G. Sharapov. Unconventional integer quantum hall effect in graphene. *Phys. Rev. Lett.*, 95:146801, 2005.

[8] K. S. Novoselov, A. K. Geim, S. V. Morozov, D. Jiang, M. I. Katsnelson, I. V. Grigorieva, S. V. Dubonos, and A. A. Firsov. Two-dimensional gas of massless dirac fermions in graphene. *Nature*, 438(7065):197–200, 2005.

[9] Yuanbo Zhang, Yan-Wen Tan, Horst L. Stormer, and Philip Kim. Experimental observation of the quantum hall effect and berry's phase in graphene. *Nature*, 438(7065):201–204, 2005.

[10] Ş Kuru, J Negro, and L M Nieto. Exact analytic solutions for a dirac electron moving in graphene under magnetic fields. *J. Phys. Condens. Matter*, 21(45):455305, 2009.

[11] Bikashkali Midya and David J Fernández. Dirac electron in graphene under supersymmetry generated magnetic fields. *J. Phys. A Math. Theor.*, 47(28):285302, 2014.

[12] David J Fernández C, Juan D García M, and Daniel O-Campa. Electron in bilayer graphene with magnetic fields leading to shape invariant potentials. *J. Phys. A Math. Theor.*, 53(43):435202, 2020.

[13] David J Fernández C, Juan D García M, and Daniel O-Campa. Bilayer graphene in magnetic fields generated by supersymmetry. *J. Phys. A Math. Theor.*, 54(24), 2021.

[14] David J. Fernández C. and Nicolás Fernández-García. Higher-order supersymmetric quantum mechanics. *AIP Conf Proc*, 744(1):236–273, 2004.

[15] L. Infeld. On a new treatment of some eigenvalue problems. *Phys. Rev.*, 59:737–747, 1941.

[16] L. Infeld and T. E. Hull. The factorization method. *Rev. Mod. Phys.*, 23:21–68, 1951.

[17] Bogdan Mielnik. Factorization method and new potentials with the oscillator spectrum. *J Math Phys*, 25(12):3387–3389, 1984.

[18] Edward Witten. Dynamical breaking of supersymmetry. *Nucl Phys B*, 188(3):513–554, 1981.

[19] Michael Martin Nieto. Relationship Between Supersymmetry and the Inverse Method in Quantum Mechanics. *Phys. Lett. B*, 145:208–210, 1984.

[20] Alexander A. Andrianov, N. V. Borisov, and Mikhail V. Ioffe. The Factorization method and quantum systems with equivalent energy spectra. *Phys. Lett. A*, 105:19–22, 1984.

[21] C V Sukumar. Supersymmetric quantum mechanics of one-dimensional systems. *J Phys A Math Gen*, 18(15):2917–2936, 1985.

[22] Erik Díaz-Bautista and David J. Fernández. Graphene coherent states. *Eur. Phys. J. Plus*, 132(11):499, 2017.

[23] E Díaz-Bautista, Y Concha-Sánchez, and A Raya. Barut–girardello coherent states for anisotropic 2d-dirac materials. *J. Phys. Condens. Matter*, 31(43):435702, 2019.

[24] E Díaz-Bautista, M Oliva-Leyva, Y Concha-Sánchez, and A Raya. Coherent states in magnetized anisotropic 2d dirac materials. *J. Phys. A Math. Theor.*, 53(10):105301, 2020.

[25] David J. Fernández and Dennis I. Martínez-Moreno. Bilayer graphene coherent states. *Eur. Phys. J. Plus*, 135(9):739, 2020.

[26] E. Díaz-Bautista, J. Negro, and L. M. Nieto. Coherent states in the symmetric gauge for graphene under a constant perpendicular magnetic field. *Eur. Phys. J. Plus*, 136(5):505, 2021.

[27] Roy J. Glauber. The quantum theory of optical coherence. *Phys. Rev.*, 130:2529–2539, 1963.

[28] Roy J. Glauber. Coherent and incoherent states of the radiation field. *Phys. Rev.*, 131:2766–2788, 1963.

[29] E. Schrödinger. An undulatory theory of the mechanics of atoms and molecules. *Phys. Rev.*, 28:1049–1070, 1926.

[30] David J Fernández C. New hydrogen-like potentials. *Lett Math Phys*, 8(4):337–343, 1984.

[31] Bogdan Mielnik and Oscar Rosas-Ortiz. Factorization: little or great algorithm? *J Phys A Math Gen*, 37(43):10007–10035, 2004.

[32] C. V. Sukumar. Supersymmetry, factorization of the Schrödinger equation and a Hamiltonian hierarchy. *J. Phys. A*, 18:L57–L61, 1985.

[33] Asim Gangopadhyaya, Jeffry V Mallow, and Constantin Rasinariu. *Supersymmetric Quantum Mechanics*. WORLD SCIENTIFIC, 2010.

[34] A. A. Andrianov, M. V. Ioffe, C. Cannata, and J.-P. Dedonder. Susy quantum mechanics with complex superpotentials and real energy spectra. *Int J Mod Phys A*, 14(17):2675–2688, 1999.

[35] A.A. Andrianov, M.V. Ioffe, F. Cannata, and J.-P. Dedonder. Second order derivative supersymmetry, q deformations and the scattering problem. *Int J Mod Phys A*, 10(18):2683–2702, 1995.

[36] David J Fernández C. Supersymmetric quantum mechanics. *AIP Conf Proc*, 1287(1):3–36, 2010.

[37] Boris F. Samsonov. New possibilities for supersymmetry breakdown in quantum mechanics and second-order irreducible darboux transformations. *Phys. Lett. A*, 263(4):274–280, 1999.

[38] David J Fernández C and Encarnación Salinas-Hernández. The confluent algorithm in second-order supersymmetric quantum mechanics. *J Phys A Math Gen*, 36(10):2537–2543, 2003.

[39] Alonso Contreras-Astorga and Axel Schulze-Halberg. The generalized zero-mode supersymmetry scheme and the confluent algorithm. *Ann Phys (N Y)*, 354:353–364, 2015.

[40] Alonso Contreras-Astorga and Axel Schulze-Halberg. On integral and differential representations of jordan chains and the confluent supersymmetry algorithm. *J. Phys. A Math. Theor.*, 48(31):315202, 2015.

[41] David Bermudez, David J. Fernández C., and Nicolás Fernández-García. Wronskian differential formula for confluent supersymmetric quantum mechanics. *Phys. Lett. A*, 376(5):692–696, 2012.

[42] David Bermudez and David J. Fernández C. Factorization method and new potentials from the inverted oscillator. *Ann Phys (N Y)*, 333:290–306, 2013.

[43] Alonso Contreras-Astorga and Axel Schulze-Halberg. Recursive representation of wronskians in confluent supersymmetric quantum mechanics. *J. Phys. A Math. Theor.*, 50(10):105301, 2017.

[44] David J. Fernández C. and Encarnación Salinas-Hernández. Wronskian formula for confluent second-order supersymmetric quantum mechanics. *Phys. Lett. A*, 338(1):13–18, 2005.

[45] David J. Fernández C, Rodrigo Muñoz, and Arturo Ramos. Second order susy transformations with 'complex energies'. *Phys. Lett. A*, 308(1):11–16, 2003.

[46] I. Razado-Colambo, J. Avila, D. Vignaud, S. Godey, X. Wallart, D. P. Woodruff, and M. C. Asensio. Structural determination of bilayer graphene on sic(0001) using synchrotron radiation photoelectron diffraction. *Sci. Rep.*, 8(1):10190, 2018.

[47] Daniel R. Cooper, Benjamin D'Anjou, Nageswara Ghattamaneni, Benjamin Harack, Michael Hilke, Alexandre Horth, Norberto Majlis, Mathieu Massicotte, Leron Vandsburger, Eric Whiteway, and Victor Yu. Experimental review of graphene. *ISRN Condens. Matter Phys.*, 2012:501686, 2012.

[48] R. R. Nair, P. Blake, A. N. Grigorenko, K. S. Novoselov, T. J. Booth, T. Stauber, N. M. R. Peres, and A. K. Geim. Fine structure constant defines visual transparency of graphene. *Science*, 320(5881):1308–1308, 2008.

[49] Toshiaki Enoki. Role of edges in the electronic and magnetic structures of nanographene. *Phys Scr*, T146:014008, 2012.

[50] A. H. Castro Neto, F. Guinea, N. M. R. Peres, K. S. Novoselov, and A. K. Geim. The electronic properties of graphene. *Rev. Mod. Phys.*, 81:109–162, 2009.

[51] S. Cahangirov, M. Topsakal, E. Aktürk, H. Şahin, and S. Ciraci. Two- and one-dimensional honeycomb structures of silicon and germanium. *Phys. Rev. Lett.*, 102:236804, 2009.

[52] Patrick Vogt, Paola De Padova, Claudio Quaresima, Jose Avila, Emmanouil Frantzeskakis, Maria Carmen Asensio, Andrea Resta, Bénédicte Ealet, and Guy Le Lay. Silicene: Compelling experimental evidence for graphenelike two-dimensional silicon. *Phys. Rev. Lett.*, 108:155501, 2012.

[53] Yasumasa Hasegawa, Rikio Konno, Hiroki Nakano, and Mahito Kohmoto. Zero modes of tight-binding electrons on the honeycomb lattice. *Phys. Rev. B*, 74:033413, 2006.

[54] M. Castillo-Celeita, E. Díaz-Bautista, and M. Oliva-Leyva. Coherent states for graphene under the interaction of crossed electric and magnetic fields. *Ann Phys (N Y)*, 421:168287, 2020.

[55] Dai-Nam Le, Van-Hoang Le, and Pinaki Roy. Conditional electron confinement in graphene via smooth magnetic fields. *Physica E Low Dimens. Syst. Nanostruct.*, 96:17–22, 2018.

[56] M Castillo-Celeita and David J Fernández C. Dirac electron in graphene with magnetic fields arising from first-order intertwining operators. *J. Phys. A Math. Theor.*, 53(3):035302, 2020.

[57] Miguel Castillo-Celeita, Alonso Contreras-Astorga, and David J. Fernández C. Photonic graphene under strain with position-dependent gain and loss. *Acta Polytechnica*, 62(1):23–29, 2022.

[58] A. K. Geim and I. V. Grigorieva. Van der waals heterostructures. *Nature*, 499(7459):419–425, 2013.

[59] Axel Schulze-Halberg and Pinaki Roy. Construction of zero-energy states in graphene through the supersymmetry formalism. *J. Phys. A Math. Theor.*, 50(36):365205, 2017.

[60] M. Oliva-Leyva and Gerardo G. Naumis. Generalizing the fermi velocity of strained graphene from uniform to nonuniform strain. *Phys. Lett. A*, 379(40):2645–2651, 2015.

[61] Gerardo G Naumis, Salvador Barraza-Lopez, Maurice Oliva-Leyva, and Humberto Terrones. Electronic and optical properties of strained graphene and other strained 2d materials: a review. *Rep. Prog. Phys.*, 80(9):096501, 2017.

[62] Aires Ferreira, J. Viana-Gomes, Johan Nilsson, E. R. Mucciolo, N. M. R. Peres, and A. H. Castro Neto. Unified description of the dc conductivity of monolayer and bilayer graphene at finite densities based on resonant scatterers. *Phys. Rev. B*, 83:165402, 2011.

[63] M. Oliva-Leyva and Gerardo G. Naumis. Understanding electron behavior in strained graphene as a reciprocal space distortion. *Phys. Rev. B*, 88:085430, 2013.

[64] M. Oliva-Leyva, J. E. Barrios-Vargas, and G. Gonzalez de la Cruz. Effective magnetic field induced by inhomogeneous fermi velocity in strained honeycomb structures. *Phys. Rev. B*, 102:035447, 2020.

[65] Rajat K Bhaduri, Jamal Sakhr, D W L Sprung, Ranabir Dutt, and Akira Suzuki. Shape invariant potentials in SUSY quantum mechanics and periodic orbit theory. *J Phys A Math Gen*, 38(11):L183–L189, 2005.

[66] R. Sandhya, S. Sree Ranjani, and A.K. Kapoor. Shape invariant potentials in higher dimensions. *Ann Phys (N Y)*, 359:125–135, 2015.

[67] Jose F. Cariñena and Arturo Ramos. Riccati equation, factorization method and shape invariance. *Rev. Math. Phys.*, 12(10):1279–1304, 2000.

[68] Bijan Kumar Bagchi. *Supersymmetry In Quantum and Classical Mechanics*. Chapman and Hall/CRC, 2000.

[69] Fred Cooper, Avinash Khare, and Uday Sukhatme. *Supersymmetry in Quantum Mechanics*. WORLD SCIENTIFIC, 2001.

[70] D Gómez-Ullate, N Kamran, and R Milson. The darboux transformation and algebraic deformations of shape-invariant potentials. *J Phys A Math Gen*, 37(5):1789–1804, 2004.

[71] David Gómez-Ullate, Yves Grandati, and Robert Milson. Rational extensions of the quantum harmonic oscillator and exceptional hermite polynomials. *J. Phys. A Math. Theor.*, 47(1):015203, 2013.

[72] Yves Grandati. Rational extensions of solvable potentials and exceptional orthogonal polynomials. *J Phys Conf Ser*, 343(1):11, 2012.

[73] I Marquette and C Quesne. Two-step rational extensions of the harmonic oscillator: exceptional orthogonal polynomials and ladder operators. *J. Phys. A Math. Theor.*, 46(15):155201, 2013.

[74] David J Fernández C and Barnana Roy. Confluent second-order supersymmetric quantum mechanics and spectral design. *Phys Scr*, 95(5):055210, 2020.

[75] A. O. Barut and L. Girardello. New "coherent" states associated with non-compact groups. *Commun. Math. Phys.*, 21(1):41–55, 1971.

[76] Robert Gilmore. Geometry of symmetrized states. *Ann Phys (N Y)*, 74(2):391–463, 1972.

[77] A. M. Perelomov. Coherent states for arbitrary lie group. *Commun. Math. Phys.*, 26(3):222–236, 1972.

[78] A. M. Perelomov. Coherent states and symmetric spaces. *Commun. Math. Phys.*, 44(2):197–210, 1975.

[79] C Aragone, G Guerri, S Salamo, and J L Tani. Intelligent spin states. *J. phys., A Math. nucl. gen.*, 7(15):L149–L151, 1974.

[80] C. Aragone, E. Chalbaud, and S. Salamó. On intelligent spin states. *J Math Phys*, 17(11):1963–1971, 1976.

[81] Michael Martin Nieto and L. M. Simmons. Coherent states for general potentials. *Phys. Rev. Lett.*, 41:207–210, 1978.

[82] Michael Martin Nieto and L. M. Simmons. Coherent states for general potentials. i. formalism. *Phys. Rev. D*, 20:1321–1331, 1979.

[83] A. Perelomov. *Generalized coherent states and their applications.* Springer-Verlag New York Inc.,New York, NY, United States, 1986.

[84] R. Gilmore. *Lie Groups, Lie Algebras, and Some of Their Applications.* Dover Publications, 2012.

[85] Erik Díaz-Bautista and Maurice Oliva-Leyva. Coherent states for dispersive pseudo-landau-levels in strained honeycomb lattices. *Eur. Phys. J. Plus*, 136(7):765, 2021.